COMPREHENSIVE MODELING AND ROBUST NONLINEAR CONTROL OF HDD SERVO SYSTEMS

CHENG GUOYANG

(B.Eng, National University of Defense Technology, China
M.Eng, Tsinghua University)

A THESIS SUBMITTED

FOR THE DEGREE OF DOCTOR OF PHILOSOPHY

DEPARTMENT OF ELECTRICAL AND COMPUTER ENGINEERING

NATIONAL UNIVERSITY OF SINGAPORE

2005

Acknowledgements

Life is a journey with myriad possibilities. Smooth or bumpy it may turn out to be, we are always indebted to those who come along our way and make this journey a unique experience.

First, I would like to express my heart-felt gratitude to my advisors, Prof. Ben M. Chen and Prof. T.H. Lee, for their constructive suggestions and constant supports during this research. Especially, I would like to thank Prof. Chen for his valuable guidance, without which this thesis could never have come into existence. Moreover, his passion for life and the capability to maintain a perfect balance between academic duty and real life have inspired us with the belief that an active career can be pursued while enjoying one's life.

Special thanks go to Dr. Kemao Peng, with whom I have the pleasure of working together. His experience and expertise impressed me very much, and I have been benefiting from his help.

I am much grateful to the professors in the department of electrical and computer engineering, whose lectures have prepared me for a career in the area of control and automation, and those who have enlightened me in one way or the other. I am also grateful to our administrative staff for being considerate and helpful. Meanwhile, I want to extend my grateful thanks to the folks in Control and Simulation Lab, with whom I have enjoyed more than three years' happy and memorable life.

My deepest appreciation should go to my family for the love and support given to me over the years. I am also obliged to old friends, Xinmin Liu, Wenguang Kim, Yuntian Xu, and many others for their understanding and encouragement.

Finally, I wish to thank the National University of Singapore for providing me the scholarship and the opportunity for pursuing a higher degree.

Contents

Summary

The HDD (hard disk drive) industry is now moving towards smaller disk drives with larger capacity. As the track density gets higher, a more stringent TMR (track mis-registration) budget is imposed for servo design. This calls for a careful study of the subtle dynamics of HDD servo mechanism, and further exploration of servo control techniques.

This thesis begins with an investigation of some robust linear and nonlinear control techniques for servo system design. First, the Robust and Perfect Tracking (RPT) control technique is introduced, which can be used to design a low-order parameterized controller with fast tracking speed and low overshoot as well as strong robustness. Then a so-called enhanced Composite Nonlinear Feedback (CNF) control technique is developed, which has a new feature of removing static error caused by disturbances while retaining the mainstay of the original CNF, *i.e.*, fast settling in set point tracking tasks.

To facilitate CNF control design, a MATLAB toolkit with a user-friendly graphical interface is then developed. The toolkit can be utilized to design a fast and smooth tracking controller for a class of linear systems with actuator and other nonlinearities as well as with external disturbances. The toolkit is capable of displaying both time-domain and frequency-domain responses, and generating control laws of state feedback and measurement feedback. The usage of the toolkit is illustrated by practical examples on servo design.

Next, research efforts are directed toward the practical design of HDD servo systems. A major step is to establish a comprehensive model for the voice coil motor (VCM) used in HDDs. The approach of physical effect analysis is applied to derive a physical model of a microdrive VCM actuator, which explicitly incorporates nonlinear effects, such as flex cable

nonlinearity and pivot bearing friction. The parameters of the model are then identified using a Monte Carlo process together with the time- and frequency-domain responses of the actual system. Verification will show that the resulting model does capture the main features of the VCM actuator.

With the HDD model in hand, the philosophy for servo system design is straightforward. First, try to cancel those unwanted nonlinearities as identified in the model, and then treat the uncompensated portion as external disturbances and choose an appropriate control methodology to minimize their adverse effects on closed-loop performance. A parameterized track following controller is first designed for the microdrive using the RPT control combined with integral and nonlinear compensation. Next, a servo system, which is capable of track following and short span seeking as well for the microdrive, is designed using the enhanced CNF control combined with nonlinearity pre-compensation. Simulation and Experiments are carried out to evaluate the effectiveness of the designs.

The above designs are based on the single-stage system. Next, a dual-stage actuated HDD servo system, which adds a secondary piezoelectric microactuator to work with the existing VCM actuator, is designed and implemented. In the design, the low frequency characteristics of the piezoelectric microactuator are utilized to estimate its displacement and the concept of open loop inverse control is adopted to control the microactuator loop. The VCM actuator is controlled with the same techniques as in single-stage case, specifically, RPT, CNF and PID control are successively applied for the purpose of comparison. Simulation and implementation results are presented and compared.

To conclude this thesis, the main results of this research, including the strengths and the limitations therein, are summarized. Some possible directions for future research are also included.

List of Figures

List of Tables

Chapter 1

Introduction

The first hard disk drive (HDD), IBM RAMAC 305, appeared in 1956. Five decades later, HDDs have evolved into a huge industry with an annual sales revenue of tens of billions of US dollars. Today, hard disk drives serve as the major storage media in computer systems. Moreover, they are finding increasing applications in consumer electronic devices, such as music player, digital camera, camcorder, mobile phone, *etc.* Along with the development of HDDs, HDD servo system, which is a supporting sub-system in each hard disk drive, has been extensively studied, both by the industry and the academic circle. New developments of hard disk drives impose more stringent demand on the servo systems and call for further research. This chapter gives a brief account of HDD servo systems, and the relevant research efforts in this area, which provide the background and motivation for this research topic.

1.1 HDD Servo Systems

Modern hard disk drives are rooted in the so-called Winchester technology developed by IBM in the 1970s. The Winchester technology featured a smaller, lighter read/write (R/W) head that was designed to ride on an air film of only 18 microinches thick above the disk surface. Moreover, it combined one or more magnetic disk platters and read/write mechanisms in a sealed module, which minimized contamination and enhanced reliability. The resulting higher capacity, faster performance and lower maintenance cost made Winchester

technology the dominant standard for the HDD industry.

Although there have been many new developments in the relevant technologies since then, the framework of Winchester remains the same and still prevails today. Typically, a hard disk drive of this framework is composed of six major components:

1. Device enclosure, which provides a safe space for other inner components and prevents contamination. It consists of two parts, *i.e.*, baseplate and cover.

2. Disk platters, on which there are concentric circles or tracks where data are stored. Each disk platter is made of Al-Mg alloy or glass substrate coated with magnetic recording medium and lubricant.

3. Spindle motor assembly, which supports and drives the disk platters to rotate at constant speed in working condition. It contains some disk clamps, a brushless DC motor with a ball bearing or more recently a fluid dynamic bearing for reduced acoustic noise and high rotating speed.

4. Actuator assembly, which is the servo mechanism to move and position R/W heads. It contains a Voice Coil Motor (VCM), a pivot bearing, arms to support the head/suspension assembly, and a flex cable carrying signal to and from the R/W heads and VCM.

5. Head/suspension assembly, which consists of a suspension, a gimbal, a slider and a R/W head. The R/W head is used to read and write data on the disk, and it can be a thin-film, or magneto-resistive (MR), or giant magneto-resistive (GMR) head.

6. Electronics card, which provides interface to host computer, power drivers for spindle motor and VCM, read/write electronics and servo demodulator, controller chip for timing control and control of interface, micro processor(s) for servo control, and etc.

An important performance indicator for HDDs is the so-called access time, which is defined as the summation of seek time and rotational latency. Seek time is the time (in

milliseconds) it takes to move the R/W heads from current position to a desired track location. Rotational latency is the average time (in milliseconds) the R/W heads must wait for the target sector on the disk to pass under them once the R/W heads are moved to the desired target track. It is determined as half of the rotation period of the disks, which in turn is related to the constant rotation speed of the spindle motor, typically at 3600, 4500, 5400 and 7200 to 15,000 revolutions per minute (RPM).

To improve the performance of HDDs, the access time should be as small as possible. Since the rotational latency is fixed by the spindle speed, more attention should be given to reduce the seek time. The seek time is a measure of how fast the head positioning mechanism in hard disk drives can move the R/W heads to a desired track. Current disk drives use the VCM actuator assembly as the servo mechanism to move and position the R/W head, while research for new servo mechanisms, *e.g.*, dual-stage actuated system, is under way. In the dual-stage system, a microactuator is added to actuate the suspension or slider, to provide a faster and finer movement for the R/W heads.

This thesis mainly deals with HDD head positioning servo system (or in short, HDD servo system). The two main functions of HDD head positioning servo mechanism are track seeking and track following. Track seeking moves the R/W heads from the present track to a specified destination track in minimum time using a bounded control effort. Track following maintains the heads as close as possible to the destination track center while information is being read from or written to the disk. To ensure reliable data reading and writing, it is required that during track following stage, the deviation of R/W heads from target track center, *i.e.*, the position error signal (PES), should not exceed the so-called Track Mis-Registration (TMR) budget, which is normally defined as 5% of track pitch. Here track pitch is simply the reciprocal of track density, which is measured by TPI (Track Per Inch).

The main objective in HDD servo system design is to ensure fast track seeking and precise track following in the face of power limitation, various disturbances and uncertainties in real application environment. Hence, closed-loop control has to be designed and implemented. This is feasible because hard disk drives have either dedicated servo or embedded servo from which the PES can be read out and used for feedback control. To design such an HDD servo system, two steps are to be followed: first, a mathematical model which captures the inherent dynamics of HDD servo mechanism has to be established; next, a suitable control strategy is applied to design a servo controller based on the derived model. Current trend of the HDD industry is towards disk drives with smaller form factor (namely, the diameter of the disk platters) and higher capacity, which requires that the tracks on disk surface be arranged as closely as possible. The higher track density will impose a more stringent TMR budget on HDD servo systems, and hence more demanding tasks with the modeling and control design. This calls for a more careful study of the dynamic characteristics of HDD servo mechanism and further exploration of control design technology.

1.2 Brief Literature Review

Over the years, the subject of HDD servo systems has received much attention from the control community. Many research efforts have been devoted to the modeling and control of HDD servo systems. In what follows, the main results available in this area are outlined.

Conventionally, HDD servo mechanism, to be specific, the VCM actuator, is modeled by a dominant second order system coupled with some high frequency resonant modes (see *e.g.*, Franklin *et al.* [26], Mamun *et al.* [48] and Chen *et al.* [12]). This linear model captures the main characteristics of HDD servo mechanism and seems to work quite well in conventional disk drives with larger form factor. However, various disturbances and nonlinear effects are not included in this model, hence it may not be good enough for the new generation disk

drives in which the nonlinear effects become more prominent with respect to higher track density. To address this problem, several attempts have been made during the past few years. Wang *et al.* [65] applied time domain technique to model the pivot nonlinearity in disk drives while Abramovitch *et al.* [1] resorted to frequency domain technique to model the same nonlinearity, *i.e.*, friction effect. Wang [66] studied the frictional nonlinearity in a small disk drive and proposed several models, *i.e.*, two-preload, preload+2-slope spring, hysteretic 2-slope, and preload+hysteretic damping, to describe the friction effect. Those models are basically the revision and/or combination of existing classical friction models, and they captures the characteristics of friction to some extent. Chang *et al.* [8] used relay function to model and identify pivot friction in HDDs. Gong *et al.* [29] tackled the pivot nonlinearity in HDDs by the use of a Dahl hysteresis model. Yan *et al.* [73] modeled and compensated the pivot nonlinearity in disk drives by using the Leuven integrated friction model. These efforts have contributed to our understanding of the nonlinear behavior in HDDs, more or less. However, the above modeling methodologies are mainly based on empirical modeling and experimental fitting. They are weak in providing theoretical insights into the nonlinearity structure of HDD servo mechanism.

So far, various control strategies have been developed to design servo controllers for HDDs, ranging from conventional PID to more advanced control techniques (see *e.g.*, Abramovitch and Franklin [2], Chen *et al.* [12]). The PID is a simple yet effective control technique and is still widely used in today's commercial HDDs. When it comes to fast track seeking under limited control effort, PID may give way to the proximate time-optimal servomechanism (PTOS), which is a modification of the well known time-optimal control (TOC) and was first proposed by Workman [71]. Both PID and PTOS are time domain techniques. Meanwhile, frequency domain techniques, such as notch filter/band pass filter (see *e.g.*, Ehrlich *et al.* [21] and Kobayashi *et al.* [39]) and disturbance observer (see *e.g.*,

Ishikawa and Tomizuka [36, 37], White *et al.* [69]) have also been proposed to reject disturbances at certain frequency region and improve the tracking performance of HDD servo systems. Although the above control techniques are still useful in the HDD industry, more research need to be done to meet the challenges of the new generation hard disk drives.

With the development of micro processor, especially the Digital Signal Processor (DSP) technology, more complex modern control techniques are being implemented on HDD servo systems. LQG/LTR has been applied to improve the TMR index of HDDs (Chang *et al.* [9]). Adaptive schemes have also been proposed to suppress resonant modes (Wu *et al.* [72]) and compensate pivot friction (Wang *et al.* [68]) respectively in HDD servo systems. Li *et al.* [43] designed an H_2 optimal tracking controller which achieved the highest track-per-inch in hard disk drives with given disturbance models. Learning based control (see *e.g.*, Cao and Xu [7]) and optimization techniques (Lee [40]) have also been utilized to minimize PES (position error signal) in hard disk drives. Goh *et al.* [28] used Robust and Perfect Tracking (RPT) approach to design an HDD tracking controller which is simple in structure yet has desirable performance and robustness. Venkataramanan *et al.* [63] proposed a mode switching controller which combines PTOS and RPT together and thus can perform track seeking and track following as well. And recently, Chen *et al.* [13] developed the so-called Composite Nonlinear Feedback (CNF) control technique, which has been successfully applied to design an HDD servo system with superior properties such as fast response, small overshoot and seamless unification of track seeking and track following without any switching element.

In recent years, more and more attention has been given to the so-called dual-stage servo design, in which the existing VCM actuator is used as a primary stage to perform large but coarse movement, while a secondary micro-actuator is employed to provide finer and faster positioning. The two most popular micro-actuators for dual-stage system

are suspension-mounted PZT (piezoelectric) actuator and slider-mounted MEMS (Micro Electric-Mechanical System) micro-actuator. Dual-stage servo design aims to use the two different actuators to their advantages, so as to enhance the combined performance. It is important to make sure that there is no destructive interactions between the VCM control loop and the microactuator loop. Guo *et al.* [30] proposed several configurations for dual-stage servo design, such as the parallel loop, master-slave loop, decoupled loop, etc. Several design schemes for dual-stage HDD servo systems have been reported, basically following the aforementioned configurations, probably with some modifications. Guo *et al.* [31], Hu *et al.* [35] and Suh *et al.* [61] utilized the well-known LQG/LTR method to design the dual-stage actuated HDD servo systems. Schroeck *et al.* [60] proposed a so-called PQ method to design compensator for dual-input/single-output (DISO) systems (among which is the dual-stage HDD servo system). This PQ method converts the control problem for a DISO system into two SISO control designs, and the relative contribution of the two control loops can be explicitly taken into account. However, overall stability is not guaranteed for the case when one of the loops is inactive. Kim *et al.* [38] applied the idea of zero-phase error tracking controller to minimize the destructive interaction effect when two control loops are combined in a decoupled configuration. Lee *et al.* [41] introduced a new performance index, i.e., destructive interference, to express the degree of cooperation between both actuators in the dual-stage actuated system, and the measure of destructive interference is then minimized to produce a dual-stage actuator control design with desired time and frequency responses. Pang *et al.* [54] proposed the use of PZT suspension-based micro-actuator as a secondary actuator and a displacement sensor simultaneously (so-called Self-Sensing Actuation, SSA), by which the dual-stage servo system can be decoupled into two loops for track-following control design and individual sensitivity optimization. Peng *et al.* [57] combined the Composite Nonlinear Feedback (CNF) control with filtering technique

within a model-based decoupled configuration to design a dual-stage servo system with a piezoelectric actuator. And the resulting dual-stage servo system has achieved significant improvement over single-stage counterpart in HDD track seeking and following.

The above control schemes have greatly improved the performance of HDD servo systems and helped to pave the way for the development of new generation hard disk drives with smaller form factor yet larger capacity. However, relatively few research efforts have been devoted to the inherent nonlinearities in disk drive servo mechanism. It should be noted that, Wang [66] studied pivot friction in a small disk drive and designed several compensators, either a robust or an adaptive one, to cope with this friction nonlinearity. Simulation results [66] indicated a significant improvement on PES (Position Error Signal) over existing controllers, but experiments results were not available to verify such improvement. When it comes to the new generation hard disk drives where friction and nonlinear effects become conspicuous, existing control schemes and techniques may not work well and hence the need for further investigations.

1.3 Motivation and Contributions of This Research

As mentioned earlier, most of the studies in HDD servo systems assume a linear model for HDD VCM actuator except that some researchers do include an add-on nonlinear model to accommodate friction and nonlinear effects. Such add-on models are cooked up from experimental observations and they are prone to variations in different systems. Moreover, they generally are lacking in theoretical foundation and are not quite helpful in controller design. It would be more desirable to have a model which is rooted in physical principle and thus can provide meaningful insight into the nonlinear characteristics in HDD servo mechanism. Such a model will be valuable in both controller design and simulation. The inadequacy of modeling is inevitably accompanied by a compromise of the subsequent con-

troller design. A controller designed based on a pure linear model cannot be expected to handle the nonlinear effects efficiently in precision systems such as HDD servo systems. Treating those nonlinear effects as a lumped disturbance is a rough-cut approach, which ends up with a trade-off between performance and robustness. Very few of the existing control techniques are able to achieve a good transient response without steady state bias in HDD track following tasks. Even for the CNF control technique, which has been successfully used to design a 3.5 inch disk drive servo system that is capable of fast settling in track seeking and track following, the problem of steady state bias still occurs, due to the existence of nonlinearity in the VCM actuator. The reasons behind this are quite clear now. Firstly, nonlinearity is not modeled and compensated; Secondly, the current version of CNF control is not able to handle disturbances.

The above problems pose a strong motivation for further research on modeling and control of HDD servo systems, with special attention to the nonlinear effects therein. The research efforts have led to fruitful contributions, both theoretically and practically.

The theoretical part of contributions is the development of an enhanced composite nonlinear feedback (CNF) control technique together with a MATLAB toolkit support. The new technique can be used to design a fast, smooth and accurate tracking controller for linear systems subject to actuator saturation and constant disturbances. The enhanced CNF control preserves those superior transient performance of the original CNF, *i.e.,* , fast response and low overshoot in set-point tracking, and at the same time has an additional capacity of eliminating steady state bias due to disturbances. To facilitate the design process of CNF control, a MATLAB toolkit with a user-friendly graphical interface has been developed. With the toolkit, user can easily choose controller structure, tune and re-tune the controller parameters and test the performance via simulation. The toolkit is capable of displaying both time-domain and frequency-domain responses on its main panel, and

generating three different types of control laws, namely, the state feedback, the full order measurement feedback and the reduced order measurement feedback controllers. The toolkit can be utilized to design servo systems that deal with point-and-shoot fast targeting.

The practical part of contributions is on the HDD servo system design. A comprehensive model, which captures not only the dominant linear characteristics but also the inherent nonlinearity of HDD head positioning servo mechanism, has been established for a microdrive. The nonlinear effects are identified from the perspective of physical law so that the resulting model can provide insightful explanation for nonlinearity structure in HDDs. Moreover, this model is in a clear form so that it is convenient for nonlinearity compensation in subsequent controller design. With such a model at hand, servo systems have been designed. Specifically, a track following controller is designed for the microdrive using Robust and Perfect Tracking (RPT) control technique combined with nonlinear compensation and integral enhancement. Then, a servo system, which can perform track seeking and track following all-in-one without any explicit switching element, is designed using the enhanced CNF control technique. Simulation and Experimental results indicate that the designs are very successful. Next, contributions have also been made on the design and implementation of a dual-stage actuated HDD servo system, in which an additional piezoelectric microactuator is mounted on top of the conventional VCM actuator to provide a faster and finer positioning, while the existing VCM actuator is used to move the R/W head assembly for large but coarse positioning. The RPT and the enhanced CNF control techniques are once again adopted in the servo system design. Simulation and experiments show that the dual-stage systems achieve significant improvement in track following and seeking, in rejecting repeatable-runouts (RROs) disturbances, which demonstrate the great potential of microactuator in HDD servo systems.

The enhanced CNF control technique with the MATLAB toolkit, the comprehensive

model and servo system designs for the microdrive, and the design and implementation of the dual-stage servo system, compose an integrated methodology for HDD servo system design. These results can be expected to bring new perspective to the servo design for commercial hard disk drives. As the HDD industry is moving towards smaller disk drives with larger capacity, higher track density and hence tighter specifications on servo performance pose a great challenge for servo engineers. By providing a comprehensive solution for modeling and control of HDD servo systems, we are, to some extent, paving the way for the new generation hard disk drives. Moreover, the modeling methodology and the control techniques developed here should be useful for general servo systems as well.

Before proceeding to the next chapter, which goes into the details of some control techniques for servo systems, it is helpful to have an overview of this thesis.

1.4 Outline of This Thesis

This thesis is dedicated to the methodology of modeling and control design for HDD head positioning servo systems. It begins with an introduction of this research interest. It is noted that friction and nonlinear effects have become the major impediments to servo performance in the new generation HDDs. Moreover, this problem has not received much attention from the HDD servo community so far, which makes it worthwhile to devote research efforts towards modeling and compensation of friction and nonlinearities in HDD servo systems. These are the main points of this chapter.

In the next chapter, or Chapter 2, some robust linear and nonlinear control techniques for servo system design are investigated. First introduced is a so-called robust and perfect tracking (RPT) control technique, which enables control engineers to design a low-order parameterized controller which still results in a closed-loop system with fast tracking speed and low overshoot as well as strong robustness. Next, the theory of enhanced composite

nonlinear feedback (CNF) control technique is developed, which is an extension of the previous work by Chen *et al.* (see *e.g.*, [12,13]). The enhanced CNF control has a feature of removing the uncompensated portion of friction and nonlinearities while maintaining those nice properties of the original CNF control, such as fast response and little or no overshoot in set point tracking tasks.

Chapter 3 presents a MATLAB toolkit with a user-friendly graphical interface for CNF (composite nonlinear feedback) control system design. The toolkit can be utilized to design a fast and smooth tracking controller for a class of linear systems with actuator and other nonlinearities as well as with external disturbances. There are basically two steps to the design of a CNF controller, *i.e.*, design of a linear feedback law to yield a closed-loop system with a small damping ratio for a quick response, and design of a nonlinear feedback law on top of the linear law to increase the damping ratio of the closed-loop system at steady state and hence reduce the overshoot caused by the linear part. An integrator will be added to the overall controller design if there are external disturbances. A nonlinearity pre-compensation will be implemented if there are plant nonlinearities that can be canceled using certain output feedback. The toolkit is capable of displaying both time-domain and frequency-domain responses on its main panel, and generating three different types of control laws, namely, the state feedback, the full order measurement feedback and the reduced order measurement feedback controllers. The usage and design procedure of the toolkit will be illustrated by some examples on servo design.

Chapter 4 deals with the modeling of the voice coil motor (VCM) with rotary pivot bearing friction and flex cable nonlinearity in a micro hard disk drive. The model of VCM actuators is generally recognized as a linear model and built through the measured frequency response. However, the fact is, the VCM actuator has some inherent nonlinearities, such as flex cable nonlinearity and pivot bearing friction. These nonlinearities will result

in large modeling errors and consequently deteriorate the performance of head positioning servo systems. This problem is more noticeable in small and micro HDDs and becomes a headache for servo engineers in this area. To effectively tackle the HDD servo problem, nonlinear effects should be carefully studied and incorporated into the model of the servo mechanism. In this chapter, a comprehensive model of the VCM actuator, including friction and nonlinear characteristics, is established. This will be achieved through a careful examination of the configuration and structure of the actual system and through a thorough analysis of its physical effects together with its time-domain and frequency-domain responses. Verification will also be carried out to show that the established model indeed captures the characteristics of the VCM actuator.

Chapter 5 is focused on the design of HDD servo systems based on the model derived in the previous chapter. The philosophy for servo system design is rather simple. Once the model of the friction and nonlinearities of the VCM actuator is obtained, a pre-compensation scheme can first be applied to cancel as much as possible all these unwanted elements in the servo system. Next, by treating the uncompensated portion as external disturbances, the HDD servo problem can be formulated into a robust control framework. Based on this idea, a track following controller is designed using the Robust and Perfect Tracking (RPT) control technique with an integral enhancement and nonlinearity compensation. The resulting controller is parameterized and amenable to online tuning and hardware implementation. Further more, a servo system, which is expected to perform track following and short span seeking as well for the micro drive, is designed. The control strategy to be adopted is the enhanced Composite Nonlinear Feedback (CNF) control technique combined with a simple friction and nonlinearity pre-compensation scheme. Simulations and experiments will be carried out to verify the effectiveness of the designs.

Chapter 6 presents the design and implementation of a dual-stage actuated hard disk

drive (HDD) servo system, in which an additional piezoelectric microactuator is mounted on top of the conventional voice-coil-motor (VCM) actuator to provide a faster and finer positioning of the R/W head onto a target track. In the design, the low frequency characteristics of the piezoelectric microactuator are utilized to estimate its displacement and accordingly the displacement of the VCM actuator, which simplifies the subsequent servo design. The microactuator is controlled through a simple static gain together with an appropriately designed filter, and the VCM actuator is controlled using the well-established single-stage servo control methodology. Three alternative controllers will be designed for the VCM actuator, based on RPT (robust and perfect tracking), CNF(composite nonlinear feedback) and PID respectively. Simulation and experimental results will be provided to show that the dual-stage servo systems have great potential in HDDs.

Chapter 7 contains a summary of the research results, their strengths and limitations and then outlines some possible scopes for future research.

Chapter 2

Robust and Nonlinear Control Techniques for Servo Systems

This chapter presents some control techniques that are useful in servo system design. To be specific, a so-called robust and perfect tracking (RPT) control technique will first be introduced, which can be used to design a low-order parameterized controller such that the controlled output almost perfectly tracks a given reference signal, *i.e.*, to track the given reference signal with arbitrarily fast settling time in the face of external disturbances and initial conditions. Next, the theory of an enhanced Composite Nonlinear Feedback (CNF) control technique will be developed, which is capable of removing steady state bias due to disturbances, and at the same time maintaining the superior transient property of the original CNF control, *i.e.*, fast and smooth settling in set point tracking tasks.

2.1 Introduction

Most of today's advanced control techniques are model-based, i.e., they are highly dependent on the plant model, which is normally a mathematical description of the plant, based on some simplifications and assumptions. A controller designed for a nominal model may not work well on the practical system. This leads to the topic of robust control, which aims to

design a controller not just for a single plant but for a class of plants, in the face of plant uncertainty and external disturbances.

In the case of HDD servo system, it is usually modeled by a linear second order system. However, there are many resonant modes in the high frequency region. In the low frequency region, there are toque disturbances, such as pivot bearing friction and flex cable nonlinearity. Other factors, *e.g.*, repeatable run-outs (RRO) and windage, are also influential. For easy implementation, it is desirable to design a low order servo controller based on a simplified HDD model (the nominal model), but at the same time some extent of robustness of stability and performance must be maintained for the controller to be workable or effective in practical environment where a single controller is expected to work for a whole batch of hard disk drives.

For more than two decades, robust control has been a hot spot among the control community. So far, many design techniques have been developed, among which is the so-called robust and perfect tracking (RPT) control, which was proposed and solved by Liu, Chen and Lin [45]. This technique enables control engineers to design a low-order controller which still results in a closed-loop system with fast tracking speed and low overshoot as well as strong robustness. This control technique has been successfully used in the servo design for a conventional 3.5 inch hard disk drive [28]. It will be further used HDD servo system design in later chapters, but with some enhancements.

The aforementioned RPT technique is a pure linear control technique by itself. However, every physical system in our life is essentially nonlinear. For example, many practical systems have actuator saturation and other nonlinearities such as friction. The important features of systems with nonlinearities may be sacrificed if they are analyzed and designed through linear techniques alone (see, *e.g.*, [13] and [34]). Hence, nonlinear control comes into the picture. Traditionally, when dealing with point-and-shoot fast targeting for systems with

actuator saturation, one would naturally think of using the well known time-optimal control (also known as the bang-bang control), which uses maximum acceleration and maximum deceleration for a predetermined time period. Unfortunately, it is well known that the classical time-optimal control is not robust with respect to the system uncertainties and measurement noises. It can hardly be used in any real situation. For asymptotic tracking situations, Workman [71] proposed the so-called proximate time-optimal servomechanism (PTOS), which is basically a modified version from the traditional time-optimal control to overcome its drawback of non-robustness with respect to uncertainties and noises.

Recently, Lin *et al.* [44] proposed a composite control law to improve the tracking performance under state feedback for a class of second order systems with input saturation. The idea was later extended by Chen *et al.* [13] to general single-input-and-single-output (SISO) systems under measurement feedback and successfully applied to solve a servo problem for a computer hard disk drive. The new technique, called composite nonlinear feedback (CNF) control technique, can be utilized to design a fast and smooth tracking controller for general SISO systems (even with input saturation). It was shown in [13] that the CNF control has the potential to beat the traditional time-optimal control or the proximate time-optimal servomechanism (PTOS) design method in set point asymptotic tracking. In this chapter, the CNF control technique will be further extended to systems with external disturbances, especially with unknown constant disturbances, which are existent almost in all physical systems (e.g., the HDD servo system) and generate steady state bias to the system output.

In what follows, the Robust and Perfect Tracking (RPT) control technique will first be introduced. Then, we will proceed to develop the so-called enhanced composite nonlinear feedback (CNF) control technique.

2.2 Robust and Perfect Tracking Control

For easy reference, we recall in this section the robust and perfect tracking (RPT) control technique, which was proposed and solved by Liu, Chen and Lin [45].

2.2.1 Problem Formulation

The robust and perfect tracking problem is to design a controller such that the resulting closed-loop system is asymptotically stable and the controlled output almost perfectly tracks a given reference signal in the presence of any initial conditions and external disturbances. By almost tracking we mean the ability of a controller to track a given reference signal with arbitrarily fast settling time in the face of external disturbances and initial conditions. More specifically, RPT deals with the following multivariable linear time-invariant system,

$$\Sigma \; : \; \begin{cases} \dot{x} = A\ x + B\ \ u + E\ w, & x(0) = x_0, \\ y = C_1\ x \qquad\quad + D_1\ w, \\ h = C_2\ x + D_2\ u, \end{cases} \tag{2.1}$$

where $x \in \mathbb{R}^n$ is the state, $u \in \mathbb{R}^m$ is the control input, $w \in \mathbb{R}^{\mathsf{q}}$ is the external disturbance, $y \in \mathbb{R}^{\mathsf{p}}$ is the measurement output, and $h \in \mathbb{R}^\ell$ is the output to be controlled. We also assume that the pair (A, B) is stabilizable and (A, C_1) is detectable. For future references, we define Σ_{P} and Σ_{Q} to be the subsystems characterized by the matrix quadruples (A, B, C_2, D_2) and (A, E, C_1, D_1), respectively. Given the external disturbance $w \in L_p$, $p \in [1, \infty)$, and any reference signal vector, $r \in \mathbb{R}^\ell$ with r, $\dot{r}$, $\cdots$, $r^{(\kappa-1)}$, $\kappa \geq 1$, being available, and $r^{(\kappa)}$ being either a vector of delta functions or in L_p, the robust and perfect tracking (RPT) problem for the system (2.1) is to find a parameterized dynamic measurement control law of the following form

$$\begin{cases} \dot{v} = A_{\mathrm{cmp}}(\varepsilon)v + B_{\mathrm{cmp}}(\varepsilon)y + G_0(\varepsilon)r + \cdots + G_{\kappa-1}(\varepsilon)r^{(\kappa-1)}, \\ u = C_{\mathrm{cmp}}(\varepsilon)v + D_{\mathrm{cmp}}(\varepsilon)y + H_0(\varepsilon)r + \cdots + H_{\kappa-1}(\varepsilon)r^{(\kappa-1)}, \end{cases} \tag{2.2}$$

such that when (2.2) is applied (2.1), we have

1. There exists an $\varepsilon^* > 0$ such that the resulting closed-loop system with $r = 0$ and $w = 0$ is asymptotically stable for all $\varepsilon \in (0, \varepsilon^*]$; and

2. Let $h(t, \varepsilon)$ be the closed-loop controlled output response and let $e(t, \varepsilon)$ be the resulting tracking error, i.e., $e(t, \varepsilon) := h(t, \varepsilon) - r(t)$. Then, for any initial condition of the state, $x_0 \in \mathbb{R}^n$,

$$J_p(x_0, w, r, \varepsilon) := \|e\|_p \to 0 \ \text{ as } \ \varepsilon \to 0. \tag{2.3}$$

Note that in the above formulation we introduce some additional information besides the reference signal r, i.e., $\dot{r}, \ddot{r}, \cdots, r^{(\kappa-1)}$, as additional controller inputs. In general, these additional signals can easily be generated without any extra costs. Also, it is simple to see that when $r(t) \equiv 0$, the proposed problem reduces to the well known perfect regulation problem with measurement feedback.

It is shown in [45] that the above RPT problem is solvable if and only if the following conditions are satisfied:

1. (A, B) is stabilizable and (A, C_1) is detectable;

2. (A, B, C_2, D_2) is minimum phase and right invertible;

3. $Ker(C_2) \supseteq C_1^{-1}\{Im(D_1)\} \equiv \{v | C_1 v \in Im(D_1)\}$.

Here we note that $Ker(\cdot)$ and $Im(\cdot)$ denote respectively the kernel and image of the appropriate matrix. Also, note that for the case when $D_1 = 0$, the last item implies that $Ker(C_2) \supseteq Ker(C_1)$.

In what follows, we are going to solve the proposed robust and perfect tracking problem by explicitly constructing parameterized controllers for two cases: the state feedback and the reduced order measurement feedback.

2.2.2 The State Feedback Case

When all states of the plant are measured for feedback, the problem can be solved by a static control law. We construct in this subsection a parameterized state feedback control law,

$$u = F(\varepsilon)x + H_0(\varepsilon)r + \cdots + H_{\kappa-1}(\varepsilon)r^{(\kappa-1)}, \tag{2.4}$$

which solves the robust and perfect tracking (RPT) problem for (2.1) under the given conditions. It is simple to note that we can rewrite the given reference in the following form,

$$\frac{d}{dt}\begin{pmatrix} r \\ \vdots \\ r^{(\kappa-2)} \\ r^{(\kappa-1)} \end{pmatrix} = \begin{bmatrix} 0 & I_\ell & \cdots & 0 \\ \vdots & \vdots & \ddots & \vdots \\ 0 & 0 & \cdots & I_\ell \\ 0 & 0 & \cdots & 0 \end{bmatrix} \begin{pmatrix} r \\ \vdots \\ r^{(\kappa-2)} \\ r^{(\kappa-1)} \end{pmatrix} + \begin{bmatrix} 0 \\ \vdots \\ 0 \\ I_\ell \end{bmatrix} r^{(\kappa)}. \tag{2.5}$$

Combining (2.5) with the given system, we obtain the following augmented system,

$$\Sigma_{\text{AUG}} : \begin{cases} \dot{\boldsymbol{x}} = \boldsymbol{A}\ \boldsymbol{x} + \boldsymbol{B}\ u + \boldsymbol{E}\ \boldsymbol{w} \\ \boldsymbol{y} = \quad \boldsymbol{x} \\ e = \boldsymbol{C}_2\ \boldsymbol{x} + \boldsymbol{D}_2\ u \end{cases} \tag{2.6}$$

where

$$\boldsymbol{w} := \begin{pmatrix} w \\ r^{(\kappa)} \end{pmatrix}, \quad \boldsymbol{x} := \begin{pmatrix} r \\ \vdots \\ r^{(\kappa-2)} \\ r^{(\kappa-1)} \\ x \end{pmatrix}, \tag{2.7}$$

$$\boldsymbol{A} = \begin{bmatrix} 0 & I_\ell & \cdots & 0 & 0 \\ \vdots & \vdots & \ddots & \vdots & \vdots \\ 0 & 0 & \cdots & I_\ell & 0 \\ 0 & 0 & \cdots & 0 & 0 \\ 0 & 0 & \cdots & 0 & A \end{bmatrix}, \quad \boldsymbol{B} = \begin{bmatrix} 0 \\ \vdots \\ 0 \\ 0 \\ B \end{bmatrix}, \quad \boldsymbol{E} = \begin{bmatrix} 0 & 0 \\ \vdots & \vdots \\ 0 & 0 \\ 0 & I_\ell \\ E & 0 \end{bmatrix}, \tag{2.8}$$

and

$$\boldsymbol{C}_2 = [\,-I_\ell \quad 0 \quad 0 \quad \cdots \quad 0 \quad C_2\,], \quad \boldsymbol{D}_2 = D_2. \tag{2.9}$$

It is then straightforward to show that the subsystem from u to e in the augmented system (2.6), i.e., the quadruple $(\boldsymbol{A}, \boldsymbol{B}, \boldsymbol{C}_2, \boldsymbol{D}_2)$, is right invertible and has the same infinite zero structure as that of $\Sigma_{\rm P} : (A, B, C_2, D_2)$. Furthermore, its invariant zeros contain those of $\Sigma_{\rm P}$ and $\ell \times \kappa$ extra ones at $s = 0$. We are now ready to present a step-by-step algorithm to construct the required control law of the form (2.4).

Step 2.2.S.1. This step is to transform the subsystem from u to e of the augmented system (2.6) into the structural form of the special coordinate basis (see *e.g.*, [11, 15, 45, 59]), i.e., to find nonsingular state, input and output transformations Γ_s, Γ_i and Γ_o

$$x = \Gamma_s \tilde{x}, \quad e = \Gamma_o \tilde{e}, \quad u = \Gamma_i \tilde{u}, \tag{2.10}$$

such that the system can be put into the following form,

$$\tilde{x} = \begin{pmatrix} x_a^0 \\ x_a^- \\ x_c \\ x_d \end{pmatrix}, \quad \tilde{e} = \begin{pmatrix} e_0 \\ e_d \end{pmatrix}, \quad \tilde{u} = \begin{pmatrix} u_0 \\ u_d \\ u_c \end{pmatrix}, \tag{2.11}$$

$$x_d = \begin{pmatrix} x_1 \\ x_2 \\ \vdots \\ x_{m_d} \end{pmatrix}, \quad e_d = \begin{pmatrix} e_1 \\ e_2 \\ \vdots \\ e_{m_d} \end{pmatrix}, \quad u_d = \begin{pmatrix} u_1 \\ u_2 \\ \vdots \\ u_{m_d} \end{pmatrix}, \tag{2.12}$$

and

$$\dot{x}_a^0 = A_{aa}^0 x_a^0 + B_{0a}^0 e_0 + L_{ad}^0 e_d + E_a^0 \boldsymbol{w}, \tag{2.13}$$

$$\dot{x}_a^- = A_{aa}^- x_a^- + B_{0a}^- e_0 + L_{ad}^- e_d + E_a^- \boldsymbol{w}, \tag{2.14}$$

$$\dot{x}_c = A_{cc}x_c + B_c\left[E^-_{ca}x^-_a + E^0_{ca}x^0_a\right] + B_{0c}e_0 + L_{cd}e_d + B_c u_c + E_c\boldsymbol{w}, \tag{2.15}$$

$$e_0 = C^0_{0a}x^0_a + C^-_{0a}x^-_a + C_{0c}x_c + C_{0d}x_d + u_0, \tag{2.16}$$

and for each $i = 1, \cdots, m_d$,

$$\dot{x}_i = A_{q_i}x_i + L_{i0}e_0 + L_{id}e_d + E_{di}\boldsymbol{w} + B_{q_i}\left[u_i + E^0_{ia}x^0_a + E^-_{ia}x^-_a + E_{ic}x_c + \sum_{j=1}^{m_d} E_{ij}x_j\right], \tag{2.17}$$

$$e_i = C_{q_i}x_i, \quad e_d = C_d x_d. \tag{2.18}$$

Here the states x^0_a, x^-_a, x_c and x_d are respectively of dimensions n^0_a, n^-_a, n_c and $n_d = \sum_{i=1}^{m_d} q_i$, while x_i is of dimension q_i for each $i = 1, \cdots, m_d$. The control vectors u_0, u_d and u_c are respectively of dimensions m_0, m_d and $m_c = m - m_0 - m_d$ while the output vectors e_0 and e_d are respectively of dimensions $p_0 = m_0$ and $p_d = m_d$. The matrices A_{q_i}, B_{q_i} and C_{q_i} have the following form:

$$A_{q_i} = \begin{bmatrix} 0 & I_{q_i-1} \\ 0 & 0 \end{bmatrix}, \quad B_{q_i} = \begin{bmatrix} 0 \\ 1 \end{bmatrix}, \quad C_{q_i} = [1,\ 0,\ \cdots,\ 0]. \tag{2.19}$$

Assuming that x_i, $i = 1, 2, \cdots, m_d$, are arranged such that $q_i \le q_{i+1}$, the matrix L_{id} has the particular form

$$L_{id} = [\, L_{i1} \quad L_{i2} \quad \cdots \quad L_{ii-1} \quad 0 \quad \cdots \quad 0\,]. \tag{2.20}$$

The last row of each L_{id} is identically zero. Moreover, the eigenvalues of A^0_{aa} are all at the origin, and the eigenvalues of A^-_{aa} are all in the left half complex plane, i.e., they are stable. Also, the pair (A_{cc},B_c) is controllable.

Step 2.2.S.2. Choose an appropriate dimensional matrix F_c such that

$$A^c_{cc} = A_{cc} - B_c F_c \tag{2.21}$$

is asymptotically stable. The existence of such an F_c is guaranteed by the property that (A_{cc}, B_c) is completely controllable.

Step 2.2.S.3. For each x_i of x_d, which is associated with the infinite zero structure of $\Sigma_{\rm P}$ or the subsystem from u to e of (2.6), we choose an F_i such that

$$p_i(s) = \prod_{j=1}^{q_i}(s - \lambda_{ij}) = s^{q_i} + F_{i1}s^{q_i-1} + \cdots + F_{iq_{i-1}}s + F_{iq_i} \tag{2.22}$$

with all λ_{ij} being in $\mathbb{C}^-$ and closed under complex conjugation. Let

$$F_i = [\, F_{iq_i} \quad F_{iq_{i-1}} \quad \cdots \quad F_{i1} \,], \quad i = 1, \cdots, m_d. \tag{2.23}$$

Step 2.2.S.4. Next, we construct

$$\boldsymbol{F}(\varepsilon) = -\Gamma_i \begin{bmatrix} C_{0a}^0 & C_{0a}^- & C_{0c} & C_{0d} \\ E_{da}^0 & E_{da}^- & E_{dc} & E_d + F_d(\varepsilon) \\ E_{ca}^0 & E_{ca}^- & F_c & 0 \end{bmatrix} \Gamma_s^{-1}, \tag{2.24}$$

where

$$E_{da}^0 = \text{blkdiag}\left\{E_{1a}^0, \cdots, E_{m_da}^0\right\} \tag{2.25}$$

$$E_{da}^- = \text{blkdiag}\left\{E_{1a}^-, \cdots, E_{m_da}^-\right\} \tag{2.26}$$

$$E_{dc} = \text{blkdiag}\left\{E_{1c}, \cdots, E_{m_dc}\right\} \tag{2.27}$$

$$E_d = \begin{bmatrix} E_{11} & \cdots & E_{1m_d} \\ \vdots & \ddots & \vdots \\ E_{m_d1} & \cdots & E_{m_dm_d} \end{bmatrix}, \tag{2.28}$$

$$F_d(\varepsilon) = \text{blkdiag}\left\{\frac{F_1}{\varepsilon^{q_1}}S_1(\varepsilon), \frac{F_2}{\varepsilon^{q_2}}S_2(\varepsilon), \cdots, \frac{F_{m_d}}{\varepsilon^{q_{m_d}}}S_{m_d}(\varepsilon)\right\}, \tag{2.29}$$

and where

$$S_i(\varepsilon) = \text{diag}\left\{1, \varepsilon, \varepsilon^2, \cdots, \varepsilon^{q_i-1}\right\}. \tag{2.30}$$

Step 2.2.S.5. Finally, we partition

$$\boldsymbol{F}(\varepsilon) = [\, H_0(\varepsilon) \quad \cdots \quad H_{\kappa-1}(\varepsilon) \quad F(\varepsilon) \,], \tag{2.31}$$

where $H_i(\varepsilon) \in \mathbb{R}^{m\times\ell}$ and $F(\varepsilon) \in \mathbb{R}^{m\times n}$. This ends the constructive algorithm. ♢

We have the following result (see [45]).

Theorem 2.1. Consider the given system (2.1) with its external disturbance $w \in L_p$, $p \in [1, \infty)$, its initial condition $x(0) = x_0$. Assume that the conditions of solvability are satisfied, and all the states are measured for feedback, i.e., $C_1 = I$ and $D_1 = 0$. Then, for any reference signal $r(t)$, which has all its i-th order derivatives, $i = 0, 1, \cdots, \kappa - 1$, $\kappa \geq 1$, being available and $r^{(\kappa)}(t)$ being either a vector of delta functions or in L_p, the proposed robust and perfect tracking (RPT) problem is solved by the control law of (2.4) with $F(\varepsilon)$ and $H_i(\varepsilon)$, $i = 0, 1, \cdots, \kappa - 1$, as given in (2.31). $\diamondsuit$

2.2.3 The Measurement Feedback Case

We now present solutions to the robust and perfect tracking problem via reduced order measurement feedback control laws. For simplicity of presentation, we assume that matrices C_1 and D_1 have already been transformed into the following forms,

$$C_1 = \begin{bmatrix} 0 & C_{1,02} \\ I_k & 0 \end{bmatrix} \quad \text{and} \quad D_1 = \begin{bmatrix} D_{1,0} \\ 0 \end{bmatrix}, \tag{2.32}$$

where $D_{1,0}$ is of full row rank. Before we present a step-by-step algorithm to construct a parameterized reduced order measurement feedback controller, we first partition the following system

$$\begin{cases} \dot{x} = A\ x + B\ u + [\,E \quad I_n\,]\ \tilde{w}, \\ y = C_1\ x \qquad\quad + [\,D_1 \quad 0\,]\ \tilde{w}, \end{cases} \tag{2.33}$$

in conformity with the structures of C_1 and D_1 in (2.32), i.e.,

$$\begin{cases} \begin{pmatrix} \dot{x}_1 \\ \dot{x}_2 \end{pmatrix} = \begin{bmatrix} A_{11} & A_{12} \\ A_{21} & A_{22} \end{bmatrix} \begin{pmatrix} x_1 \\ x_2 \end{pmatrix} + \begin{bmatrix} B_1 \\ B_2 \end{bmatrix} u + \begin{bmatrix} E_1 & I_k & 0 \\ E_2 & 0 & I_{n-k} \end{bmatrix} \tilde{w}, \\ \begin{pmatrix} y_0 \\ y_1 \end{pmatrix} = \begin{bmatrix} 0 & C_{1,02} \\ I_k & 0 \end{bmatrix} \begin{pmatrix} x_1 \\ x_2 \end{pmatrix} + \begin{bmatrix} D_{1,0} & 0 & 0 \\ 0 & 0 & 0 \end{bmatrix} \tilde{w}, \end{cases} \tag{2.34}$$

where

$$\tilde{w} = \begin{pmatrix} w \\ x_0 \cdot \delta(t) \end{pmatrix}. \tag{2.35}$$

Obviously, $y_1 = x_1$ is directly available and hence need not to be estimated. Next, we define $\Sigma_{\rm QR}$ to be characterized by

$$(A_{\rm R}, E_{\rm R}, C_{\rm R}, D_{\rm R}) = \left(A_{22}, \begin{bmatrix} E_2 & 0 & I_{n-k} \end{bmatrix}, \begin{bmatrix} C_{1,02} \\ \\ A_{12} \end{bmatrix}, \begin{bmatrix} D_{1,0} & 0 & 0 \\ \\ E_1 & I_k & 0 \end{bmatrix} \right). \tag{2.36}$$

It is again straightforward to verify that $\Sigma_{\rm QR}$ is right invertible with no finite and infinite zeros. Moreover, $(A_{\rm R}, C_{\rm R})$ is detectable if and only if (A, C_1) is detectable. We are ready to present the following algorithm.

Step 2.2.R.1. For the given reference $r(t)$ and the given system (2.1), we again assume that all the state variables of (2.1) are measurable and follow the procedures of the previous subsection to define an auxiliary system,

$$\begin{cases} \dot{\boldsymbol{x}} = \boldsymbol{A}\ \boldsymbol{x} + \boldsymbol{B}\ u + \boldsymbol{E}\ \boldsymbol{w} \\ \\ \boldsymbol{y} = \quad \boldsymbol{x} \\ \\ e = \boldsymbol{C}_2\ \boldsymbol{x} + \boldsymbol{D}_2\ u \end{cases} \tag{2.37}$$

Then, we follow Steps 2.2.S.1 to 2.2.S.5 of the algorithm of the previous subsection to construct a state feedback gain matrix

$$\boldsymbol{F}(\varepsilon) = \begin{bmatrix} H_0(\varepsilon) & \cdots & H_{\kappa-1}(\varepsilon) & F(\varepsilon) \end{bmatrix}. \tag{2.38}$$

Let us partition $F(\varepsilon)$ in conformity with x_1 and x_2 of (2.34) as follows,

$$F(\varepsilon) = \begin{bmatrix} F_1(\varepsilon) & F_2(\varepsilon) \end{bmatrix}. \tag{2.39}$$

Step 2.2.R.2. Let $K_{\rm R}$ be an appropriate dimensional constant matrix such that the eigenvalues of

$$A_{\rm R} + K_{\rm R} C_{\rm R} = A_{22} + \begin{bmatrix} K_{\rm R0} & K_{\rm R1} \end{bmatrix} \begin{bmatrix} C_{1,02} \\ \\ A_{12} \end{bmatrix} \tag{2.40}$$

are all in $\mathbb{C}^-$. This can be done because $(A_{\rm R}, C_{\rm R})$ is detectable.

Step 2.2.R.3. Let

$$G_{\rm R} = \begin{bmatrix} -K_{\rm R0}, & A_{21} + K_{\rm R1} A_{11} - (A_{\rm R} + K_{\rm R} C_{\rm R}) K_{\rm R1} \end{bmatrix}, \tag{2.41}$$

and

$$\left.\begin{aligned} A_{\rm cmp}(\varepsilon) &= A_{\rm R} + B_2F_2(\varepsilon) + K_{\rm R}C_{\rm R} + K_{\rm R1}B_1F_2(\varepsilon), \\ B_{\rm cmp}(\varepsilon) &= G_{\rm R} + (B_2 + K_{\rm R1}B_1)\,[\,0, \quad F_1(\varepsilon) - F_2(\varepsilon)K_{\rm R1}\,], \\ C_{\rm cmp}(\varepsilon) &= F_2(\varepsilon), \\ D_{\rm cmp}(\varepsilon) &= [\,0, \quad F_1(\varepsilon) - F_2(\varepsilon)K_{\rm R1}\,]. \end{aligned}\right\} \tag{2.42}$$

Step 2.2.R.4. Finally, we obtain the following reduced order measurement feedback control law,

$$\begin{cases} \dot{v} = A_{\rm cmp}(\varepsilon)v + B_{\rm cmp}(\varepsilon)y + G_0(\varepsilon)r + \cdots + G_{\kappa-1}(\varepsilon)r^{(\kappa-1)}, \\ u = C_{\rm cmp}(\varepsilon)v + D_{\rm cmp}(\varepsilon)y + H_0(\varepsilon)r + \cdots + H_{\kappa-1}(\varepsilon)r^{(\kappa-1)}, \end{cases} \tag{2.43}$$

where for $i = 0, 1, \cdots, \kappa - 1$,

$$G_i(\varepsilon) = (B_2 + K_{\rm R1}B_1)H_i(\varepsilon). \tag{2.44}$$

This completes the construction of the reduced order controller. ♢

The following theorem is due to [45].

Theorem 2.2. Consider the given system (2.1) with its external disturbance $w \in L_p$, $p \in [1, \infty)$, its initial condition $x(0) = x_0$. If the conditions of solvability are satisfied, then, for any reference signal $r(t)$, which has all its i-th order derivatives, $i = 0, 1, \cdots, \kappa-1$, $\kappa \geq 1$, being available and $r^{(\kappa)}(t)$ being either a vector of delta functions or in L_p, the proposed robust and perfect tracking (RPT) problem is solved by the parameterized reduced order measurement feedback control laws of (2.43). ♢

2.3 Enhanced Composite Nonlinear Feedback Control

We develop in this section an enhanced version of the composite nonlinear feedback (CNF) control design, which is capable of removing constant bias in servo systems. A common approach for removing bias resulting from constant disturbances is to add an integrator to the controller. With this idea in mind we incorporate an additional integration action to enhance the original CNF control. The new approach will retain the fast settling property

of the original CNF control and at the same time have an additional capacity of eliminating steady state bias due to disturbances.

2.3.1 Problem Formulation

The rationale of CNF technique is rooted in the seminal paper of Lin *et al.* [44] where they proposed an add-in nonlinear feedback term to supplement the stabilizing linear controller so as to speed up the settling process of set point tracking tasks for second order linear systems with input amplitude constraint. Inspired by this idea, Chen *et al.* [12] developed the Composite Nonlinear Feedback (CNF) control technique, for more general linear systems with input saturation but without external disturbances. A controller designed via CNF technique consists of two parts, a linear part and a nonlinear part. The linear feedback part is responsible for stability and fast response of the closed-loop system, while at the same time not exceeding the actuator limits for the desired reference input level. The nonlinear part serves to increase the damping and accordingly smooth out the overshoot when the controlled output approaches the target reference. The resulting controlled system can be expected to achieve fast and smooth settling in set point tracking tasks. This CNF technique has been successfully applied to design an HDD servo system that is able to perform track seeking and track following all-in-one with superior performance and yet without any explicit switching element.

The original CNF technique assumes no disturbances in the plant. When the given system does have disturbances, the resulting system output under CNF control generally can not asymptotically match the target reference without knowing *a priori* the level of bias. In the case of micro drives, there are noticeable friction and nonlinearities in the VCM actuator, and normally a perfect cancellation cannot be expected. Under such circumstance, the original CNF technique alone does not seem to provide a complete solution for servo system design. This motivated us to come up with this enhanced composite nonlinear feedback

(CNF) control technique, which is basically an extension of the original one. Compared to the result of [12, 13], the new technique has an additional feature of removing constant bias and rejecting disturbances. As will be seen from the simulation and implementation results in later chapters, the enhanced CNF technique is very efficient and successful for tracking control.

To proceed, let us consider a linear system with an amplitude constrained actuator, characterized by

$$\begin{cases} \dot{x} = A\,x + B\,\mathrm{sat}(u) + Ew, \;\; x(0) = x_0 \\ y = C_1\,x, \\ h = C_2\,x, \end{cases} \tag{2.45}$$

where $x \in \mathbb{R}^n$, $u \in \mathbb{R}$, $y \in \mathbb{R}^p$, $h \in \mathbb{R}$ and $w \in \mathbb{R}$ are respectively the state, control input, measurement output, controlled output and disturbance input of the system. A, B, C_1, C_2 and E are appropriate dimensional constant matrices. The function, sat: $\mathbb{R} \to \mathbb{R}$, represents the actuator saturation defined as

$$\mathrm{sat}(u) = \mathrm{sgn}(u)\,\min\{\; u_{\max},\; |u|\;\}, \tag{2.46}$$

with $u_{\max}$ being the saturation level of the input. The following assumptions on the given system are made:

1. (A, B) is stabilizable,

2. (A, C_1) is detectable,

3. (A, B, C_2) is invertible and has no invariant zero at $s = 0$,

4. w is bounded unknown constant disturbance, and

5. h is also measurable, *i.e.*, h is part of the measurement output.

Note that all these assumptions are fairly standard for tracking control. We aim to design an enhanced CNF control law for the system with disturbances such that the resulting

controlled output would track a target reference (set point), say r, as fast and as smooth as possible without having steady state error. We first follow the usual practice to augment an integrator into the given system. Such an integrator will eventually become part of the final control law. To be more specific, we define an auxiliary state variable,

$$\dot{z} := e := h - r = C_2 x - r, \tag{2.47}$$

which is implementable as h is assumed to be measurable, and augment it into the given system as follows,

$$\begin{cases} \dot{\bar{x}} = \bar{A}\,\bar{x} + \bar{B}\,\mathrm{sat}(u) + \bar{B}_{\mathrm{r}}\,r + \bar{E}\,w, \\ \bar{y} = \bar{C}_1\,\bar{x}, \\ h = \bar{C}_2\,\bar{x}, \end{cases} \tag{2.48}$$

where

$$\bar{x} = \begin{pmatrix} z \\ x \end{pmatrix}, \quad \bar{x}_0 = \begin{pmatrix} 0 \\ x_0 \end{pmatrix}, \quad \bar{y} = \begin{pmatrix} z \\ y \end{pmatrix}, \tag{2.49}$$

and

$$\bar{A} = \begin{bmatrix} 0 & C_2 \\ 0 & A \end{bmatrix}, \ \bar{B} = \begin{bmatrix} 0 \\ B \end{bmatrix}, \ \bar{B}_{\mathrm{r}} = \begin{bmatrix} -1 \\ 0 \end{bmatrix}, \ \bar{E} = \begin{bmatrix} 0 \\ E \end{bmatrix}, \ \bar{C}_1 = \begin{bmatrix} 1 & 0 \\ 0 & C_1 \end{bmatrix}, \ \bar{C}_2 = [\,0 \quad C_2\,]. \tag{2.50}$$

Note that under Assumptions 1 and 3, the pair $(\bar{A}, \bar{B})$ is stabilizable. This can be justified by considering the rank property of the following matrices:

$$\mathrm{rank}\,[\,\lambda I - \bar{A} \quad \bar{B}\,] = \mathrm{rank} \begin{bmatrix} \lambda & -C_2 & 0 \\ 0 & \lambda I - A & B \end{bmatrix}, \tag{2.51}$$

which is either equal to $1 + \mathrm{rank}\,[\,\lambda I - A \quad B\,]$, if $\lambda \neq 0$, or equal to

$$\mathrm{rank} \begin{bmatrix} -C_2 & 0 \\ \lambda I - A & B \end{bmatrix} = \mathrm{rank} \begin{bmatrix} \lambda I - A & B \\ C_2 & 0 \end{bmatrix} = n + 1, \tag{2.52}$$

if $\lambda = 0$. The equality in (2.52) holds because (A, B, C_2) is assumed to have no invariant zeros at $s = 0$. Clearly, it follows that the uncontrollable modes of $(\bar{A}, \bar{B})$, if any, are identical to those of (A, B). Hence, $(\bar{A}, \bar{B})$ is stabilizable as (A, B) is assumed to be stabilizable.

Next, we proceed to carry out the design of enhanced CNF control laws for two different cases, *i.e.*, the state feedback case and the reduced order measurement feedback case. The full order measurement feedback case is straightforward once the result for the reduced order case is established. We note that the procedure for designing the enhanced CNF control laws is a natural extension of that of [12, 13]. The enhanced control laws are, however, capable of removing steady state bias.

2.3.2 The State Feedback Case

We first investigate the case when all the state variables of the plant (2.48) are measurable, *i.e.*, $\bar{y} = \bar{x}$. The procedure that generates an enhanced CNF state feedback law will be done in three steps. That is, in the first step, a linear feedback control law will be designed, in the second step, the design of nonlinear feedback control will be carried out, and lastly, in the final step, the linear and nonlinear feedback laws will be combined to form an enhanced CNF control law.

Step 2.3.s.1: Design a linear feedback control law,

$$u_{\mathrm{L}} = F\bar{x} + G\,r, \tag{2.53}$$

where F is chosen such that 1) $\bar{A} + \bar{B}F$ is an asymptotically stable matrix, and 2) the closed-loop system $\bar{C}_2(sI - \bar{A} - \bar{B}F)^{-1}\bar{B}$ has certain desired properties. Let us partition $F = [\,F_{\mathrm{z}} \quad F_{\mathrm{x}}\,]$ in conformity with z and x. The general guideline in designing such an F is to place the closed-loop pole of $\bar{A} + \bar{B}F$ corresponding to the integration mode, z, to be sufficiently closer to the imaginary axis compared to the rest eigenvalues, which implies that F_{z} is a relatively small scalar. The remaining closed-loop poles of $\bar{A} + \bar{B}F$ should be placed to have a dominating pair with a small damping ratio, which in turn would yield a fast rise time in the closed-loop system

response. Next, G is chosen as

$$G = -[C_2(A + BF_{\mathrm{x}})^{-1}B]^{-1}, \tag{2.54}$$

which is well defined as (A, B, C_2) is assumed to have no invariant zeros at $s = 0$ and $A + BF_{\mathrm{x}}$ is nonsingular whenever $\bar{A} + \bar{B}F$ is stable and F_{z} is relatively small.

Step 2.3.s.2: Given a positive definite symmetric matrix $W \in \mathbb{R}^{(n+1)\times(n+1)}$, we solve the following Lyapunov equation:

$$(\bar{A} + \bar{B}F)'P + P(\bar{A} + \bar{B}F) = -W, \tag{2.55}$$

for $P > 0$. Such a solution is always existent as $(\bar{A} + \bar{B}F)$ is asymptotically stable. Next, we define

$$G_{\mathrm{e}} := \begin{bmatrix} 0 \\ \\ -(A + BF_{\mathrm{x}})^{-1}BG \end{bmatrix} \quad \text{and} \quad \bar{x}_{\mathrm{e}} := G_{\mathrm{e}}\, r. \tag{2.56}$$

The nonlinear feedback portion of the enhanced CNF control law, u_{N}, is given by

$$u_{\mathrm{N}} = \rho(r, h)\bar{B}'P(\bar{x} - \bar{x}_{\mathrm{e}}), \tag{2.57}$$

where $\rho(r, h)$ is a smooth, non-positive and non-decreasing function of $|h - r|$, to be used to gradually change the system closed-loop damping ratio to yield a better tracking performance. The choices of the design parameters, $\rho(r, h)$ and W, will be discussed later.

Step 2.3.s.3: The linear feedback control law and nonlinear feedback portion derived in the previous steps are now combined to form an enhanced CNF control law,

$$u = u_{\mathrm{L}} + u_{\mathrm{N}} = F\bar{x} + G\, r + \rho(r, h)\bar{B}'P(\bar{x} - \bar{x}_{\mathrm{e}}). \tag{2.58}$$

We have the following result.

Theorem 2.3. *Consider the given system (2.45) with $y = x$ and the disturbance w being bounded by a non-negative scalar τ_w, i.e., $|w| \le \tau_w$. Let*

$$\gamma := 2\tau_w \lambda_{\max}(PW^{-1}) \left(\bar{E}' P \bar{E}\right)^{1/2}. \tag{2.59}$$

Then, for any $\rho(r,h)$, which is a smooth, non-positive and non-decreasing function of $|h-r|$, and tends to a constant as $t \to +\infty$, the enhanced CNF control law (2.58) will drive the system controlled output h to track the step reference of amplitude r from an initial state $\bar{x}_0$ asymptotically without steady state error, provided that the following conditions are satisfied:

1. *There exist positive scalars $\delta \in (0,1)$ and $c_\delta > \gamma^2$ such that*

$$\forall \bar{x} \in \boldsymbol{X}(F, c_\delta) := \left\{ \bar{x} \ : \ \bar{x}' P \bar{x} \le c_\delta \right\} \quad \Rightarrow \quad |F\bar{x}| \le (1-\delta) u_{\max}. \tag{2.60}$$

2. *The initial condition, $\bar{x}_0$, satisfies*

$$\bar{x}_0 - \bar{x}_{\rm e} \in \boldsymbol{X}(F, c_\delta). \tag{2.61}$$

3. *The level of the target reference, r, satisfies*

$$|H\, r| \le \delta u_{\max}, \tag{2.62}$$

where $H := FG_{\rm e} + G$.

Proof. For simplicity, we drop the variable r, h in $\rho(r,h)$ throughout this proof. Noting that

$$\begin{aligned}
\bar{A}\bar{x}_e + \bar{B}Hr + \bar{B}_{\rm r} r &= \bar{A}\bar{x}_{\rm e} + \bar{B}(FG_{\rm e} + G)r + \bar{B}_{\rm r} r \\
&= (\bar{A} + \bar{B}F)\bar{x}_{\rm e} + \bar{B}_{\rm r} r + \bar{B}Gr \\
&= \begin{bmatrix} 0 & C_2 \\ BF_{\rm z} & A + BF_{\rm x} \end{bmatrix} \begin{bmatrix} 0 \\ -(A+BF_{\rm x})^{-1}BG \end{bmatrix} r + \begin{bmatrix} -1 \\ 0 \end{bmatrix} r + \begin{bmatrix} 0 \\ BG \end{bmatrix} r \\
&= \begin{bmatrix} -C_2(A+BF_{\rm x})^{-1}BG \\ -BG \end{bmatrix} r + \begin{bmatrix} -1 \\ BG \end{bmatrix} r = 0,
\end{aligned} \tag{2.63}$$

and letting $\tilde{x} = \bar{x} - \bar{x}_{\rm e}$, then the dynamics equation of the augmented plant in (2.48) can be expressed as,

$$\begin{aligned}
\dot{\tilde{x}} = \dot{\bar{x}} &= \bar{A}(\tilde{x} + \bar{x}_{\rm e}) + \bar{B}\,\mathrm{sat}(u) + \bar{B}_{\rm r}\,r + \bar{E}w \\
&= (\bar{A} + \bar{B}F)\tilde{x} + \bar{A}\bar{x}_{\rm e} - \bar{B}F\tilde{x} + \bar{B}\,\mathrm{sat}(u) + \bar{B}_{\rm r}\,r + \bar{E}w, \\
&= (\bar{A} + \bar{B}F)\tilde{x} + \bar{B}\,[\mathrm{sat}(u) - F\tilde{x} - Hr] + \big(\bar{A}\bar{x}_{\rm e} + \bar{B}Hr + \bar{B}_{\rm r}\,r\big) + \bar{E}w \\
&= (\bar{A} + \bar{B}F)\tilde{x} + \bar{B}\,v + \bar{E}w, \qquad (2.64)
\end{aligned}$$

where

$$v := \mathrm{sat}(u) - F\tilde{x} - H\,r. \qquad (2.65)$$

Clearly, the composite nonlinear feedback control law (2.58) can now be rewritten as,

$$u = F\tilde{x} + H\,r + \rho\bar{B}'P\tilde{x}. \qquad (2.66)$$

Next, for $\tilde{x} \in \boldsymbol{X}(F, c_\delta)$ and $|H\,r| \le \delta u_{\max}$, we have

$$|F\tilde{x} + H\,r| \le |F\tilde{x}| + |H\,r| \le u_{\max}.$$

Now, the range of v can be determined for the following three cases:

Case 1. $|u| \le u_{\max}$. For this case, it follows from (2.65) and (2.66) that

$$v = \mathrm{sat}(u) - F\tilde{x} - Hr = \rho\bar{B}'P\tilde{x}.$$

Case 2. $u > u_{\max}$. We have

$$\begin{aligned}
v &= \mathrm{sat}(u) - F\tilde{x} - Hr = u_{\max} - (F\tilde{x} + Hr) > 0, \\
v &= \mathrm{sat}(u) - F\tilde{x} - Hr < u - (F\tilde{x} + Hr) = \rho\bar{B}'P\tilde{x}.
\end{aligned}$$

Case 3. $u < -u_{\max}$. Similarly, for this case, we have

$$\rho\bar{B}'P\tilde{x} < v < 0.$$

Obviously, for all possible situations, we can always write v as

$$v = q\rho\bar{B}'P\tilde{x}, \tag{2.67}$$

for some non-negative variable $q \in [0, 1]$. Thus, for the case when $\tilde{x} \in \boldsymbol{X}(F, c_\delta)$ and $|Hr| \leq \delta u_{\max}$, the closed-loop system comprising the given augmented plant (2.48) and the enhanced CNF control law (2.58) can be expressed as the following:

$$\dot{\tilde{x}} = (\bar{A} + \bar{B}F + q\rho\bar{B}\bar{B}'P)\tilde{x} + \bar{E}w. \tag{2.68}$$

In what follows, we will show that (2.68) is stable provided that the initial condition, $\bar{x}_0$, the target reference, r, and the disturbance, w, satisfy those conditions listed in the theorem. Let us define a Lyapunov function:

$$V = \tilde{x}'P\tilde{x}. \tag{2.69}$$

For easy derivation, we introduce a matrix S such that $P = S'S$. We then obtain the derivative of V which is calculated along the trajectory of the system (2.68),

$$\begin{aligned}
\dot{V} &= \dot{\tilde{x}}'P\tilde{x} + \tilde{x}'P\dot{\tilde{x}} \\
&= \tilde{x}'[(\bar{A} + \bar{B}F)'P + P(\bar{A} + \bar{B}F)]\tilde{x} + 2q\rho\tilde{x}'P\bar{B}\bar{B}'P\tilde{x} + 2\tilde{x}'P\bar{E}w \\
&\leq -\tilde{x}'W\tilde{x} + 2\tilde{x}'P\bar{E}w \\
&= -\tilde{x}'S'SP^{-1}WP^{-1}S'S\tilde{x} + 2\tilde{x}'S'S\bar{E}w \\
&\leq -\lambda_{\min}(SP^{-1}WP^{-1}S')\tilde{x}'S'S\tilde{x} + 2\|S\tilde{x}\| \cdot \|S\bar{E}\|\tau_w \\
&= -\lambda_{\min}(P^{-1}W)\tilde{x}'P\tilde{x} + 2\tau_w(\tilde{x}'P\tilde{x})^{1/2}(\bar{E}'P\bar{E})^{1/2} \\
&= -\lambda_{\min}(P^{-1}W)(\tilde{x}'P\tilde{x})^{1/2}\left[(\tilde{x}'P\tilde{x})^{1/2} - 2\tau_w\lambda_{\max}(PW^{-1})(\bar{E}'P\bar{E})^{1/2}\right] \\
&= -\lambda_{\min}(P^{-1}W)(\tilde{x}'P\tilde{x})^{1/2}\left[(\tilde{x}'P\tilde{x})^{1/2} - \gamma\right].
\end{aligned} \tag{2.70}$$

Note that we have used the matrix properties: i) $z'Xz \geq \lambda_{\min}(X)z'z$, where X is a symmetric matrix; ii) $\lambda(XY) = \lambda(YX)$, if both X and Y are square matrices; and iii) $\lambda(XY) > 0$

if $X > 0$ and $Y > 0$. Clearly, the closed-loop system in the absence of the disturbance, w, has $\dot{V} < 0$ and thus is asymptotically stable.

With the presence of the disturbance, w, and with $\tilde{x}(0) = \bar{x}_0 - \bar{x}_e \in \boldsymbol{X}(F, c_\delta)$, where $c_\delta > \gamma^2$, the corresponding trajectory of (2.68) will remain in $\boldsymbol{X}(F, c_\delta)$. As ρ converges to some constant value over time, the system of (2.68) will degenerate into a linear time-invariant system and its trajectory will eventually settle into a point on a ball characterized by $\{\tilde{x} : \tilde{x}' P \tilde{x} \leq \tilde{\gamma}^2\}$ with $\tilde{\gamma} \leq \gamma$. Since $z(t) = \int_0^t e(\tau) d\tau$ converges to a constant, it is clear that the tracking error $e(t) \to 0$ as $t \to \infty$. This completes the proof of Theorem 2.3. $\diamondsuit$

2.3.3 The Measurement Feedback Case

In practical situations, it is unrealistic to assume that all the state variables of a given plant are measurable. In what follows, we will design an enhanced CNF control law using only information measurable from the plant. In principle, we can design either a full order measurement feedback control law, for which its dynamical order will be identical to that of the given plant, or a reduced order measurement feedback control law, in which we make full use of the measurement output and estimate only the unknown part of the state variable. As such, the dynamical order of the controller will be reduced. It is more feasible to implement controllers with smaller dynamical order. Hence we will focus on the development of reduced order measurement feedback control law.

For simplicity of presentation, we assume that C_1 in the measurement output of the given plant (2.45) is already in the form,

$$C_1 = [\, I_p \quad 0 \,]. \tag{2.71}$$

The augmented plant (2.48) can then be partitioned as the following:

$$\left\{\begin{array}{rcl} \begin{pmatrix} \dot{z} \\ \dot{x}_1 \\ \dot{x}_2 \end{pmatrix} &=& \begin{bmatrix} 0 & C_{21} & C_{22} \\ 0 & A_{11} & A_{12} \\ 0 & A_{21} & A_{22} \end{bmatrix} \begin{pmatrix} z \\ x_1 \\ x_2 \end{pmatrix} + \begin{bmatrix} 0 \\ B_1 \\ B_2 \end{bmatrix} \mathrm{sat}(u) + \begin{bmatrix} -1 \\ 0 \\ 0 \end{bmatrix} r + \begin{bmatrix} 0 \\ E_1 \\ E_2 \end{bmatrix} w, \\ \bar{y} &=& \begin{bmatrix} 1 & 0 & 0 \\ 0 & I_p & 0 \end{bmatrix} \begin{pmatrix} z \\ x_1 \\ x_2 \end{pmatrix}, \\ h &=& [\,0 \quad C_{21} \quad C_{22}\,] \begin{pmatrix} z \\ x_1 \\ x_2 \end{pmatrix}, \end{array}\right. \tag{2.72}$$

where

$$\begin{pmatrix} z \\ x_1 \\ x_2 \end{pmatrix} = \bar{x}, \quad \begin{pmatrix} z(0) \\ x_1(0) \\ x_2(0) \end{pmatrix} = \begin{pmatrix} 0 \\ x_{10} \\ x_{20} \end{pmatrix} = \bar{x}_0, \quad \bar{y} = \begin{pmatrix} z \\ y \end{pmatrix} = \begin{pmatrix} z \\ x_1 \end{pmatrix}. \tag{2.73}$$

Clearly, z and x_1 are readily available and need not be estimated. We only need to estimate x_2. There are two main steps in designing a reduced order measurement feedback control law: i) the construction of a full state feedback gain matrix F; and ii) the construction of a reduced order observer gain matrix K_{R}. The construction of the gain matrix F is totally identical to that given in the previous subsection, which can be partitioned in conformity with z, x_1 and x_2, as follows:

$$F = [\,F_z \quad F_1 \quad F_2\,]. \tag{2.74}$$

The reduced order observer gain matrix K_{R} is chosen such that the poles of $A_{22} + K_{\mathrm{R}} A_{12}$ are placed in appropriate locations in the open-left half plane.

Next, we choose a positive definite matrix $W \in \mathbb{R}^{(n+1)\times(n+1)}$, let $P > 0$ be the solution to the Lyapunov equation

$$(\bar{A} + \bar{B}F)'P + P(\bar{A} + \bar{B}F) = -W. \tag{2.75}$$

Now the reduced order enhanced CNF control law is given as follows,

$$\dot{x}_{\mathrm{v}} = (A_{22} + K_{\mathrm{R}} A_{12}) x_{\mathrm{v}} + [A_{21} + K_{\mathrm{R}} A_{11} - (A_{22} + K_{\mathrm{R}} A_{12}) K_{\mathrm{R}}] y + (B_2 + K_{\mathrm{R}} B_1)\,\mathrm{sat}(u), \tag{2.76}$$

and

$$u = F\begin{pmatrix} z \\ x_1 \\ x_{\rm v} - K_{\rm R} y \end{pmatrix} + Gr + \rho(r,h)\bar{B}'P\left[\begin{pmatrix} z \\ x_1 \\ x_{\rm v} - K_{\rm R} y \end{pmatrix} - \bar{x}_{\rm e}\right], \tag{2.77}$$

where G is as defined in (2.54) and $\rho(r,h)$ is a smooth, non-positive and non-decreasing function of $|h-r|$, to be chosen to yield a desired performance.

Further more, given another positive definite matrix $W_{\rm R} \in \mathbb{R}^{(n-p)\times(n-p)}$ with

$$W_{\rm R} > F_2'\bar{B}'PW^{-1}P\bar{B}F_2, \tag{2.78}$$

let $Q_{\rm R} > 0$ be the solution to the Lyapunov equation

$$(A_{22} + K_{\rm R}A_{12})'Q_{\rm R} + Q_{\rm R}(A_{22} + K_{\rm R}A_{12}) = -W_{\rm R}. \tag{2.79}$$

Note that such a $Q_{\rm R}$ exists as $A_{22} + K_{\rm R}A_{12}$ is asymptotically stable.

We have the following result.

Theorem 2.4. *Consider the given system (2.45) with the disturbance w being bounded by a non-negative scalar τ_w, i.e., $|w| \le \tau_w$. Let*

$$\gamma_R := 2\tau_w\lambda_{\max}\left(\begin{bmatrix} P & 0 \\ 0 & Q_R \end{bmatrix}\begin{bmatrix} W & -P\bar{B}F_2 \\ -F_2'\bar{B}'P & W_R \end{bmatrix}^{-1}\right)\left[\bar{E}'P\bar{E} + (E_2 + K_R E_1)'Q_R(E_2 + K_R E_1)\right]^{1/2}. \tag{2.80}$$

Then, there exists a scalar $\hat{\rho} > 0$ such that for any $\rho(r,h)$, which is a smooth, non-positive and non-decreasing function of $|h-r|$ with $|\rho(r,h)| \le \hat{\rho}$, and tends to a constant as $t \to +\infty$, the enhanced reduced order CNF control law of (2.76) and (2.77) will drive the system controlled output h to track the step reference of amplitude r asymptotically without steady state error, provided that the following conditions are satisfied:

1. *There exist positive scalars $\delta \in (0,1)$ and $c_{R\delta} > \gamma_R^2$ such that*

$$\forall \bar{x} \in \boldsymbol{X}(F, c_{R\delta}) := \left\{ \bar{x} \ : \ \bar{x}'\begin{bmatrix} P & 0 \\ 0 & Q_R \end{bmatrix}\bar{x} \le c_{R\delta} \right\} \quad \Rightarrow \quad |\begin{bmatrix} F & F_2 \end{bmatrix}\bar{x}| \le (1-\delta)u_{\max}. \tag{2.81}$$

2. *The initial conditions, $\bar{x}_0$ and $x_{\rm v0} = x_{\rm v}(0)$, satisfy*

$$\begin{pmatrix} \bar{x}_0 - \bar{x}_{\rm e} \\ x_{\rm v0} - x_{20} - K_R\, x_{10} \end{pmatrix} \in \boldsymbol{X}(F, c_{R\delta}). \tag{2.82}$$

3. The level of the target reference, r, satisfies

$$|H\, r| \leq \delta u_{\max}, \tag{2.83}$$

where H is the same as that defined in Theorem 2.3.

Proof: The result follows from similar lines of reasoning as those given in Theorem 2.3 and those for the measurement feedback case in [13]. ♢

2.3.4 Selection of W and the Nonlinear Gain $\rho(r, h)$

The procedures for selecting the design parameter W and the nonlinear gain $\rho(r, h)$ for the enhanced CNF control law are the same as those for the usual CNF design given in [13]. We recall below the selection procedures for W and $\rho(r, h)$ from [13] for completeness. Basically, the freedom to choose the function $\rho(r, h)$ is used to tune the control law so as to improve the performance of the closed-loop system as the controlled output, h, approaches the set point, r. Since the main purpose of adding the nonlinear part to the CNF or the enhanced CNF controller is to speed up the settling time, or equivalently to contribute a significant value to the control input when the tracking error, $r - h$, is small. The nonlinear part, in general, will be in action when the control signal is far away from its saturation level, and thus it will not cause the control input to hit its limits. Under such a circumstance, the closed-loop system comprising the augmented plant in (2.48) and the enhanced CNF control law can be expressed as:

$$\dot{\tilde{x}} = (\bar{A} + \bar{B}F + \rho\bar{B}\bar{B}'P)\tilde{x} + \bar{E}w. \tag{2.84}$$

We note that the additional term $\rho(r, h)$ does not affect the stability of the estimators. It is now clear that eigenvalues of the closed-loop system in (2.84) can be changed by the function $\rho(r, h)$. Such a mechanism can be interpreted using the classical feedback control concept as shown in Figure 2.1, where the auxiliary system $G_{\text{aux}}(s)$ is defined as:

$$G_{\text{aux}}(s) := C_{\text{aux}}(sI - A_{\text{aux}})^{-1}B_{\text{aux}} := \bar{B}'P(sI - \bar{A} - \bar{B}F)^{-1}\bar{B}. \tag{2.85}$$

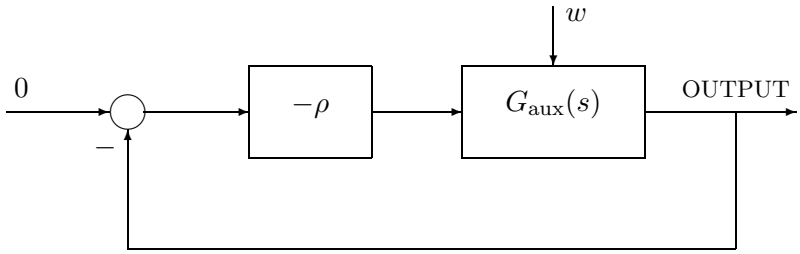

Figure 2.1: Interpretation of the nonlinear function $\rho(r, h)$.

Following the result of [13], we can show that $G_{\text{aux}}(s)$ is stable and invertible with a relative degree equal to 1, and is of minimum phase with n stable invariant zeros.

The invariant zeros of $G_{\text{aux}}(s)$ play an important role in selecting the poles of the closed-loop system of (2.84). The poles of the closed-loop system approach the locations of the invariant zeros of $G_{\text{aux}}(s)$ as $|\rho|$ becomes larger and larger. We would like to note that there is freedom in pre-selecting the locations of these invariant zeros. This can actually be done by selecting an appropriate $W > 0$. In general, we can employ the result of Chen and Zheng [14] on finite and infinite zero assignment to select the invariant zeros of $G_{\text{aux}}(s)$, which are corresponding to the closed-loop poles for larger $|\rho|$, such that the dominant ones have a large damping ratio, which in turn will yield a smaller overshoot. We refer interested readers to [13].

The selection of the nonlinear function $\rho(r, h)$ is relatively simple once the desired invariant zeros of $G_{\text{aux}}(s)$ are obtained. The following choice of $\rho(r, h)$ is a smooth, non-positive and non-decreasing function of $|h - r|$:

$$\rho(r, h) = -\beta \left| \mathrm{e}^{-\alpha|h-r|} - \mathrm{e}^{-\alpha|h(0)-r|} \right|, \tag{2.86}$$

where α and β are appropriate positive scalars that can be chosen to yield a desired performance, *i.e.*, fast settling time and small overshoot. This function $\rho(r, h)$ changes from 0 to $\rho^* = -\beta \left| 1 - \mathrm{e}^{-\alpha|h(0)-r|} \right|$ as the tracking error approaches zero. At the initial stage, when the controlled output, h, is far away from the final set point, $\rho(r, h)$ is small in amplitude

and the effect of the nonlinear part on the overall system is very limited. When the controlled output, h, approaches the set point r, $\rho(r,h) \to \rho^*$, and the nonlinear control law will become influential. In general, the parameter ρ^* should be chosen such that the poles of $\bar{A} + \bar{B}F + \rho^*\bar{B}\bar{B}'P$ are in the desired locations, *e.g.*, the dominant poles should have a large damping ratio, which would reduce the overshoot of the output response. Finally, we note that the choice of $\rho(r,h)$ is non-unique. Any function would work so long as it has similar properties of that given in (2.86).

2.4 Concluding Remarks

In this chapter, we have outlined the robust and perfect tracking (RPT) control technique, which can be used to design a parameterized controller to track a given reference signal with arbitrarily fast settling time in the face of external disturbances and initial conditions. Further more, we have developed the enhanced Composite Nonlinear Feedback (CNF) control technique, which has a new capability of removing steady state error due to disturbances, and at the same time retains the mainstay of the original CNF control, *i.e.*, fast response and low overshoot in servo tracking. These control techniques will be adopted to solve HDD servo problems in later chapters.

Chapter 3

A MATLAB Toolkit for Composite Nonlinear Feedback Control

In the previous chapter, we have developed the enhanced CNF (composite nonlinear feedback) control technique. However, its design procedure is somewhat involved. It is desirable to have some software tools to facilitate the design. This motivated us to come up with a MATLAB toolkit for CNF control, to be presented in this chapter. The toolkit can be utilized to design a fast and smooth tracking controller for a class of linear systems with actuator and other nonlinearities as well as with external disturbances. The usage and design procedure of the toolkit are illustrated by two practical examples on the servo design for a hard disk drive and a magnetic tape drive.

3.1 Introduction

Linear control technologies have come a long way and proved successful in many applications. Nonlinear control is relatively naive and is now meticulously finding applications in the real world. A smart combination of linear and nonlinear control techniques, which takes full advantage of both techniques, can lead to a desirable solution for practical control problems. This is exactly the motivation of the CNF (composite nonlinear feedback) control

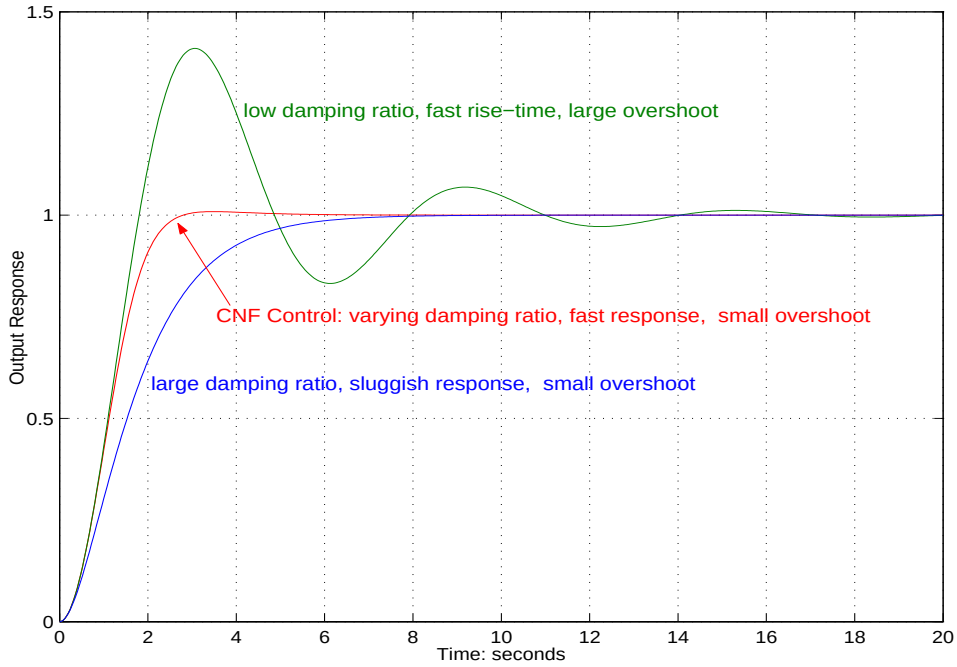

Figure 3.1: The rationale of CNF control.

technique. The rationale of this technique is actually quite intuitive and can be explained from the step response of a second order system (see Figure 3.1): If the damping ratio of the conjugate poles is small, the output will have a fast response (rise-time) accompanied with a large overshoot; If the damping ratio is large, the overshoot may be small or non-existent, but the output response will be sluggish. The core of CNF is to bring together the good points of both cases, by continuously scheduling the damping ratio of the dominant closed-loop poles, that is, to make the dominant damping ratio grow from a small value at the beginning to a large value at the end. This is achieved by introducing a nonlinear feedback term to supplement the fundamental stabilizing linear feedback control law. Since the birth of the CNF control [13, 44], there have been some further developments. Especially, He *et al.* [32] extended the CNF technique to general MIMO linear systems with actuator saturation. In Chapter 2, the CNF technique has been extended to general SISO systems with external unknown constant disturbances.

The CNF design involves some matrix calculations and parameter selections. Especially

with those parameters for forming the nonlinear feedback law, some tuning and re-tuning are needed in order to obtain the best possible solutions. Hence, it is desirable to have a toolkit to facilitate the design process. This motivated us to develop a MATLAB toolkit with a user-friendly graphical interface for the CNF control system design. With the help of the rich collection of m-functions in MATLAB and the powerful simulation capacity of its SIMULINK, we develop a toolkit for the CNF control technique. The toolkit can be utilized to design fast and smooth tracking controllers for general linear systems with actuator saturation and other nonlinearities such as friction, as well as external disturbances. The CNF design procedure essentially involves design of a linear feedback law for closed-loop stability and quick response, and design of a nonlinear feedback law on top of the linear part to smooth out overshoot and speed up the settling. A nonlinearity pre-compensation will be implemented if there are plant nonlinearities that can be canceled using certain output feedback. An integrator will also be added to the overall controller design if there are external disturbances. The toolkit is capable of displaying both time-domain and frequency-domain responses on its main panel, and generating three different types of control laws, namely, the state feedback, the full order measurement feedback and the reduced order measurement feedback controllers. The toolkit can be utilized to design servo systems that deal with point-and-shoot fast targeting.

The outline of this chapter is as follows: In Section 3.2, we briefly recall the design procedure of the CNF control technique for general linear systems with input saturation and external disturbances. Section 3.3 presents the software framework and user interfaces of the toolkit, while Section 3.4 illustrates the usage of the toolkit through the design of a hard disk drive servo system and a magnetic tape drive servo system. Finally, we draw some concluding remarks in Section 3.5.

3.2 Theoretical Formulation

In this section, we recall the theoretical background of a control scheme for plants with nonlinearities and with CNF control. Note that the plants considered here are far more general than those covered in the previous chapter. To be precise, we consider a given plant characterized by the following dynamics equations:

$$\begin{cases} \dot{x} = A\,x + B\,\mathrm{sat}(g(y) + u) + Ew, \;\; x(0) = x_0 \\ y = C_1\,x, \\ h = C_2\,x + D_2\,\mathrm{sat}(g(y) + u), \end{cases} \tag{3.1}$$

where $x \in \mathbb{R}^n$, $u \in \mathbb{R}^m$, $y \in \mathbb{R}^p$, $h \in \mathbb{R}^l$ and $w \in \mathbb{R}^q$ are respectively the state, control input, measurement output, controlled output and disturbance input of the system; $g(y)$ is a nonlinear function representing the plant nonlinearities; and A, B, C_1, C_2, D_2 and E are appropriate dimensional constant matrices. The function, $sat()$, represents the actuator saturation defined as

$$\mathrm{sat}(u) = \mathrm{sgn}(u)\,\min\{\; u_{\max},\; |u|\;\}, \tag{3.2}$$

with $u_{\max}$ being the saturation level of the input. In the case of MIMO systems where u is likely a vector, the above definition applies to every element of u. The following assumptions on the given system are made:

1. (A, B) is stabilizable and (A, C_1) is detectable;

2. (A, B, C_2, D_2) is invertible and has no invariant zero at $s = 0$;

3. w is bounded unknown constant disturbance; and

4. h is also measurable, *i.e.*, h is part of the measurement output.

These assumptions are fairly standard for tracking control problems.

3.2.1 CNF Control: State Feedback Case

We first summarize in the following the step-by-step design procedure for constructing a CNF control law for the state feedback case, *i.e.*, for the case when $y = x$.

STEP 1: Given a target reference r, we define an auxiliary state variable,

$$\dot{z} := \kappa_{\rm i} e := \kappa_{\rm i}(h - r), \tag{3.3}$$

where $\kappa_{\rm i}$ is the integration gain matrix of full rank. The augmented system is as follows,

$$\begin{cases} \dot{\bar{x}} = \bar{A}\,\bar{x} + \bar{B}\,\mathrm{sat}(g(y) + u) + \bar{B}_{\rm r}\,r + \bar{E}\,w, \\ \bar{y} = \bar{C}_1\,\bar{x}, \\ h = \bar{C}_2\,\bar{x} + D_2\,\mathrm{sat}(g(y) + u), \end{cases} \tag{3.4}$$

where

$$\bar{x} = \begin{pmatrix} z \\ x \end{pmatrix}, \quad \bar{x}_0 = \begin{pmatrix} 0 \\ x_0 \end{pmatrix}, \quad \bar{y} = \begin{pmatrix} z \\ y \end{pmatrix}, \tag{3.5}$$

$$\bar{C}_1 = \begin{bmatrix} I_l & 0 \\ 0 & C_1 \end{bmatrix}, \quad \bar{C}_2 = [\,0 \quad C_2\,], \tag{3.6}$$

and

$$\bar{A} = \begin{bmatrix} 0 & \kappa_{\rm i} C_2 \\ 0 & A \end{bmatrix}, \quad \bar{B} = \begin{bmatrix} \kappa_{\rm i} D_2 \\ B \end{bmatrix}, \quad \bar{B}_{\rm r} = \begin{bmatrix} -\kappa_{\rm i} \\ 0 \end{bmatrix}, \quad \bar{E} = \begin{bmatrix} 0 \\ E \end{bmatrix}. \tag{3.7}$$

Note that this step is not necessary if the given plant does not have external disturbances.

STEP 2: Design a linear feedback control law,

$$u_{\rm L} = F\bar{x} + G\,r, \tag{3.8}$$

where F is chosen such that 1) $\bar{A} + \bar{B}F$ is an asymptotically stable matrix, and 2) the closed-loop system $\bar{C}_2(sI - \bar{A} - \bar{B}F)^{-1}\bar{B}$ has certain desired properties. Let us partition $F = [\,F_{\rm z} \quad F_{\rm x}\,]$ in conformity with z and x. The general guideline in designing such an F is to place the closed-loop pole(s) of $\bar{A} + \bar{B}F$ corresponding to

the integration mode, z, to be sufficiently closer to the imaginary axis compared to the rest eigenvalues, which implies that $F_{\rm z}$ is relatively small (in norm). The remaining closed-loop poles of $\bar{A}+\bar{B}F$ should be placed to have a dominant pair with a small damping ratio, which in turn would yield a fast rise time in the closed-loop response. Finally, G is chosen as

$$G = G_0'(G_0G_0')^{-1} \tag{3.9}$$

with

$$G_0 = D_2 - (C_2 + D_2F_{\rm x})(A+BF_{\rm x})^{-1}B. \tag{3.10}$$

STEP 3: Given a positive definite symmetric matrix $W \in \mathbb{R}^{(n+l)\times(n+l)}$, we solve the following Lyapunov equation:

$$(\bar{A}+\bar{B}F)'P + P(\bar{A}+\bar{B}F) = -W, \tag{3.11}$$

for $P > 0$. Such a solution is always existent as $(\bar{A}+\bar{B}F)$ is asymptotically stable. The nonlinear feedback portion of the CNF control law, $u_{\rm N}$, is then given by

$$u_{\rm N} = \rho(r,h)\bar{B}'P(\bar{x}-\bar{x}_{\rm e}), \tag{3.12}$$

where

$$\bar{x}_{\rm e} := G_{\rm e}\, r \quad \text{with} \quad G_{\rm e} := \begin{bmatrix} 0 \\ \\ -(A+BF_{\rm x})^{-1}BG \end{bmatrix}. \tag{3.13}$$

and $\rho(r,h)$, with $h-r$ being the tracking error, is a smooth, non-positive and non-decreasing function of $\|h-r\|$, to be used to gradually change the closed-loop poles' damping ratios to yield a better tracking performance. The following nonlinear function $\rho(r,h)$ has been suggested:

$$\rho(r,h) = -\beta\left|{\rm e}^{-\alpha\|h-r\|} - {\rm e}^{-\alpha\|h(0)-r\|}\right|, \tag{3.14}$$

where α and β are positive scalars or diagonal matrices with dimensions consistent with the input u. They can be tuned to yield appropriate performance. Also note that

the matrix, W, is generally used to tune the desired closed-loop poles at the steady state situation. The detailed interpretations of these design parameters can be found in Chapter 2 (see also Chen et al. [13]).

STEP 4: The linear feedback control law and nonlinear feedback portion derived in the previous steps together with a nonlinearity pre-compensation are now combined to form a CNF control law,

$$u = u_{\text{pre}} + u_{\text{L}} + u_{\text{N}} = -g(y) + F\bar{x} + G\,r + \rho(r,h)\bar{B}'P(\bar{x} - \bar{x}_{\text{e}}). \tag{3.15}$$

3.2.2 CNF Control: Measurement Feedback Case

In most cases, not all state variables are measurable for feedback control, hence an observer might be needed to estimate state vector x. This is the measurement feedback case, where the state variable, x, contained in $\bar{x}$ of the CNF state feedback law (3.15) will be replaced by an estimation using either a full order or a reduced order observer. In what follows, we outline the design procedure of observer. The detailed derivation is rather involved. We refer interested readers to [12] and [13] for more details.

It should be noted that, in the following derivation, we assume that plant nonlinearity has been pre-compensated beforehand, i.e., the control input u in the relevant equations does not include the term u_{pre}.

Full Order Observer

A linear full order observer can be designed as follows,

$$\dot{\hat{x}} = (A + KC_1)\hat{x} - Ky + B\,\text{sat}(u). \tag{3.16}$$

where K is a gain matrix such that $A + KC_1$ is asymptotically stable and the resulting closed-loop system has desired properties. Such a K exists since (A, C_1) is detectable.

Reduced Order Observer

In general, it is not necessary to estimate all the n states of x in measurement feedback laws, since there are already p states that are measurable, if C_1 is of maximal rank. As such, it is possible to design a reduced order observer, which has a dynamical order less than that of the given plant.

For the moment, we assume that C_1 is already in the form of

$$C_1 = [\, I_p \quad 0 \,]. \tag{3.17}$$

Then, the measurement subsystem of (3.1) without disturbances can be rewritten as,

$$\begin{cases} \begin{pmatrix} \dot{x}_1 \\ \\ \dot{x}_2 \end{pmatrix} = \begin{bmatrix} A_{11} & A_{12} \\ \\ A_{21} & A_{22} \end{bmatrix} \begin{pmatrix} x_1 \\ \\ x_2 \end{pmatrix} + \begin{bmatrix} B_1 \\ \\ B_2 \end{bmatrix} \mathrm{sat}(u),\ x_0 = \begin{pmatrix} x_{10} \\ \\ x_{20} \end{pmatrix} \\ \\ y \quad = \ [\ \ I_p \quad\quad 0\ \ ] \begin{pmatrix} x_1 \\ \\ x_2 \end{pmatrix} \end{cases} \tag{3.18}$$

where the original state x is partitioned into two parts, x_1 and x_2 with $y \equiv x_1$. Thus, we will only need to estimate x_2 in the reduced order measurement feedback design. Next, we choose a K_{R} such that $A_{22} + K_{\mathrm{R}} A_{12}$ is asymptotically stable. Such a stabilizing K_{R} exists, as it was shown in Chen [10] that (A_{22}, A_{12}) is detectable if and only if (A, C_1) is detectable.

The reduced order observer is given by

$$\dot{x}_v = A_o x_v + B_{oy} y + B_{ou}\, \mathrm{sat}(u) \tag{3.19}$$

where

$$\begin{cases} A_o = A_{22} + K_{\mathrm{R}} A_{12}, \\ \\ B_{ou} = B_2 + K_{\mathrm{R}} B_1, \\ \\ B_{oy} = A_{21} + K_{\mathrm{R}} A_{11} - A_o K_{\mathrm{R}} \end{cases} \tag{3.20}$$

The estimate of state x is given by

$$\hat{x} = \begin{pmatrix} y \\ \\ x_v - K_{\mathrm{R}} y \end{pmatrix}. \tag{3.21}$$

General Case of matrix C_1

When C_1 is not in the standard form, we choose a matrix

$$T = \begin{bmatrix} C_1 \\ \\ C_\perp \end{bmatrix} \tag{3.22}$$

where the rows of $C_\perp$ are the basis vectors of the null space of C_1. It can be verified that T is invertible if C_1 is of maximal row rank. Now we apply transformation $\tilde{x} = Tx$ to the original system and ignore disturbance, we arrive at the following subsystem of standard form:

$$\Sigma_o : \begin{cases} \dot{\tilde{x}} = \tilde{A}\tilde{x} + \tilde{B}sat(u), \\ \\ y = [\, I_p \quad 0 \,]\, \tilde{x} \end{cases} \tag{3.23}$$

with

$$\begin{cases} \tilde{A} = TAT^{-1}, \\ \\ \tilde{B} = TB \end{cases} \tag{3.24}$$

Now a reduced order observer can be designed to estimate $\tilde{x}$:

$$\begin{cases} \dot{x}_v = \tilde{A}_o x_v + \tilde{B}_{oy} y + \tilde{B}_{ou}\, \mathrm{sat}(u), \\ \hat{\tilde{x}} = \begin{pmatrix} y \\ \\ x_v - \tilde{K}_{\mathrm{R}} y \end{pmatrix} \end{cases} \tag{3.25}$$

Then the estimate of x is given by

$$\hat{x} = T^{-1}\hat{\tilde{x}} = T^{-1} \begin{pmatrix} y \\ \\ x_v - \tilde{K}_{\mathrm{R}} y \end{pmatrix}. \tag{3.26}$$

In all cases, the observer (whether full order or reduced order) for estimating x can be cast into the following form:

$$\begin{cases} \dot{x}_v = A_o x_v + B_{oy} y + B_{ou}\, \mathrm{sat}(u), \\ \\ \hat{x} = C_o x_v + D_o y \end{cases} \tag{3.27}$$

3.2.3 Auxiliary Analysis Tools

Root locus

The nonlinear part of CNF control will become influential only when the tracking error, $r - h$, gets smaller. Thus in general the control input does not hit its limits. Under such a circumstance, the closed-loop system will have an error dynamics as follows:

$$\dot{\tilde{x}} = (\bar{A} + \bar{B}F)\tilde{x} + \rho \bar{B}\bar{B}' P \tilde{x} + \bar{E}w. \tag{3.28}$$

Now it is easy to see that eigenvalues of the closed-loop system can be changed by changing the function $\rho(r,h)$. The error dynamics of (3.28) can be cast into the classical feedback context if we define an auxiliary system $G_{aux}(s)$ as follows:

$$G_{aux}(s) := C_{aux}(sI - A_{aux})^{-1}B_{aux} := \bar{B}'P(sI - \bar{A} - \bar{B}F)^{-1}\bar{B}. \tag{3.29}$$

It then follows from the classical control theory that the closed-loop poles, which are the function of the tuning parameter ρ, will start from the open-loop poles, i.e., the eigenvalues of $\bar{A} + \bar{B}F$, when $\rho = 0$, and end up at the open-loop zeros (including the zero at the infinity) as $|\rho| \to \infty$. As such, the root locus of the auxiliary system $G_{aux}(s)$ provides an intuitive method for observing the evolution of the closed-loop poles, which is useful for controller design and parameter tuning.

Since the invariant zeros of $G_{aux}(s)$ play an important role in selecting the poles of the closed-loop system, we should, in general, select a set of invariant zeros, which correspond to the closed-loop poles for larger $|\rho|$, such that the dominant ones have a large damping ratio, which in turn will yield a small overshoot. This can be achieved by selecting an appropriate weighting matrix $W > 0$.

The above analysis is based on SISO plants. For MIMO plants, the concept of root locus is not quite intuitive. However, by stepping over the values of $\rho(r,h)$, we can still plot the locus of the closed-loop poles as determined by (3.28).

Loop Transfer Function

In classical control context, bandwidth and gain/phase margins are important measures for evaluation of a control design. These measures can be observed from the bode plots of the sensitivity/complementary sensitivity functions and open-loop transfer function. For simplicity, here we only consider the steady state situation, when $\rho(r,h)$ approaches a constant value ρ^* and control saturation is inactive. Four cases are considered here.

Case 1: State feedback without integral

The control input becomes (assuming that plant nonlinearity has been pre-compensated beforehand)

$$u = Fx + Gr + \rho^* B'P(x - x_e) = F_c \cdot x + G_c \cdot r, \tag{3.30}$$

where

$$F_c = F + \rho^* B'P, \;\; G_c = G - \rho^* B'PG_e. \tag{3.31}$$

Now from the controlled system

$$\begin{cases} \dot{x} = Ax + Bu, \\ h = C_2 x + D_2 u, \\ u = F_c \cdot x + G_c \cdot r \end{cases} \tag{3.32}$$

we can get the closed-loop transfer function from reference r to output h as follows,

$$H(s) = (C_2 + D_2F_c)[sI - (A + BF_c)]^{-1}BG_c + D_2G_c, \tag{3.33}$$

and the open loop transfer function is simply

$$L(s) = F_c(sI - A)^{-1}B. \tag{3.34}$$

Case 2: State feedback with integral

Consider the controlled and augmented system

$$\begin{cases} \dot{\bar{x}} = \bar{A}\bar{x} + \bar{B}u + B_r r, \\ h = \bar{C}_2\bar{x} + D_2 u = [\,0 \quad C_2\,]\,\bar{x} + D_2 u, \\ u = F_c \cdot \bar{x} + G_c \cdot r \end{cases} \tag{3.35}$$

the closed-loop transfer function from reference r to output h is given by

$$H(s) = (\bar{C}_2 + D_2F_c)[sI - (\bar{A} + \bar{B}F_c)]^{-1}(B_r + \bar{B}G_c) + D_2G_c, \tag{3.36}$$

and the open loop transfer function is

$$L(s) = F_c(sI - \bar{A})^{-1}\bar{B}. \tag{3.37}$$

Case 3: Measurement feedback without integral

Consider the observer-based controller

$$\begin{cases} \dot{x}_v = A_o x_v + B_{oy} y + B_{ou}\, u, \\ \hat{x} = C_o x_v + D_o y, \\ u = F_c \cdot \hat{x} + G_c \cdot r \end{cases} \tag{3.38}$$

and the system to be controlled

$$\begin{cases} \dot{x} = Ax + Bu, \\ y = C_1 x, \\ h = C_2 x + D_2 u \end{cases} \tag{3.39}$$

we have the following

$$\begin{cases} \begin{pmatrix} \dot{x} \\ \dot{x}_v \end{pmatrix} = A_{cl} \begin{pmatrix} x \\ x_v \end{pmatrix} + B_{cl} \cdot r, \\ h = C_{cl} \begin{pmatrix} x \\ x_v \end{pmatrix} + D_{cl} \cdot r \end{cases} \tag{3.40}$$

where

$$\begin{cases} A_{cl} = \begin{bmatrix} A + BF_cD_oC_1 & BF_cC_o \\ B_{ou}F_cD_oC_1 + B_{oy}C_1 & A_o + B_{ou}F_cC_o \end{bmatrix}, \\ B_{cl} = \begin{bmatrix} BG_c \\ B_{ou}G_c \end{bmatrix}, \\ C_{cl} = \begin{bmatrix} C_2 + D_2F_cD_oC_1 & D_2F_cC_o \end{bmatrix}, \\ D_{cl} = D_2G_c \end{cases} \tag{3.41}$$

Now the closed-loop transfer function from reference r to output h is simply

$$H(s) = C_{cl}(sI - A_{cl})^{-1}B_{cl} + D_{cl}, \tag{3.42}$$

and the open loop transfer function is

$$L(s) = F_c[C_o(sI - A_o - B_{ou}F_cC_o)^{-1}(B_{oy} + B_{ou}F_cD_o) + D_o]C_1(sI - A)^{-1}B. \tag{3.43}$$

Case 4: Measurement feedback with integral

Consider the augmented system

$$\begin{cases} \dot{\bar{x}} = \bar{A}\bar{x} + \bar{B}u + B_r r, \\ \bar{y} = \begin{pmatrix} z \\ y \end{pmatrix} = \bar{C}_1\bar{x} = \begin{bmatrix} I_l & 0 \\ 0 & C_1 \end{bmatrix} \bar{x}, \\ h = \bar{C}_2\bar{x} + D_2u = \begin{bmatrix} 0 & C_2 \end{bmatrix} \bar{x} + D_2u \end{cases} \tag{3.44}$$

and the observer-based controller

$$\begin{cases} \dot{x}_v = A_o x_v + B_{oy} y + B_{ou}\, u, \\ \hat{x} = C_o x_v + D_o y, \\ u = F_c \cdot \begin{pmatrix} z \\ \hat{x} \end{pmatrix} + G_c \cdot r = F_x \hat{x} + F_z z + G_c \cdot r \end{cases} \tag{3.45}$$

where F_z and z correspond to integral augmentation.

The closed-loop system is

$$\begin{cases} \begin{pmatrix} \dot{\bar{x}} \\ \dot{x}_v \end{pmatrix} = A_{cl} \begin{pmatrix} \bar{x} \\ x_v \end{pmatrix} + B_{cl} \cdot r, \\ h = C_{cl} \begin{pmatrix} \bar{x} \\ x_v \end{pmatrix} + D_{cl} \cdot r \end{cases} \tag{3.46}$$

where

$$\begin{cases} A_{cl} = \begin{bmatrix} \bar{A} + \bar{B} F_x D_o \,[\,0 \quad C_1\,] + \bar{B} F_z \,[\,I_l \quad 0\,] & \bar{B} F_x C_o \\ (B_{ou} F_x D_o + B_{oy})\,[\,0 \quad C_1\,] + B_{ou} F_z \,[\,I_l \quad 0\,] & A_o + B_{ou} F_x C_o \end{bmatrix}, \\ B_{cl} = \begin{bmatrix} B_r + \bar{B} G_c \\ B_{ou} G_c \end{bmatrix}, \\ C_{cl} = \left[\bar{C}_2 + D_2 F_x D_o \,[\,0 \quad C_1\,] + D_2 F_z \,[\,I_l \quad 0\,], \quad D_2 F_x C_o\right], \\ D_{cl} = D_2 G_c \end{cases} \tag{3.47}$$

Now the closed-loop transfer function from reference r to output h is of the same form as (3.42), and the open loop transfer function is

$$\begin{aligned} L(s) = \big\{ & F_x C_o (sI - A_o - B_{ou} F_x C_o)^{-1} (B_{oy}\,[\,0 \quad I_l\,] + B_{ou}\,[\,F_z \quad F_x D_o\,]) + [\,F_z \quad F_x D_o\,] \big\} \\ & \times \bar{C}_1 (sI - \bar{A})^{-1} \bar{B}. \end{aligned} \tag{3.48}$$

3.3 Software Framework and User Guide

The CNF control toolkit is developed under the latest version of MATLAB, i.e., MATLAB 6.5, together with SIMULINK 5.0. It fully utilizes the graphical user interface (GUI) resources of MATLAB and provides a user-friendly graphical interface. The main interface of the toolkit consists of three panels, i.e., the panel for conducting simulation, the panel for setting up system data and the panel for specifying an appropriate controller. We illustrate these panels in details in the following:

SIMULATION PANEL: The simulation panel as shown in Figure 3.2 is the main portion of the CNF control toolkit. Users can specify directly on the panel the simulation parameters, such as the set point for the target reference, the duration of simulation and the sampling period. Users can also define the tracking performance indicator and obtain the result for settling time and steady state bias of the controlled output response. For example, in Figure 3.2, the settling time is defined as the time when the controlled output of the closed-loop system enters the neighborhood of ± 0.025 of the given set point. Alternatively, one can define such a neighborhood in terms of the percentage of final target instead of the absolute error bound.

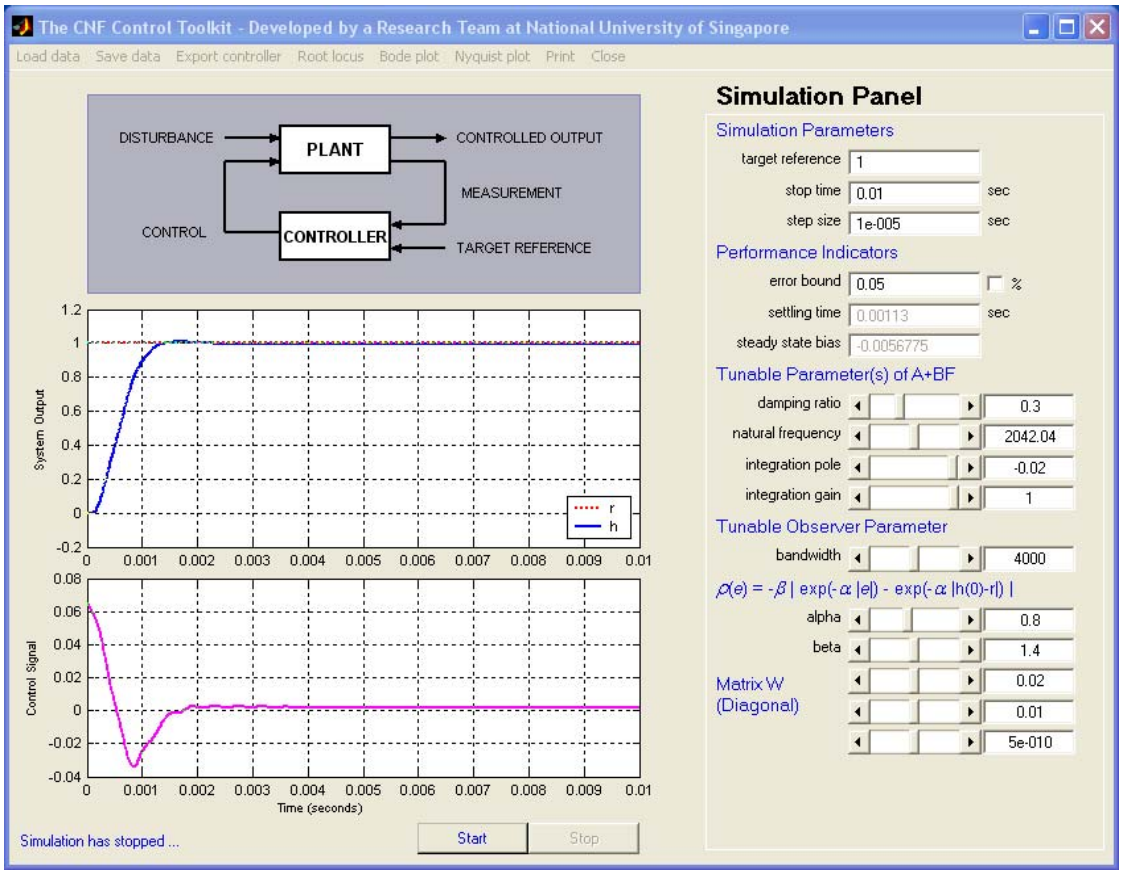

Figure 3.2: The simulation panel of the CNF control toolkit.

As mentioned in the previous section, the CNF controller consists of two parts: a linear part and a nonlinear part. On the simulation panel, users are able to tune

the properties of the linear part by selecting appropriate values of the damping ratio and natural frequency of the dominant modes of the linear state feedback dynamical matrix, i.e., $A+BF$. The rest eigenvalues of $A+BF$ are placed 3 times faster than the dominant modes with a Butterworth pattern. Such an arrangement is purely for the simplification of the control system design. The pole corresponding to the integrator part, if applicable, can be tuned on this main panel as well. Alternatively, users are allowed to apply the H_2 design with a tunable parameter ϵ, or directly specify a state feedback gain matrix in the controller setup panel without any tunable parameters.

Design parameters for the nonlinear part of the CNF controller, i.e., W and $\rho(r,h)$, can also be tuned online on the main simulation panel. In particular, the parameters α and β for the nonlinear function $\rho(r,h)$ of (2.86) can be easily adjusted using the computer mouse or by directly keying their values onto the spaces provided.

There are two windows in the simulation panel for displaying the system controlled output response and the control input signal, together with a block diagram showing the structure of the overall control system. Using the right button of the computer mouse to click on the window displaying the output response and control signal, users will be prompted by a small text window showing options to re-draw the plots on a new pop-out window or export the simulation data to the MATLAB workspace. By clicking on the box labeled with PLANT, there will be a new panel opened for users to enter data for the plant. Similarly, clicking on the box labeled with CONTROLLER will lead to another new panel, which will allow users to specify an appropriate controller structure and enter preliminary controller parameters. Detailed information for these two panels will be given later.

Finally, we have also implemented the following commands and functions on the simulation panel for saving and loading data as well as for evaluating the frequency

domain properties of the overall control system:

1. Load Data: This function is used to load data previously saved in the CNF control toolkit.

2. Save Data: This command is to save the system and controller data entered for future use.

3. Export Controller: This function is to export the data of the CNF controller obtained to the MATLAB workspace. The controller data are given in the following format:

$$\left.\begin{aligned} \dot{z} &= \kappa_{\rm i}(h-r) \\ \dot{x}_{\rm v} &= A_{\rm cmp}\, x_{\rm v} + B_{\rm ycmp}\, y + B_{\rm ucmp}\, {\rm sat}(\bar{u}) \\ \hat{x} &= C_{\rm cmp}\, x_{\rm v} + D_{\rm cmp}\, y \\ \bar{u} &= F \begin{pmatrix} z \\ \hat{x} \end{pmatrix} + G\, r + \rho(r,h) F_{\rm n} \left[\begin{pmatrix} z \\ \hat{x} \end{pmatrix} - G_{\rm e}\, r \right] \\ u &= \bar{u} - g(y) \end{aligned}\right\} \tag{3.49}$$

where $A_{\rm cmp}$, $B_{\rm ycmp}$, $B_{\rm ucmp}$, $C_{\rm cmp}$, $D_{\rm cmp}$, F, $F_{\rm n}$, G, $G_{\rm e}$ are constant vectors or matrices, and $\rho(r,h)$ and $g(y)$ are some nonlinear functions. All these parameters will be saved under a structured workspace variable in the MATLAB command window.

4. Root Locus: It is to generate the locus of the closed-loop poles of the controlled system with the CNF controller with respect to the change of the nonlinear function $\rho(r,h)$.

5. Bode Plot: It is to generate the Bode magnitude and phase responses of the open-loop system comprising the plant and the controller in the steady state situation when the nonlinear gain ρ is converging to a constant. This function can be used to evaluate the frequency domain properties of the controlled system, such as gain and phase margins.

6. Nyquist Plot: Similar to the Bode plot given above. Note that for both the Bode and Nyquist plots, users are allowed to specify a frequency range of interest in radian.

7. Print: This function is to print the items shown on the simulation panel.

8. Close: This command is to close up the CNF control toolkit.

PLANT MODEL SETUP PANEL: A setup panel as shown in Figure 3.3 for entering system data will be opened when the box labeled PLANT in the main simulation panel has been activated. In addition to the state space model of the given plant specified in (3.1), the toolkit allows users to specify resonant modes of the plant as well on this panel. We note that high frequency resonant modes are existing almost in all physical systems. Because of the complexity of resonant modes, they are generally ignored or simplified in the controller design stage. However, they should be and have to be included in the simulation and evaluation of the overall control system design.

Each time a plant model is keyed in or modified on the panel, the toolkit will automatically run a checkup on the validity of the given model, i.e., to check the stabilizability, detectability, invertibility and other requirements. Users will be warned if the solvability conditions for the CNF tracking control are not satisfied and of course users can not proceed to the step of controller design.

CONTROLLER SETUP PANEL: As the core of this toolkit, the CNF controller design is to be proceeded in a configurable and convenient fashion. A controller setup panel as shown in Figure 3.4 will be opened when the user has activated the box marked with CONTROLLER in the main simulation panel. This panel carries a block diagram for an adjustable controller configuration, which will automatically refresh if the user has made any change or re-selection on the controller structure. Users need to decide

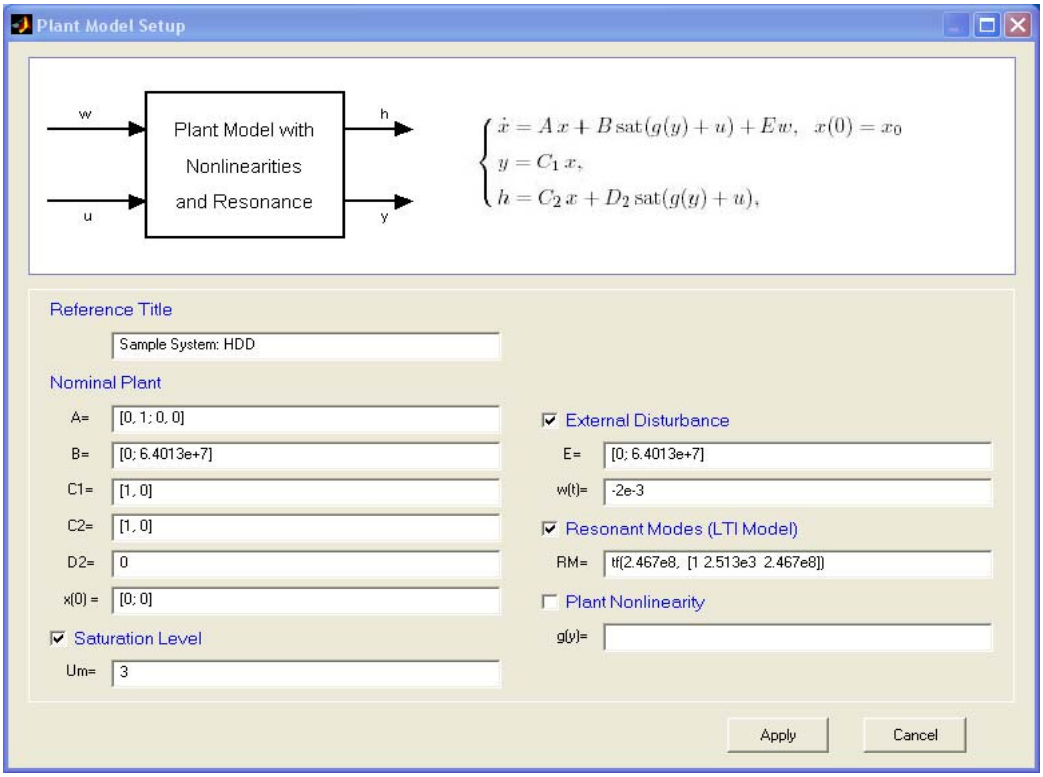

Figure 3.3: The panel for the plant model setup.

a controller structure first before proceeding to specify the corresponding controller parameters.

The following are the options available for the controller in the CNF control toolkit:

1. If the given plant has some nonlinearities, users should choose the pre-compensation option and enter an appropriate nonlinear function $g(y)$ to cancel as many nonlinearities as possible.

2. If the plant has some unknown constant disturbances or other types of disturbances, users should select a controller structure with integrator to remove the steady state bias.

3. Based on the properties of the given plant and personal interest, users can then choose a controller with either one of the following options:

   (a) State feedback;

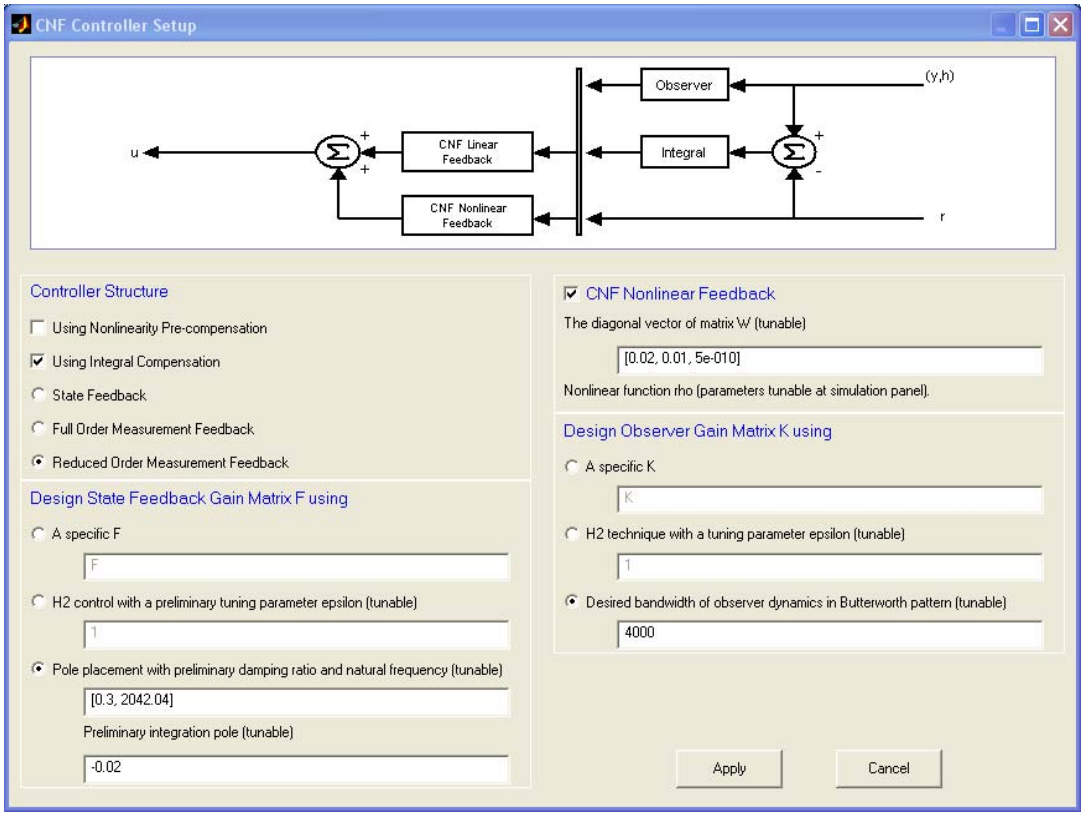

Figure 3.4: The panel for the CNF controller setup.

(b) Full order measurement feedback;

(c) Reduced order measurement feedback.

When it comes to the design of the state feedback gain F, users have three choices: Users can either specify an explicit matrix (obtained through any other design methodologies) for F, or apply the H_2 design with a parameter ϵ, or use the pole placement method characterized by the damping ratio and natural frequency of the dominant poles and integration pole (if applicable). For the pole placement method, the rest of the closed-loop poles are placed three times faster than the dominant pair with a Butterworth pattern.

For the H_2 design approach, the state feedback gain, F, is computed by solving the

following ϵ-perturbed H_2 algebraic Riccati equation (H_2-ARE):

$$A'P_2 + P_2A + \tilde{C}_2'\tilde{C}_2 - (P_2B + \tilde{C}_2'\tilde{D}_2)(\tilde{D}_2'\tilde{D}_2)^{-1}(\tilde{D}_2'\tilde{C}_2 + B'P_2) = 0, \tag{3.50}$$

for a stabilizing $P_2 \geq 0$, where

$$\tilde{C}_2 = \begin{bmatrix} C_2 \\ \epsilon I \\ 0 \end{bmatrix} \quad \text{and} \quad \tilde{D}_2 = \begin{bmatrix} D_2 \\ 0 \\ \epsilon I \end{bmatrix} \tag{3.51}$$

The state feedback gain, F, is then given by

$$F = -(\tilde{D}_2'\tilde{D}_2)^{-1}(\tilde{D}_2'\tilde{C}_2 + B'P_2). \tag{3.52}$$

In the case of measurement feedback control, users also have three choices for the design of the observer gain K: an explicit matrix for K, or H_2 design with a parameter ϵ (a dual version of state feedback), or using the pole placement method to organize the observer poles into the pattern of a Butterworth filter with bandwidth ω_o. In any cases, the corresponding parameters can be further tuned on the simulation panel to yield a satisfactory performance for the overall system..

Although the CNF control toolkit is meant to design a composite nonlinear feedback controller (for which the matrix W has yet to be specified), users have the option to choose only the linear portion of the CNF control law for their design. This option is particularly useful for the comparison of performances of the CNF controller and the linear controller.

3.4 Illustrative Examples

In this section, we demonstrate the usage of the CNF control toolkit by two practical examples, to be specific, a hard disk drive (HDD) servo system design and a magnetic tape drive servo design.

3.4.1 Hard Disk Drive Servo System Design

In this subsection we design a CNF controller for a conventional 3.5 inch hard disk drive. The model of this disk drive has been identified as follows (see [13]):

$$G_v(s) = \frac{6.4013\times10^7}{s^2} \cdot \frac{2.467\times10^8}{s^2 + 2.513\times10^3 s + 2.467\times10^8} \tag{3.53}$$

For CNF design, we will use the following simplified model or so-called nominal model:

$$\begin{cases} \dot{x} = \begin{bmatrix} 0 & 1 \\ 0 & 0 \end{bmatrix} x + \begin{bmatrix} 0 \\ 6.4013\times10^7 \end{bmatrix} \mathrm{sat}(u) + \begin{bmatrix} 0 \\ 6.4013\times10^7 \end{bmatrix} w, \\ y = h = [\,1 \quad 0\,]\, x, \end{cases} \tag{3.54}$$

where the state variable, x, consists of the displacement and velocity of the read/write (R/W) head of the voice-coil-motor actuator in the disk drive; y and h are simply the displacement (in micrometer) of the R/W head of the drive; w represents friction and some unknown disturbances of the system, and is set to be -0.002V for this demonstration; u is the control input, limited by ±3V. The high frequency resonance is excluded from the nominal model but will be included in simulation and robustness analysis.

For hard disk drive servo systems, the task of the controller is to move the actuator R/W head to a desired track as fast as possible and to maintain the R/W head as close as possible to the target track center when data are being read or written. To ensure reliable data reading and writing, it is required that the deviation of R/W head from the target track center should not exceed 5% of track pitch. In this demonstration, we focus our attention on designing a servo system, which will yield an optimal performance for short distance tracking. In particular, we will set the target reference $r = 1$ micrometer, which is equivalent to 1 track on the actual drive (A track density of 25 kTPI is assumed here). Thus, the settling time is defined as the total duration for the R/W head to enter the ±0.05 micrometers region of the target track.

Using the CNF control toolkit with few online adjustments on the design parameters, we manage to obtain a reduced order CNF controller that yields a very satisfactory performance. The simulation parameter setup, the plant model setup and the controller structure setup for this example have actually been presented already earlier in Figures 3.2 to 3.4, respectively. The dynamics equations of the controller is given by:

$$\begin{pmatrix} \dot{z} \\ \\ \dot{x}_{\rm v} \end{pmatrix} = \begin{bmatrix} 0 & 0 \\ \\ 0 & -4000 \end{bmatrix} \begin{pmatrix} z \\ \\ x_{\rm v} \end{pmatrix} + \begin{bmatrix} 0 \\ \\ 6.4013 \times 10^7 \end{bmatrix} \mathrm{sat}(u) + \begin{bmatrix} 1 \\ \\ -1.6 \times 10^7 \end{bmatrix} y - \begin{bmatrix} 1 \\ \\ 0 \end{bmatrix} r, \quad (3.55)$$

and

$$u = u_{\rm L} + u_{\rm N}, \quad (3.56)$$

where

$$u_{\rm L} = -\begin{bmatrix} 1.3028 \times 10^{-3} & 0.0651 & 1.9141 \times 10^{-5} \end{bmatrix} \begin{pmatrix} z \\ y - r \\ x_{\rm v} + 4000y \end{pmatrix}, \quad (3.57)$$

and

$$u_{\rm N} = \rho(r, h) \begin{bmatrix} 7.6756 & 0.0790 & 7.7548 \times 10^{-5} \end{bmatrix} \begin{pmatrix} z \\ y - r \\ x_{\rm v} + 4000y \end{pmatrix} \quad (3.58)$$

with

$$\rho(r, h) = -1.4 \left| \mathrm{e}^{-0.8|h-r|} - \mathrm{e}^{-0.8} \right|. \quad (3.59)$$

Figure 3.5 shows the controlled output response of the servo system with the obtained CNF controller. For comparison, we have also plotted the response of the resulting closed-loop system with only the linear portion, i.e., $u = u_{\rm L}$. Clearly, the servo system with the obtained CNF controller yields a much better performance. The frequency domain properties of the servo system with the CNF control law are respectively shown in Figures 3.6, 3.7 and 3.8. The results are very satisfactory.

3.4.2 Magnetic Tape Drive Servo System Design

The previous example deals with CNF controller design for a SISO plant. In this subsection we demonstrate the design for a MIMO plant, specifically, a magnetic tape drive. This

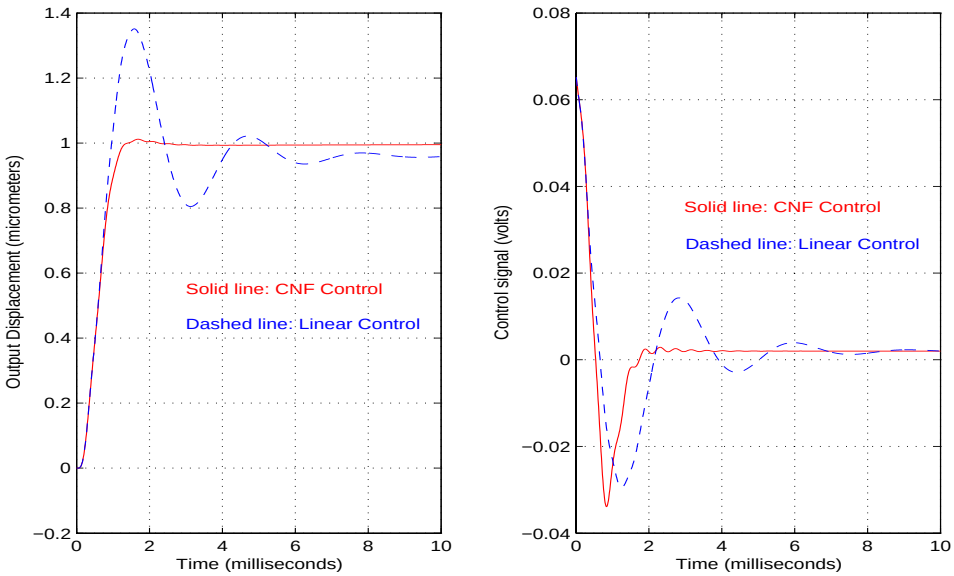

Figure 3.5: Controlled output response and control signal of the HDD servo system.

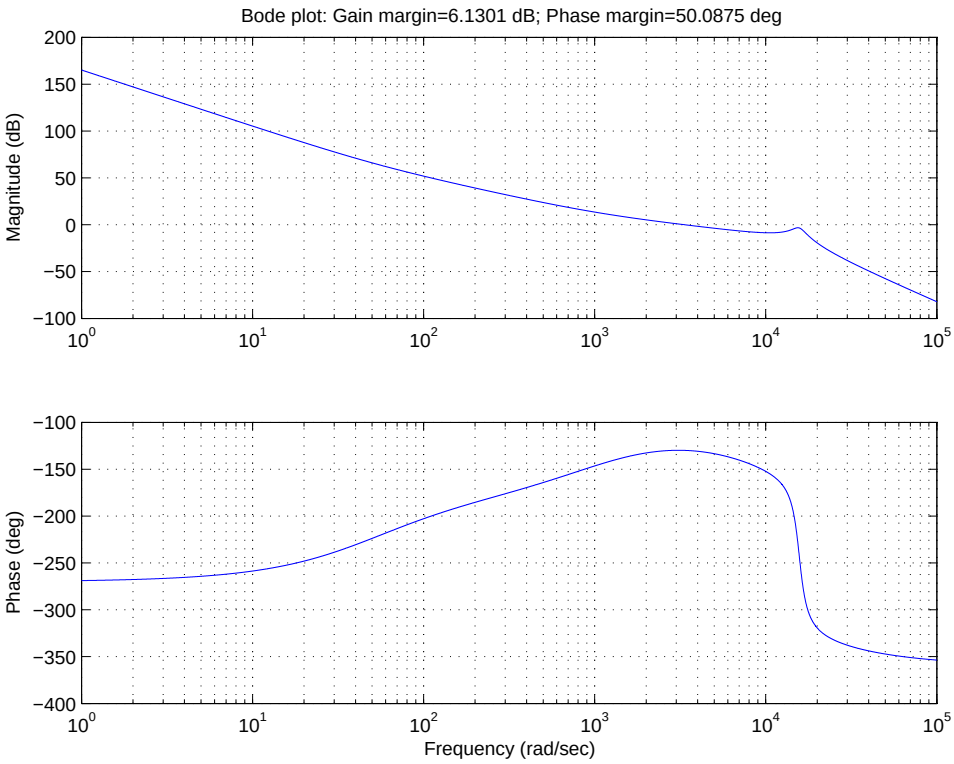

Figure 3.6: Bode plot of the open-loop transfer function of the HDD servo system.

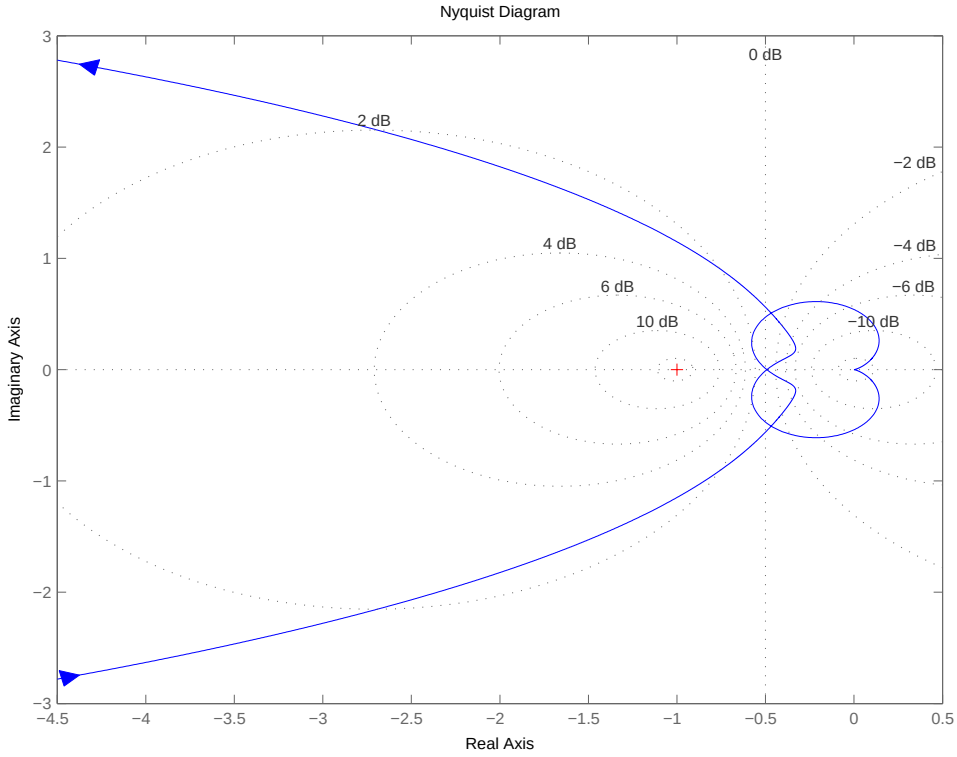

Figure 3.7: Nyquist plot of the open-loop transfer function of the HDD servo system.

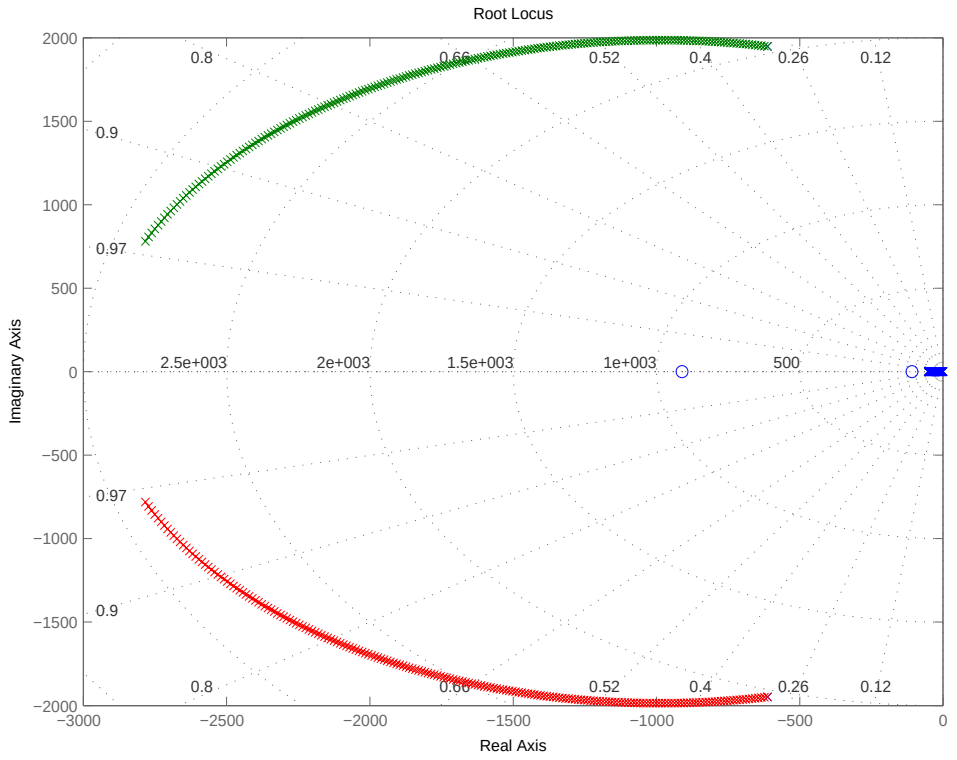

Figure 3.8: Root locus of the closed-loop HDD servo system versus function $\rho(r, h)$.

example is taken from the book of Franklin *et al.* [26], in which a time-scaled model of a magnetic tape drive is given as follows,

$$\begin{cases} \dot{x} = \begin{bmatrix} 0 & 0 & -10 & 0 \\ 0 & 0 & 0 & 10 \\ 3.315 & -3.315 & -0.5882 & -0.5882 \\ 3.315 & -3.315 & -0.5882 & -0.5882 \end{bmatrix} x + \begin{bmatrix} 0 & 0 \\ 0 & 0 \\ 8.533 & 0 \\ 0 & 8.533 \end{bmatrix} \text{sat}(u), \\ y = h = \begin{bmatrix} x_3 \\ T_e \end{bmatrix} = \begin{bmatrix} 0.5 & 0.5 & 0 & 0 \\ -2.113 & 2.113 & 0.375 & 0.375 \end{bmatrix} x. \end{cases} \tag{3.60}$$

where

$$x = [\, x_1 \quad x_2 \quad \omega_1 \quad \omega_2 \,]', \quad u = [\, i_1 \quad i_2 \,]' \tag{3.61}$$

with

x_1, x_2 = positions of tape at capstans 1 and 2, respectively (mm);

ω_1, ω_2 = angular rates of motor/capstan assembly 1 and 2, respectively (rad/sec);

i_1, i_2 = electric current inputs to drive motors 1 and 2, respectively (A);

x_3 = position of tape over read head (mm);

T_e = tension in tape (N).

The specifications for servo design are to provide a step change in position of the tape head, x_3, from zero initial condition to 1mm with a 1% settling time no larger than 2.5 seconds (time-scaled equivalent of 250 milliseconds) with less than 20% overshoot. The tape tension, T_e, should be controlled to 2N with the constraint that $0 < T_e < 4N$. The control signal, i.e., electric current (i_1, i_2) is limited to 1A at each drive motor.

It is reasonable to expect some disturbances in the real systems. Here for demonstration we assume the disturbances entering the two control input channels (i_1, i_2) are as follows,

$$w = \begin{bmatrix} 0.01 + 0.005sin(8\pi t) \\ -0.005 + 0.002sin(4\pi t) \end{bmatrix} \tag{3.62}$$

Due to the existence of disturbances, integral compensation will have to be used to remove the steady-state bias. Using the CNF control toolkit with some online tuning of the design parameters, we manage to obtain a reduced order enhanced CNF controller that yields a very satisfactory performance. We choose the damping and natural frequency of dominant poles to be 0.4 and 4 respectively, and the observer bandwidth to be 12. The matrix W is chosen as $diag(10^{-4}, 10^{-6}, 1, 1, 1, 1)$. The dynamic equations of the controller are given by:

$$\begin{cases} \dot{z} = h - r, \\ \dot{x}_{\rm v} = \begin{bmatrix} -8.4853 & 8.4853 \\ -8.4853 & -8.4853 \end{bmatrix} x_{\rm v} + \begin{bmatrix} 8.5997 & 0.0667 \\ -1.2384 & 7.2946 \end{bmatrix} \mathrm{sat}(u) + \begin{bmatrix} 14.4000 & 1.8673 \\ 14.4000 & -4.5743 \end{bmatrix} y, \\ \hat{x} = \begin{bmatrix} 8.7371\times10^{-2} & 8.7371\times10^{-2} \\ -8.7371\times10^{-2} & -8.7371\times10^{-2} \\ 9.9231\times10^{-1} & -7.6929\times10^{-3} \\ -7.6929\times10^{-3} & 9.9231\times10^{-1} \end{bmatrix} x_{\rm v} + \begin{bmatrix} 8.5173\times10^{-1} & -2.0100\times10^{-1} \\ 1.1483 & 2.0100\times10^{-1} \\ -1.6840 & -3.1317\times10^{-3} \\ 1.3055\times10^{-2} & 4.0472\times10^{-1} \end{bmatrix} y. \end{cases} \tag{3.63}$$

and

$$u = u_{\rm L} + u_{\rm N}, \tag{3.64}$$

where

$$u_{\rm L} = \begin{bmatrix} 5.7639\times10^{-4} & -1.0343\times10^{-4} & 9.8473\times10^{-2} & 4.7796\times10^{-1} \\ -2.6457\times10^{-4} & -2.3832\times10^{-4} & -6.3017\times10^{-2} & -2.0172\times10^{-1} \end{bmatrix}$$

$$\begin{bmatrix} -1.0534 & -6.1719\times10^{-1} \\ 4.8843\times10^{-1} & -1.1728 \end{bmatrix} \begin{pmatrix} z \\ \hat{x} \end{pmatrix} + \begin{bmatrix} -5.7643\times10^{-1} & 9.4061\times10^{-2} \\ 2.6473\times10^{-1} & 2.1668\times10^{-1} \end{bmatrix} r,$$

and

$$u_{\rm N} = \rho(r,h) \begin{bmatrix} -7.1689\times10^{-2} & 1.3871\times10^{-3} & -1.7387 & 9.2455\times10^{-1} \\ 3.2805\times10^{-2} & 1.4960\times10^{-3} & 1.0500 & 9.8769\times10^{-1} \end{bmatrix}$$

$$\begin{bmatrix} 2.1119 & -3.9908\times10^{-1} \\ -3.9908\times10^{-1} & 1.5554 \end{bmatrix} \left\{ \begin{pmatrix} z \\ \hat{x} \end{pmatrix} - \begin{bmatrix} 0 & 0 \\ 0 & 0 \\ 1 & -2.3663\times10^{-1} \\ 1 & 2.3663\times10^{-1} \\ 0 & 0 \\ 0 & 0 \end{bmatrix} r \right\}$$

with

$$\rho(r,h) = -\begin{bmatrix} 1.6 & 0 \\ 0 & 1.2 \end{bmatrix} \left| \mathrm{e}^{-\|h-r\|} - 0.3679 \right|. \tag{3.65}$$

Figure 3.9 shows the controlled output response of the servo system with the obtained CNF controller for the target reference $r = [1 \quad 2]^T$. The settling time are 0.745 sec and 0.77 sec respectively for the two output channels with the error bound of 1%. Since the disturbances are fictitiously added, it would be interesting to check the performance in the absence of disturbances. Simulation shows that the settling time are 0.45 sec and 0.77 sec when the disturbances are non-existent, which is a little better than the case with disturbances. These results are consistent with our intuition and indicate that the obtained CNF controller has performance robustness with respect to disturbances. Clearly, the servo system with the enhanced CNF controller meets the performance specifications stipulated before. The evolution locus of the closed-loop poles of the servo system with the enhanced CNF control law is shown in Figure 3.10, which provides some insight into the characteristics of the closed-loop system. The above results are quite impressive.

3.5 Concluding Remarks

We have presented in this chapter a composite nonlinear feedback (CNF) control toolkit for general linear systems with actuator and other nonlinearities, external disturbances, and high frequency resonance. The toolkit has been built on the MATLAB and SIMULINK environment with a user-friendly interface. All design parameters can be easily tuned online on the panels of the toolkit. The usage and design procedure of the toolkit have been illustrated through two practical examples on the servo design for a hard disk drive and a magnetic tape drive. The CNF control toolkit can be utilized to design servo systems that require fast target tracking and good robustness. It can be downloaded for free from `http://hdd.ece.nus.edu.sg/~bmchen/` for use in research and academical purposes.

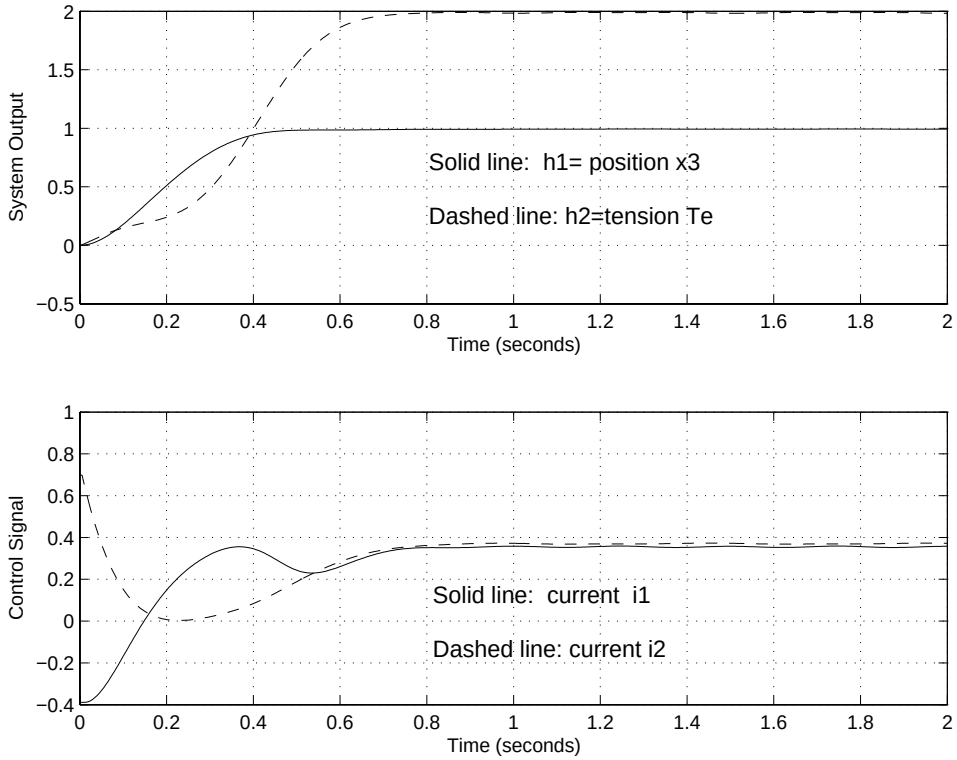

Figure 3.9: Controlled output response and control signal of the tape drive system.

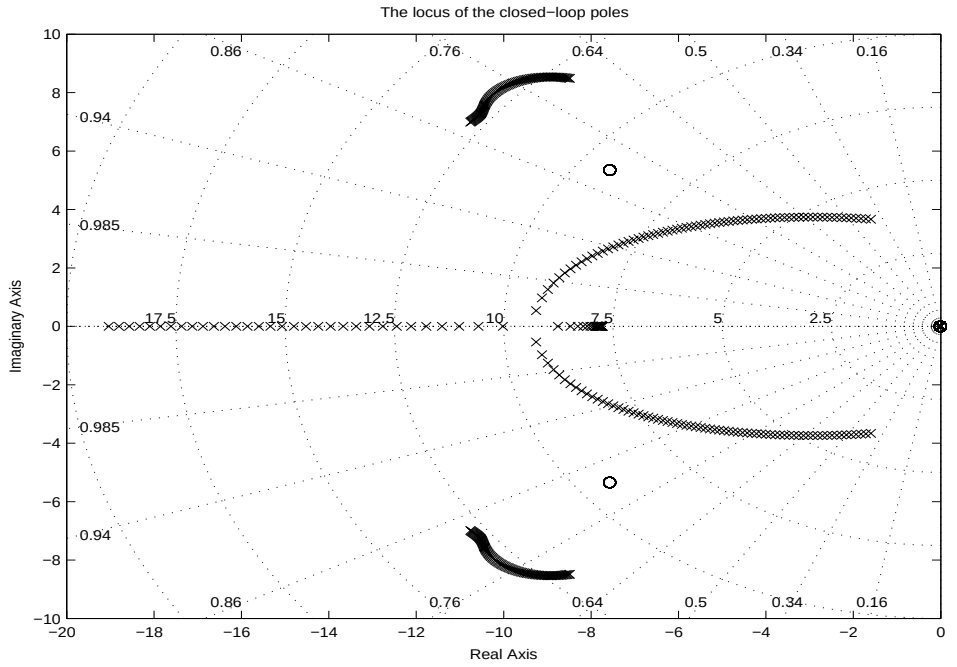

Figure 3.10: Root locus of the closed-loop tape drive system versus function $\rho(r, h)$.

Chapter 4

Comprehensive Modeling of A Micro Hard Disk Drive Actuator

Beginning from this chapter, we deal with HDD servo systems. The first step to servo system design is to establish an accurate model for the plant. The model of HDD servo systems has long been identified as a linear system without incorporating the inherent nonlinearities, such as pivot bearing friction and flex cable nonlinearity. These nonlinearities are becoming more influential in smaller disk drives and may result in large modeling errors and deteriorate the performance of head positioning servo systems. Thus, it is highly desired to completely characterize the behaviors of nonlinearities and friction in HDD servo systems. This is exactly what we are going to do in this chapter. This chapter presents a comprehensive modeling of a typical voice-coil-motor (VCM) actuator used in commercial hard disk drives. The basic idea here is to carefully examine the configuration and structure of the system through a thorough analysis of its physical effects, and then identify the structured model parameters using both time-domain and frequency-domain responses of the system. Experimental verification will show that the identified model matches very well the actual behavior of the physical system.

4.1 Introduction

Presently, HDD servo systems popularly use a VCM motor to actuate the read/write (R/W) recording arm assembly, which consists of a pivot with a ball bearing, a metal arm and a rigid suspension that holds the read/write head and slider (see Figure 4.1). The VCM motor is a DC motor that translates an input electric current into a force or acceleration as its output. Its frequency domain response without considering friction and nonlinearities matches very well to that of a double integrator (see *e.g.*, [12]) at low frequency range, typically from DC to somewhere around 1–2 kHz, and has many high frequency resonant modes.

Current trend of the HDD industry is towards smaller disk drives with higher capacity, for increasing applications in mobile environment. The new generation HDDs impose more stringent specification on the corresponding servo systems. Due to the smaller inertia of the VCM arm assembly, nonlinear effects, such as pivot bearing friction and flex cable nonlinearity, now become influential. It has been observed that nonlinearities from friction in the rotary pivot bearing and bias torque of the data flex cable in the VCM actuator may generate large residual errors and high frequency oscillations which eventually deteriorate the overall performance of head positioning servo systems. This phenomenon becomes more noticeable for micro disk drives and is one of the challenges in servo design for the new generation HDDs. The impetus to fully understand the behaviors of nonlinearities and friction in the servo systems is obvious. Actually, this motivates us to carry out a complete study and comprehensive modeling of the dynamic characteristics for the VCM actuated HDD head positioning servo systems.

Friction exists in almost all servomechanisms, behaves in features of Stribeck effect, hysteresis, stiction and varying break-away force, and appears at the physical interface between two contact surfaces moving relative to each other. The features of friction have

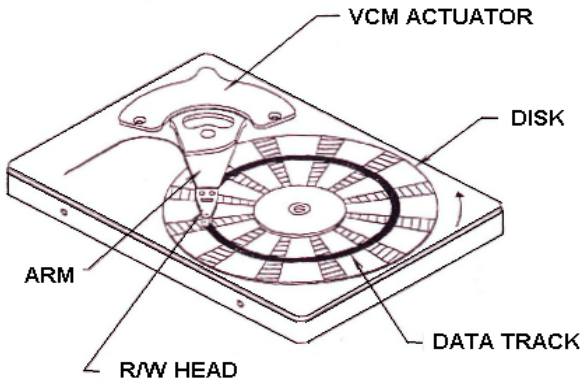

Figure 4.1: A typical HDD with a VCM actuator servo system.

been extensively explored (see *e.g.*, [3–6, 27, 49, 51–53]), but diversity exists in different systems. In recent years, there has been a significantly increased interest in friction from the industries, which is driven by strong engineering needs in a wide range of industries and availability of both precise measurement and advanced control techniques.

Although many research efforts have been directed to the modeling and control of HDD servo systems, there are only limited reports concerned with the pivot bearing friction (see *e.g.*, [1, 8, 29, 36, 37, 46, 64–66, 73]). It may be worthwhile to mention that, Wang et al. [64–66] studied the frictional nonlinearity in a small disk drive and proposed several models for it, i.e., two-preload, preload+2-slope spring, hysteretic 2-slope, and preload+hysteretic damping. These models are basically the revision and/or combination of existing classical friction models, and capture the characteristics of friction, more or less. However, they are mainly based on empirical modeling and experimental fitting and can barely provide theoretical insights into the nonlinearity mechanism of the disk drive actuator.

As for modeling methodologies for dynamic systems, one can see that diverse modeling methods have been proposed (see *e.g.*, [24, 47]), based on linear systems, where nonlinearities of plants are assumed to be tiny and negligible. As such, these methods cannot be directly applied to model plants with significant nonlinearities. The method proposed in [4] to estimate the parameters of friction in typical DC motors, is inappropriate for the VCM

actuator because of insufficient information available in HDD servo systems, in which only the relative displacement of the R/W head is measurable. One of the key steps to model systems with nonlinearities is to determine the physical structures of the nonlinear components. In this chapter, we will utilize the physical effect approach of [18] to determine the structures of nonlinearities and friction associated with the VCM actuator in a typical HDD servo system. This will be done by carefully examining and analyzing physical effects that occur in or between electromechanical parts. This process will give us a physical model of the VCM actuator, but its parameters still wait to be identified. And the headache with parameter identification over here is that there is generally no analytical solution for nonlinear differential equations, and the conventional parameter optimization techniques (such as Least Square, or Gradient-based ones) are not readily applicable in a non-LIP (linear in parameter) model. To circumvent this difficulty, we will employ a Monte Carlo process (see *e.g.*, [20, 22, 50]) to identify parameters in the structured model. We note that Monte Carlo method is very effective in approximating solutions to a variety of mathematical problems, for which their analytical solutions are hard, if not impossible, to be determined. In summary, physical effect analysis will be used to configure the structures of the nonlinearities in the VCM actuator and the Monte Carlo method will be used to identify the parameters in the structured model. After that, simulation and implementation results will be given to show that the identified model characterizes very well the behavior of the actual system.

The outline of this chapter is as follows. The structural models of nonlinearities in the VCM actuator will be determined through the physical effect analysis in Section 4.2. The parameters in the nonlinear models will then be identified using the Monte Carlo method in Sections 4.3. The verification to evaluate the obtained model will be presented in Section 4.4. Finally, we draw some concluding remarks in Section 4.5.

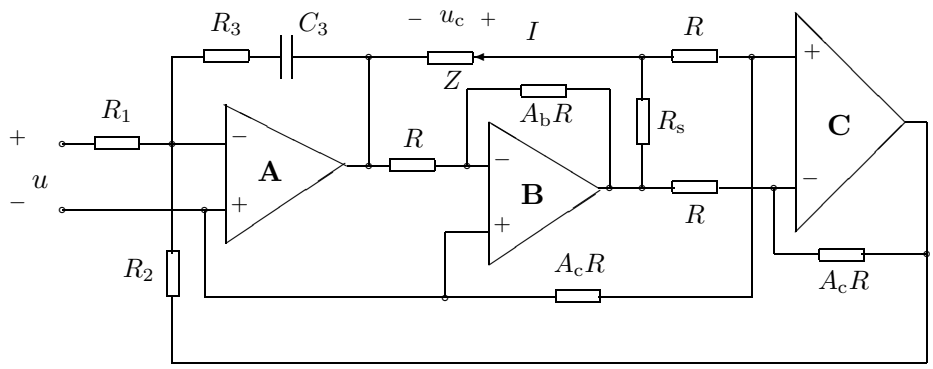

Figure 4.2: The electric circuit of a typical VCM driver.

4.2 Structural Modeling of the VCM Actuator

In this section, the physical effect analysis of [18] is used to determine the structures of nonlinearities in the VCM actuator. It is to analyze the physical effects in and between the components of the actuator, such as the stator, rotor and support plane as well as the VCM driver. The VCM actuator is designed to position the R/W head fast and precisely onto the target track, and is driven by a VCM driver, i.e., a full bridge power amplifier, which converts an input voltage into an electric current. The electric circuit of a typical VCM driver is shown in Figure 4.2, where Z represents the coil of the VCM actuator and the external input voltage is exerted directly into the VCM driver to drive the coil.

Through a detailed analysis of the VCM driver circuit in Figure 4.2, we can verify that the relationship between the driver input voltage and the current and voltage of the VCM coil is given by

$$\frac{R_s + (1+A_c)(1+A_b)R}{R_s A_c (1+A_c)(1+A_b)R} \cdot \frac{R_2}{R_1} u = \frac{1 + s\left(R_3 + \frac{R_2}{A_c + A_c A_b}\right) C_3}{1 + sR_3C_3} I + \mathcal{E}(s) u_c, \tag{4.1}$$

where

$$\mathcal{E}(s) = \frac{A_b}{(1+A_c)(1+A_b)R} \frac{1 + s\left[R_3 + \frac{R_2}{A_c A_b}\left(1 + \frac{R + RA_c}{R_s}\right)\right] C_3}{1 + sR_3C_3}, \tag{4.2}$$

u is the input voltage to the VCM driver, I and u_c are respectively the VCM coil current and voltage. $R_s \doteq 1$ ohm is a resistor sampling electric current in the coil. A_c and A_b are

the amplification ratios of the amplifier C and B respectively. $R_i (i = 1, 2, 3)$ and R are resistors. C_3 is a capacitor. With appropriate values of the resistors and the capacitor, the effect of the load can be neglected in the VCM driver to make the electric current proportional to the input voltage within the bandwidth of interest. For the IBM microdrive (DMDM-10340) used in our experimental tests in the later sections, $R_\mathrm{s} = 1\Omega$, $R_1 = 8.2$ KΩ, $R_2 = 1$ KΩ, $R_3 = 270$ KΩ, $R = 16$ KΩ, $C_3 = 270$ pF, and the amplifier gains $A_\mathrm{c} = 2$ and $A_\mathrm{b} = 4.7$. Thus, we have

$$\mathcal{E}(s) = \frac{1.7178 \times 10^{-5} \left(1 + 1.45 \times 10^{-3} s\right)}{1 + 7.29 \times 10^{-5} s},$$

which has a magnitude response ranging from -95 dB (for frequency less than 110 Hz) to -69 dB (for frequency greater than 2.2 kHz). In fact, this property generally holds for all commercial disk drives. As such, the effect of $\mathcal{E}(s)$ in (4.1) can be neglected and the relationship in (4.1) can be safely approximated as the following:

$$I = \frac{R_2}{A_\mathrm{c} R_1 R_\mathrm{s}} u = k_\mathrm{vd} u, \tag{4.3}$$

where $k_\mathrm{vd} = 0.061\mho$ is the gain of the VCM driver used in IBM DMDM-10340 microdrives.

Now let us turn to the VCM actuator assembly. The mechanical structure of a typical VCM actuator is shown in Figure 4.3. The motion of the VCM coil is driven by a permanent magnet similar to typical DC motors. The stator of the VCM motor is built of a permanent magnet. The rotor consists of a coil, a pivot and a metal arm on which the R/W head is attached. A data flex cable is connected with the R/W head through the metal arm to transfer data read from or written to the HDD discs. Typically, the rotor has a deflection angle, α, in rad (see Figure 4.3). The range of the rotor is constrained, typically up to 0.5 rad in most commercial disk drives.

Before proceeding to further derivation, we make the following assumptions on the physical system :

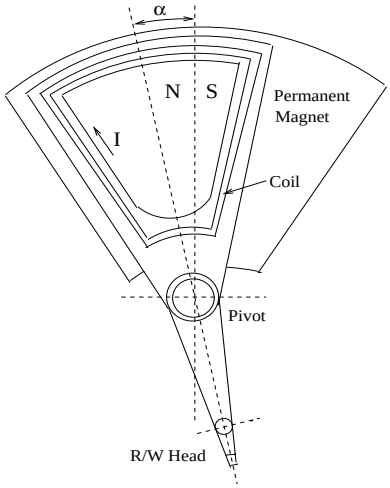

Figure 4.3: The mechanical structure of a typical VCM actuator.

1. The permanent magnet is constant; and

2. The coil is assembled strictly along the radius and concentric circle of the pivot;

Furthermore, we assume that the friction in a mechanical motion consists of Coloumb friction and viscous damping, and is characterized by a typical friction function as the following (see *e.g.*, [3, 27, 52]):

$$f(N, v, f_{\rm e}, f_{\rm v}, \mu_{\rm d}, \mu_{\rm s}) = \begin{cases} -\mu_{\rm d} N \ \mathrm{sgn}(v) - f_{\rm v} v, & v \neq 0, \\ -f_{\rm e}, & v = 0 \text{ and } |f_{\rm e}| \leq \mu_{\rm s} N, \\ -\mu_{\rm s} N \ \mathrm{sgn}(f_{\rm e}), & v = 0 \text{ and } |f_{\rm e}| > \mu_{\rm s} N, \end{cases} \tag{4.4}$$

where N is the normal load and v is the relative moving speed between two contact surfaces, $f_{\rm e}$ is the external force applied to the object, and $\mu_{\rm s} N$ is the break-away force. Furthermore, $\mu_{\rm d}$, $\mu_{\rm s}$ and $f_{\rm v}$ are respectively the dynamic, static and viscous coefficients of friction.

These assumptions are important as they enable us to derive a mathematically tractable model for the VCM actuator.

By physical law, the force $d\overrightarrow{F}$ is produced in the section with length dl in the coil with the electric current $\overrightarrow{I}$ by the permanent magnet $\overrightarrow{B}$ as follows:

$$d\overrightarrow{F} = \overrightarrow{I} \times \overrightarrow{B} \cdot dl.$$

As such for the whole coil, the cooperative force $\overrightarrow{F}$ is

$$\overrightarrow{F} = \int_{Coil+\alpha} \overrightarrow{I} \times \overrightarrow{B} \cdot dl, \tag{4.5}$$

where $Coil + \alpha$ means the rotor has deflected by α radians. The cooperative force can be decomposed into two orthogonal components. One ($\overrightarrow{F}_r$) is outwards along direction of the radius of the pivot and the other ($\overrightarrow{F}_t$) is anti-clockwise along the tangent of the pivot.

$$\overrightarrow{F} = \overrightarrow{F}_r + \overrightarrow{F}_t. \tag{4.6}$$

The torque $d\overrightarrow{T}$ is produced by $d\overrightarrow{F}$ relative to the center of the pivot as follows:

$$d\overrightarrow{T} = \overrightarrow{r} \times d\overrightarrow{F} = \overrightarrow{r} \times (\overrightarrow{I} \times \overrightarrow{B} \cdot dl),$$

where $\overrightarrow{r}$ is the vectored distance from the center of the pivot to the section with length dl in the coil. There only the component $\overrightarrow{F}_t$ produces the torque relative to the center of the pivot. For the whole coil, the torque $\overrightarrow{T}$ is

$$\overrightarrow{T} = \int_{Coil+\alpha} \overrightarrow{r} \times (\overrightarrow{I} \times \overrightarrow{B} \cdot dl). \tag{4.7}$$

Now, it is straightforward to derive that the torque T_{m}, relative to center of the pivot (along anti-clockwise is positive) and produced by the permanent magnet B_{coil} in the coil with the electric current, is given by

$$T_{\mathrm{m}} = (r_1^2 - r_2^2) B_{\mathrm{coil}} n_{\mathrm{coil}} k_{\mathrm{vd}} u, \tag{4.8}$$

r_1 and r_2 are respectively the outside and inside radius of the coil to center of the pivot, and n_{coil} is number of windings of the coil. The total external torque T_{e} applied to the VCM rotor is given as follows:

$$T_{\mathrm{e}} = T_{\mathrm{m}} - T_{\mathrm{c}}(\alpha), \tag{4.9}$$

where $T_{\mathrm{c}}(\alpha)$ is the spring torque produced by the data flex cable and is a function of the deflection angle α or the displacement of the R/W head. The friction torque produced in

the VCM actuator comes from two major sources: One is the friction in the pivot bearing and the other is between the pivot bearing and the support plane. The friction torque in the pivot bearing can be characterized as

$$T_{\mathrm{f1}} = f(N_1, r_3\dot{\alpha}, f_{\mathrm{e1}}, f_{\mathrm{v1}}, \mu_{\mathrm{d1}}, \mu_{\mathrm{s1}})r_3, \tag{4.10}$$

where f_{e1} is the external force, f_{v1}, μ_{d1} and μ_{s1} are the related friction coefficients as defined in (4.4), r_3 is the radius of the pivot to its center, and

$$N_1 = \left|F_{\mathrm{r}} + m_{\mathrm{r}}\dot{\alpha}^2\right|, \tag{4.11}$$

is the normal load, which consists of the centrifugal force $m_{\mathrm{r}}\dot{\alpha}^2$ of the rotor and the cooperative force F_{r}. Overhere, m_{r} is a constant dependent on the mass distribution of the rotor, and

$$F_{\mathrm{r}} = 2(r_1 - r_2)B_{\mathrm{coil}}n_{\mathrm{coil}}k_{\mathrm{vd}}u\alpha, \tag{4.12}$$

is the force produced in the coil by the permanent magnet and along the radius of the pivot bearing. The friction torque between the pivot bearing and the support plane can be characterized as:

$$T_{\mathrm{f2}} = f(N_2, r_3\dot{\alpha}, f_{\mathrm{e2}}, f_{\mathrm{v2}}, \mu_{\mathrm{d2}}, \mu_{\mathrm{s2}})r_3, \tag{4.13}$$

where f_{e2} is the external force, f_{v2}, μ_{d2} and μ_{s2} are the related friction coefficients as defined in (4.4), and

$$N_2 = |T_0|r_3^{-1}, \tag{4.14}$$

where N_2 is the normal load resulted from a static balance torque of the rotor, T_0. Thus, the total friction torque T_{f} produced in the VCM actuator is given by

$$T_{\mathrm{f}} = T_{\mathrm{f1}} + T_{\mathrm{f2}} = \begin{cases} -T_{\mathrm{v}}, & \dot{\alpha} \neq 0, \\ -T_{\mathrm{e}}, & \dot{\alpha} = 0 \text{ and } |T_{\mathrm{e}}| \leq T_{\mathrm{s}}, \\ -T_{\mathrm{s}}\ \mathrm{sgn}(T_{\mathrm{e}}), & \dot{\alpha} = 0 \text{ and } |T_{\mathrm{e}}| > T_{\mathrm{s}}, \end{cases} \tag{4.15}$$

where

$$T_{\rm v} = \left(\mu_{\rm d1}\left|2(r_1-r_2)B_{\rm coil}n_{\rm coil}k_{\rm vd}u\alpha + m_{\rm r}\dot{\alpha}^2\right|r_3 + \mu_{\rm d2}|T_0|\right)\mathrm{sgn}(\dot{\alpha}) + (f_{\rm v1}+f_{\rm v2})r_3^2\dot{\alpha}, \quad (4.16)$$

and

$$T_{\rm s} = 2\mu_{\rm s1}\left|(r_1-r_2)B_{\rm coil}n_{\rm coil}k_{\rm vd}u_0\alpha_0\right|r_3 + \mu_{\rm s2}|T_0|, \quad (4.17)$$

is the break-away torque, and where u_0 and α_0 are respectively the corresponding input voltage and the deflection angle for the situation when $\dot{\alpha}=0$.

Lastly, it is simple to verify that the relative displacement of the R/W head, y, is given by

$$y = 2r_4\sin\frac{\alpha}{2} \approx r_4\alpha, \quad (4.18)$$

where r_4 is the length from the R/W head to the center of the pivot. Following the Newton's law of motion, $J\ddot{\alpha} = T_{\rm e} + T_{\rm f}$, where J is the moment of inertia of the VCM rotor, we have

$$\ddot{y} = bu - \tilde{T}_{\rm c} + \tilde{T}_{\rm f}, \quad (4.19)$$

where

$$\tilde{T}_{\rm f} = \begin{cases} -\left(\left|d_1buy + d_2\dot{y}^2\right| + d_3\right)\mathrm{sgn}(\dot{y}) - d_0\dot{y}, & \dot{y}\neq 0, \\ -\tilde{T}_{\rm e}, & \dot{y}=0 \text{ and } |\tilde{T}_{\rm e}|\leq \tilde{T}_{\rm s}, \\ -\tilde{T}_{\rm s}\ \mathrm{sgn}(\tilde{T}_{\rm e}), & \dot{y}=0 \text{ and } |\tilde{T}_{\rm e}|> \tilde{T}_{\rm s}, \end{cases} \quad (4.20)$$

and where

$$\left.\begin{aligned}
\tilde{T}_{\rm e} &= -\tilde{T}_{\rm c}(y) + bu,\\
\tilde{T}_{\rm s} &= d_4 b|u_0 y_0| + d_5,\\
\tilde{T}_{\rm c} &= J^{-1} r_4 T_{\rm c}(\alpha),\\
b &= J^{-1} r_4 (r_1^2 - r_2^2) B_{\rm coil} n_{\rm coil} k_{\rm vd},\\
d_0 &= J^{-1}(f_{\rm v1} + f_{\rm v2}) r_3^2,\\
d_1 &= 2 r_3 \mu_{\rm d1} [r_4(r_1 + r_2)]^{-1},\\
d_2 &= r_3 m_{\rm r} \mu_{\rm d1} (J r_4)^{-1},\\
d_3 &= J^{-1} r_4 \mu_{\rm d2} |T_0|,\\
d_4 &= 2 r_3 \mu_{\rm 1s} [r_4(r_1 + r_2)]^{-1},\\
d_5 &= J^{-1} r_4 \mu_{\rm 2s} |T_0|,
\end{aligned}\right\} \tag{4.21}$$

with u_0 and y_0 being respectively the corresponding input voltage and the displacement for the case when $\dot{y} = 0$. It is clear now that the expressions in (4.19)–(4.21) give a complete structure of the VCM model including pivot bearing friction and nonlinearities from the data flex cable. Our next task is to identify all these parameters. Once again, we use an IBM microdrive (DMDM-10340) in our experimental test.

4.3 Identification of the Model Parameters

We proceed to identify the parameters of the VCM actuator model given in (4.19)-(4.21). We note that there are results available in the literature (see *e.g.*, [4]) to estimate friction parameters for typical DC motors for which both velocity and displacement are measurable and without constraint. Unfortunately, for the VCM actuator studied here, it is impossible to measure the time responses in constant velocity motions and only the relative displacement of the R/W head is measurable. As such, the method of [4] cannot be adopted to solve our problems. Instead, we will employ the popular Monte Carlo method (see *e.g.*, [20, 22, 50]), which has been widely used in solving engineering problems and is capable of providing

good numerical solutions.

First, it is simple to obtain from (4.19) at a steady state when $\dot{y} = 0$ and $\ddot{y} = 0$,

$$|u_0 - b^{-1}\tilde{T}_{\rm c}(y_0)| = b^{-1}|\tilde{T}_{\rm f}| \leq b^{-1}\tilde{T}_{\rm s} = d_4|u_0 y_0| + b^{-1}d_5. \tag{4.22}$$

Our experimental results show that the right hand side of (4.22) is very insignificant for small input signal u_0 and small displacement y_0. This will be confirmed later when the model parameters are fully identified. Thus, we have

$$u_0 \approx b^{-1}\tilde{T}_{\rm c}(y_0) := \tilde{T}_{\rm bc}(y_0), \tag{4.23}$$

which will be used to identify $\tilde{T}_{\rm c}(y)$ or equivalently $T_{\rm c}(\alpha)$, the spring torque produced by the data flex cable. Next, for the small neighborhood of (u_0, y_0), we can rewrite the dynamic equation of (4.19) as follows:

$$\ddot{y} = -\left.\frac{\partial \tilde{T}_{\rm c}}{\partial y}\right|_{y=y_0}(y - y_0) + b(u - u_0) + \tilde{T}_{\rm f}. \tag{4.24}$$

For small signals and by omitting the nonlinear terms, the dynamic equation (4.24) can be approximated by the following transfer function (from $u - u_0$ to $y - y_0$):

$$G_{y_0,u_0}(s) = \frac{b}{s^2 + d_0 s + \omega_{\rm p}^2}, \tag{4.25}$$

where its natural or roughly its peak frequency, $\omega_{\rm p}$, is given by

$$\omega_{\rm p} = \left(\left.\frac{\partial \tilde{T}_{\rm c}}{\partial y}\right|_{y=y_0}\right)^{\frac{1}{2}}, \tag{4.26}$$

and its static gain is given by $k_{\rm dc} = b\omega_{\rm p}^{-2}$, which implies that

$$b = k_{\rm dc}\omega_{\rm p}^2 = 4\pi^2 k_{\rm dc} f_{\rm p}^2, \tag{4.27}$$

where $f_{\rm p} = \omega_{\rm p}/(2\pi)$. Expression (4.27) will be used to estimate the parameter b. More specifically, the parameters of the dynamic models of the VCM actuator will be identified using the following procedure:

1. The nonlinear characteristics of the data flex cable or equivalently $\tilde{T}_{\rm bc}(y)$ will be initially determined using (4.23) with a set of input signal, u_0, and its corresponding output displacement, y_0. It will be fine tuned later using the Monte Carlo method.

2. The parameter b will be initially computed using measured static gains and peak frequencies as in (4.27), resulting from the dynamical responses of the actuator to a set of small input signals. Again, the identified parameter will be fine tuned later using the Monte Carlo method.

3. All system parameters will then be identified using the Monte Carlo method to match the frequency response to small input signal;

4. The high frequency resonant modes of the actuator, which have not been included in either (4.19) or (4.24), will be determined from frequency responses to input signals at high frequencies.

The above procedure will yield a fairly complete and comprehensive model including nominal dynamics, high frequency resonant modes, friction and nonlinearities of the VCM actuator. As mentioned earlier, an IBM microdrive (DMDM-10340) is chosen in our experimental test. In our experiments, the relative displacement of the R/W head is the only measurable output and is measured using a Laser Doppler Vibrometer (LDV). A dynamic signal analyzer (DSA) (Model SRS 785) is used to measure the frequency responses of the VCM actuator. The DSA is also used to record both input and output signals of time-domain responses. Square waves are generated with a dSpace DSP board installed in a personal computer. The overall experimental setup is depicted in Figure 4.4.

The time-domain response of the VCM actuator to a typical square input signal about 1Hz is shown in Figure 4.5. With a group of time-domain responses to a set of square input signals, we obtain the corresponding measurement data for the nonlinear function, $\tilde{T}_{\rm bc}(y_0)$,

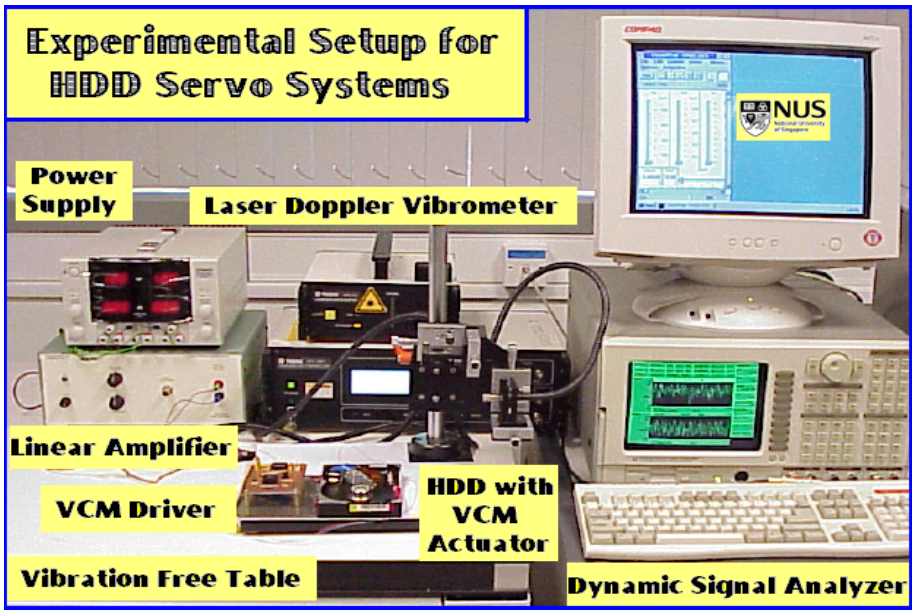

Figure 4.4: The experimental setup.

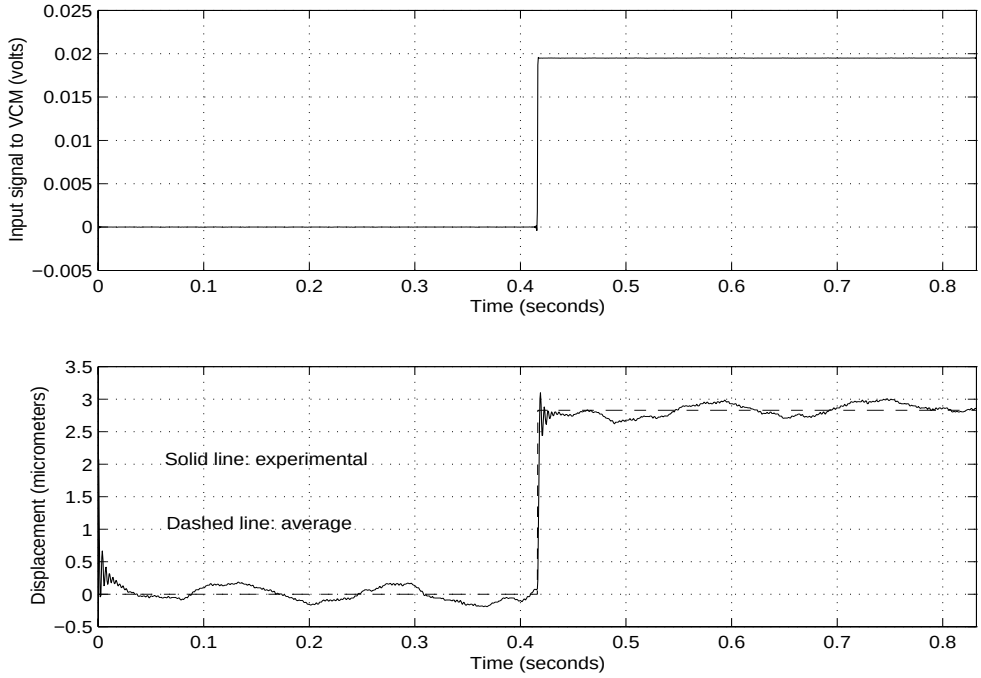

Figure 4.5: Time-domain response of the VCM actuator to a square wave input.

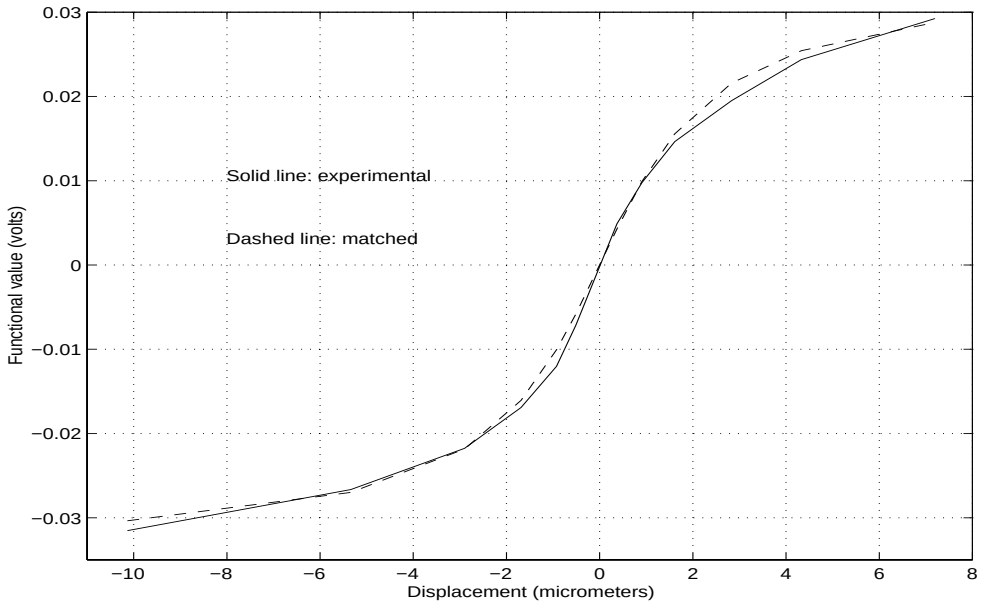

Figure 4.6: Nonlinear characteristics of the data flex cable.

which can be matched pretty nicely by an arctan function (see Figure 4.6) as the following:

$$\tilde{T}_{\rm bc}(y) = a \arctan(cy), \tag{4.28}$$

where $a = 21.8748 \times 10^{-3}$ and $c = 0.5351$. These parameters will be further fine tuned later in the Monte Carlo process.

Next, by fixing a particular input offset point u_0 and by injecting on top of u_0 a sweep of small sinusoidal signals with an amplitude of 1 mV, we are able to obtain a corresponding frequency response within the range of interest. It then follows from (4.27) that the values of the static gain, $k_{\rm dc}$, and peak frequency, $f_{\rm p}$, of the frequency response can be used to estimate the parameter, b. Figure 4.7 shows the frequency response of the system for the pair $(u_0, y_0) = (0, 0)$, which gives a static gain of 63.71 and a peak frequency of 305.24 Hz. In order to obtain a more accurate result, we repeat the above experimental tests for several pairs (u_0, y_0) and the results are shown in Table 4.1. The parameter, b, can then be more accurately determined from these data using a least square fitting,

$$\min_b \sum_{i=1}^{7} \left[b - k_{{\rm dc},i} \omega_{{\rm p},i}^2 \right]^2, \tag{4.29}$$

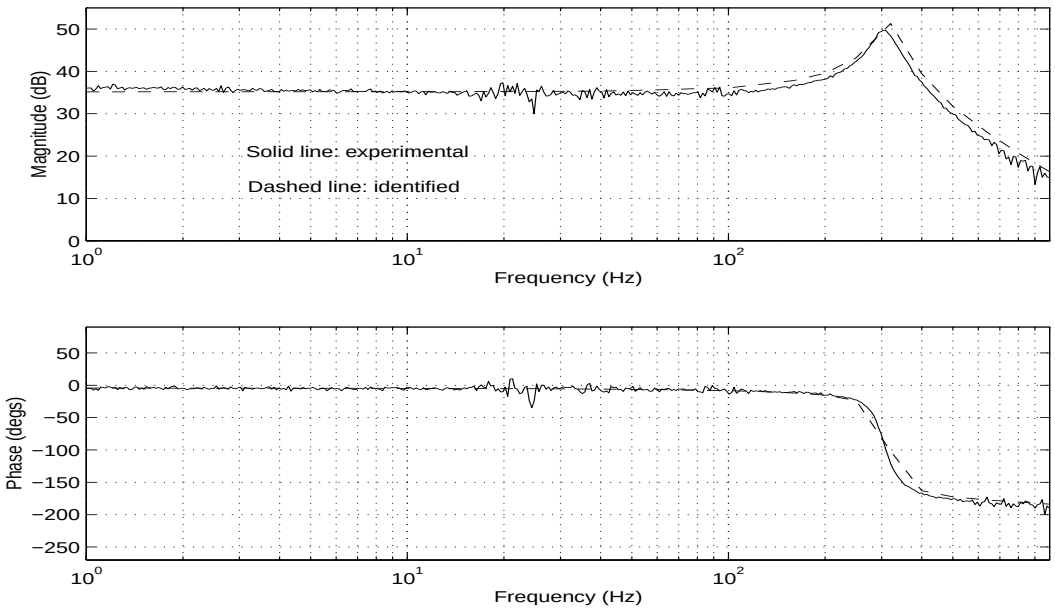

Figure 4.7: Frequency response to small signals at the steady state with $u_0 = 0$.

Table 4.1: Static gains and peak frequencies of the actuator for small inputs.

u_0 (mV)	-10	-5	0	5	10	15	20
$k_{\rm dc}$	60.73	59.06	63.71	62.43	63.72	65.12	65.50
$f_{\rm p}$ (Hz)	310.30	310.63	305.24	303.88	299.56	296.99	295.43

which gives an optimal solution $b = 2.28 \times 10^8$. Nonetheless, this parameter will again be fine tuned later in the Monte Carlo process.

Lastly, we apply a Monte Carlo process to identify all other parameters of our VCM actuator model and to fine tune those parameters, which have previously been identified. Monte Carlo processes are known as numerical simulation methods, which make use of random numbers and probability statistics to solve some complicated mathematical problems. The detailed treatments of Monte Carlo methods vary widely from field to field. Originally, a Monte Carlo experiment means to use random numbers to examine some stochastic problems. The idea can be extended to deterministic problems by pre-setting some parameters and conditions of the problems. The use of Monte Carlo methods for modeling physical

systems allows us to solve more complicated problems than we otherwise can, and provides approximate solutions to a variety of mathematical problems, whose analytical solutions are hard, if not impossible, to be derived. In what follows, a Monte Carlo process is utilized to obtain time-domain responses of the VCM actuator model in (4.19) with a set of pre-setting parameters $(b, a, c, d_0, d_1, d_2, d_3, d_4, d_5)$ and input signals. The corresponding frequency responses can then be obtained through Fourier transformation of the obtained time-domain responses. Our idea of using the Monte Carlo process is to minimize the differences between simulated frequency responses and the experimental ones by iteratively adjusting the parameters of the physical model in (4.19). The input signals in our simulations are again a combination of an offset u_0 and sinusoidal signals with a small amplitude 1 mV and several frequencies ranging from 1 Hz to 1 kHz.

Although Monte Carlo methods can only give locally minimal solutions, in our problem, however, the pre-determined nonlinear characteristics of the data flex cable and the parameter, b, have given us a rough idea on what the true solution should be. The solution within the neighborhood of the previously identified parameters is given by

$$\left.\begin{aligned} b &= 2.35 \times 10^8 \ \mu\text{m} \ / \ (\text{V}{\cdot}\text{s}^2), \\ a &= 0.02887 \ \text{V}, \\ c &= 0.5886 \ (\mu\text{m})^{-1}, \\ d_0 &= 282.6 \ \text{s}^{-1}, \\ d_1 &= 0.005 \ (\mu\text{m})^{-1}, \\ d_2 &= 0.01 \ (\mu\text{m})^{-1}, \\ d_3 &= 1.5 \times 10^4 \ \mu\text{m} \ / \ \text{s}^2, \\ d_4 &= 0.0055 \ (\mu\text{m})^{-1}, \\ d_5 &= 1.65 \times 10^4 \ \mu\text{m} \ / \ \text{s}^2. \end{aligned}\right\} \tag{4.30}$$

These parameters will be used for further verifications using the experimental setup of the actual system.

So far, we have been focusing on the low frequency components of the VCM actuator model. In fact, there are many high frequency resonant modes, which are crucial to the overall performance of HDD servo systems. The high frequency resonant modes of the VCM actuator can be obtained from frequency responses of the system in high frequency region (see *e.g.*, Figure 4.8). The transfer function that matches the responses given in Figure 4.8 is identified as follows:

$$G(s) = \frac{2.35 \times 10^8}{s^2} G_{\text{r.m.}}(s) \tag{4.31}$$

with the resonant modes being given as

$$G_{\text{r.m.}}(s) = G_{\text{r.m.1}}(s) G_{\text{r.m.2}}(s) G_{\text{r.m.3}}(s) G_{\text{r.m.4}}(s) G_{\text{r.m.5}}(s), \tag{4.32}$$

where

$$G_{\text{r.m.1}}(s) = \frac{0.8709 s^2 + 1726 s + 1.369 \times 10^9}{s^2 + 1480 s + 1.369 \times 10^9}, \tag{4.33}$$

$$G_{\text{r.m.2}}(s) = \frac{0.9332 s^2 - 805.8 s + 1.739 \times 10^9}{s^2 + 125.1 s + 1.739 \times 10^9}, \tag{4.34}$$

$$G_{\text{r.m.3}}(s) = \frac{1.072 s^2 + 925.1 s + 1.997 \times 10^9}{s^2 + 536.2 s + 1.997 \times 10^9}, \tag{4.35}$$

$$G_{\text{r.m.4}}(s) = \frac{0.9594 s^2 + 98.22 s + 2.514 \times 10^9}{s^2 + 1805 s + 2.514 \times 10^9}, \tag{4.36}$$

and

$$G_{\text{r.m.5}}(s) = \frac{7.877 \times 10^9}{s^2 + 6212 s + 7.877 \times 10^9}. \tag{4.37}$$

Finally, for easy reference, we conclude this section by explicitly expressing the identified rigid model of VCM actuator:

$$\ddot{y} = 2.35 \times 10^8 u - 6.78445 \times 10^6 \arctan(0.5886 y) + \tilde{T}_{\text{f}}, \tag{4.38}$$

where

$$\tilde{T}_{\text{f}} = \begin{cases} -\left(\left|1.175 \times 10^6 u y + 0.01 \dot{y}^2\right| + 1.5 \times 10^4\right) \operatorname{sgn}(\dot{y}) - 282.6 \dot{y}, & \dot{y} \neq 0, \\ -\tilde{T}_{\text{e}}, & \dot{y} = 0 \text{ and } |\tilde{T}_{\text{e}}| \leq \tilde{T}_{\text{s}}, \\ -\tilde{T}_{\text{s}} \operatorname{sgn}(\tilde{T}_{\text{e}}), & \dot{y} = 0 \text{ and } |\tilde{T}_{\text{e}}| > \tilde{T}_{\text{s}}, \end{cases} \tag{4.39}$$

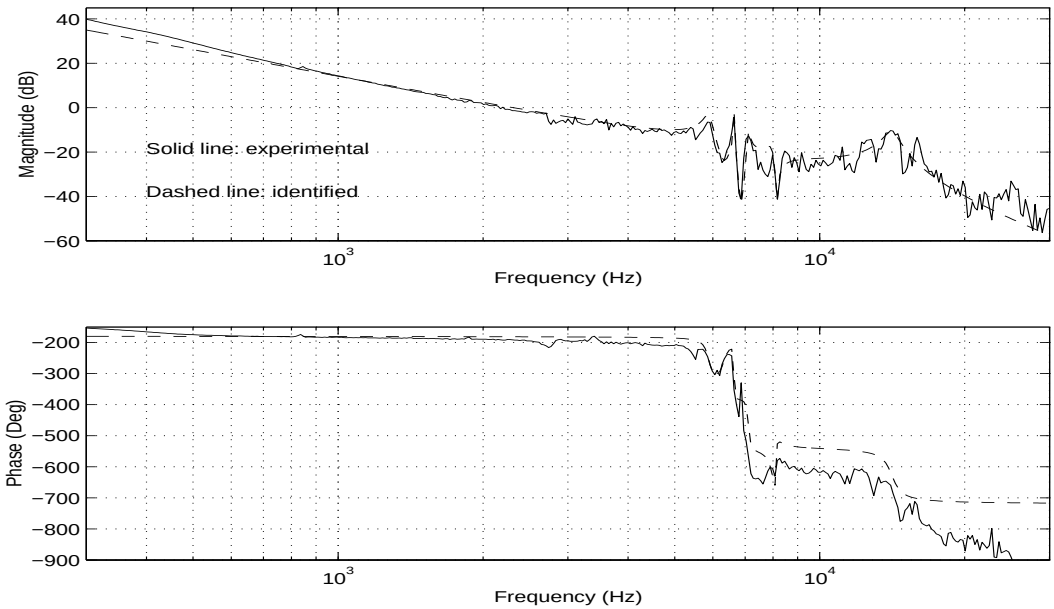

Figure 4.8: Frequency responses of the VCM actuator in the high frequency region.

and where

$$\tilde{T}_{\rm e} = 2.35 \times 10^8 \Big[u - 0.02887 \arctan\left(0.5886 y\right) \Big], \tag{4.40}$$

$$\tilde{T}_{\rm s} = 1.293 \times 10^6 |u_0 y_0| + 1.65 \times 10^4, \tag{4.41}$$

with u_0 and y_0 being respectively the corresponding input voltage and the displacement for the case when $\dot{y} = 0$. Note that in the above model, the input signal u is in voltage and the output displacement y is in micrometer. Together with high frequency resonant modes of (4.33)–(4.37), the above model presents a fairly comprehensive description of the dynamic characteristics of the VCM actuator studied. This model will be further verified using experimental tests on the actual system.

4.4 Model Verification

In order to verify the validity of the established model of the VCM actuator, we carry out a series of comparisons between the experimental results and computed results of the time-domain responses and frequency-domain responses of the actuator. The comparison of the frequency responses between experimental result and identified result is shown in

Figure 4.9. It clearly shows that the result of the identified model matches pretty well with the experimental result. The comparison of the time-domain responses is given in Figure 4.10, which shows that the simulation results typically match the trends and values of those obtained from experiments. The small fluctuations associated with experimental results are due to drift noises caused by the LDV and/or DSA.

The friction torques from simulation are shown in Figures 4.11 and 4.12, which are generated with sinusoidal input signals with an amplitude of 1 mV and frequencies at 1, 10, 100 and 200 Hz, respectively. Figure 4.11 shows the friction torques corresponding to various input signals, while Figure 4.12 shows the relationship between the equivalent friction torque and velocity of the R/W head as well as the relationship between the equivalent friction torque and equivalent external torque for the 10 Hz sinusoidal input signal. Note that the right half of Figure 4.12 provides a close-up for important details. The results clearly show the typical features of friction, such as stiction, Stribeck effect and hysteresis. With such information, we can analyze the trend of the motion. In the right-bottom corner of Figure 4.14, line AB means the R/W head is not moving. The friction torque has a mutation in point B to become smaller as the R/W head begins to move, and is increasing gradually corresponding to the increase of the velocity of the head. Once the friction torque exceeds the external torque, the head will decrease its velocity, which in turn causes the friction torque to decrease. There are several reversions of acceleration before the head gets stuck again (back to the neighborhood of point A). Such phenomenon is typical of stick-slip motion.

The comparisons of both frequency-domain and time-domain responses and the analysis on features of friction demonstrate that the identified model indeed describes the comprehensive features of the dynamics of the VCM actuator.

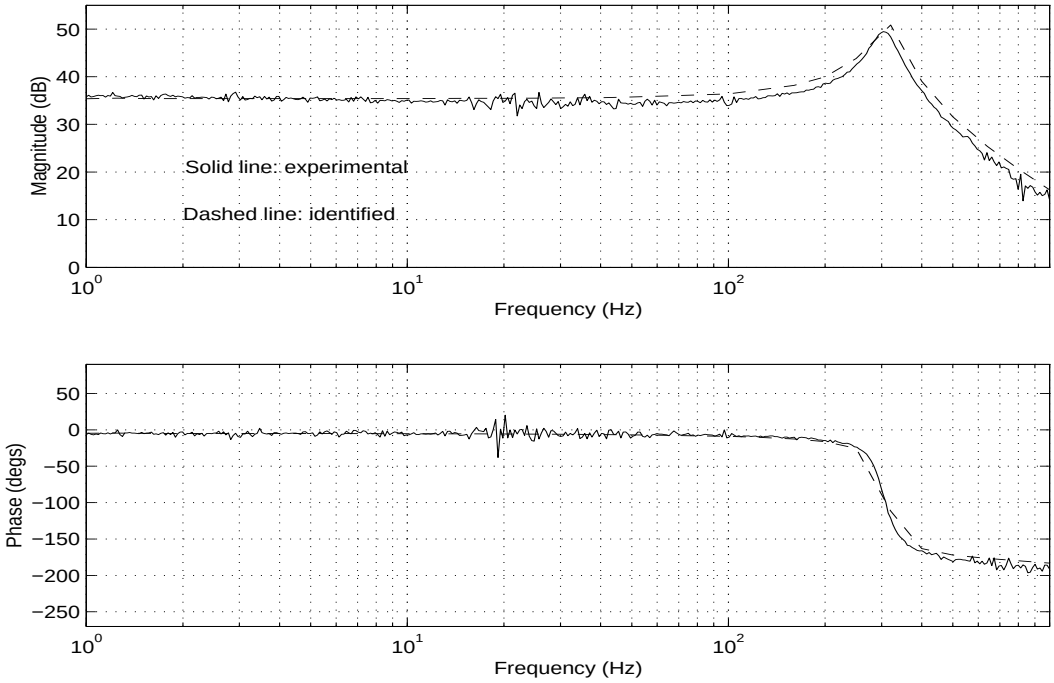

a) $u_0 = 5$ mV.

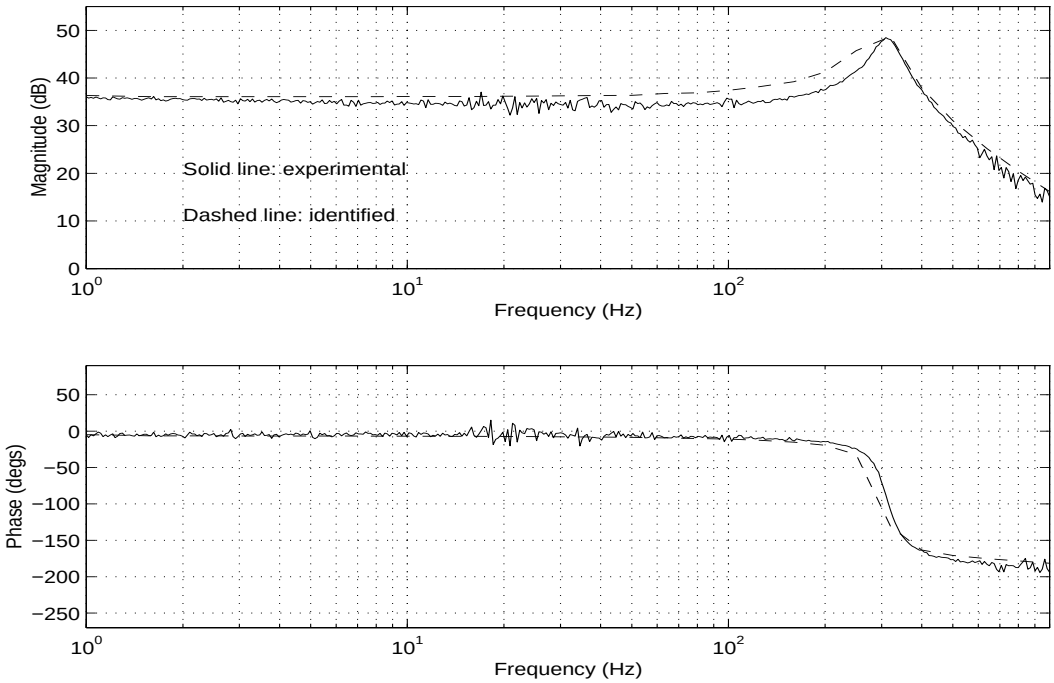

b) $u_0 = -10$ mV.

Figure 4.9: Comparison of frequency responses to small signals of the VCM actuator.

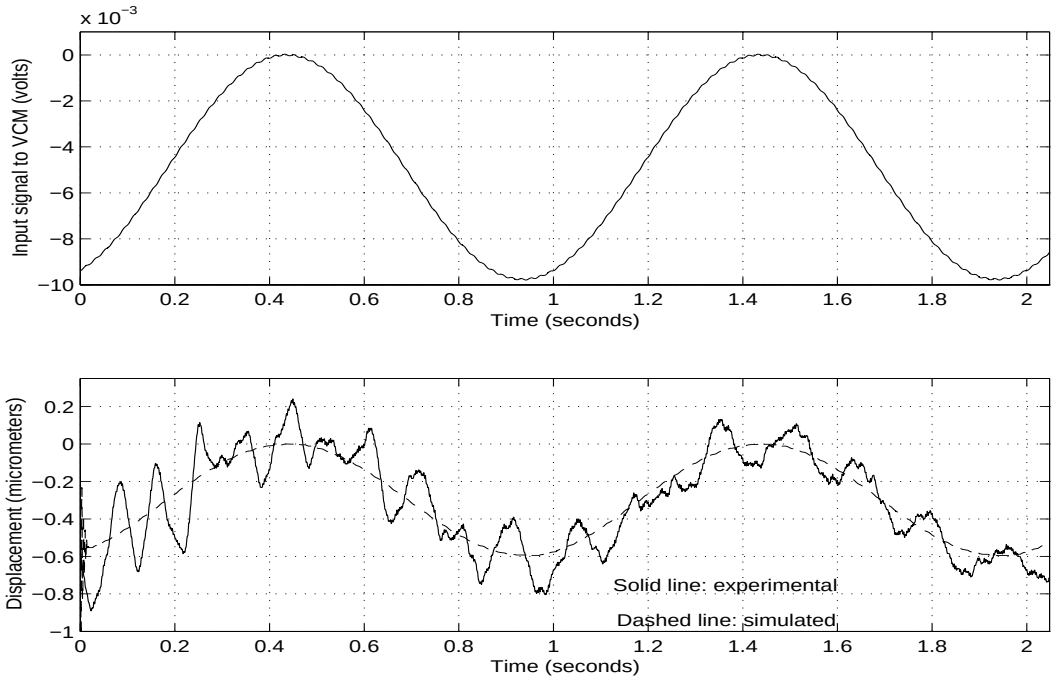

a) $u_0 = -5$ mV with a sine wave of amplitude 5 mV.

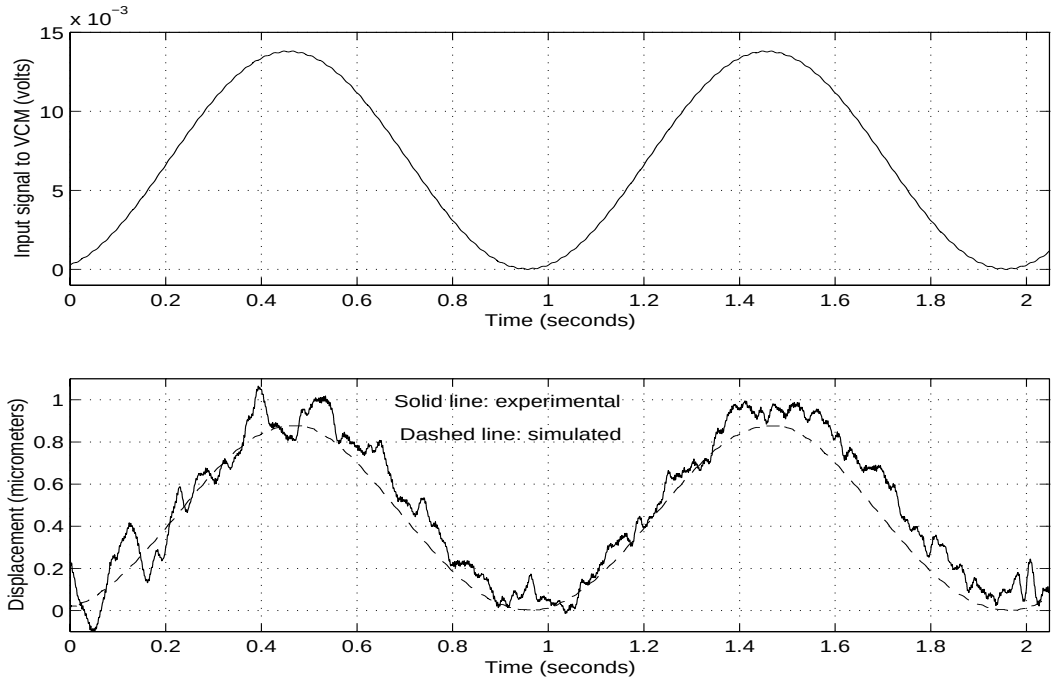

b) $u_0 = 7$ mV with a sine wave of amplitude 7 mV.

Figure 4.10: Comparison of time-domain responses of the VCM actuator.

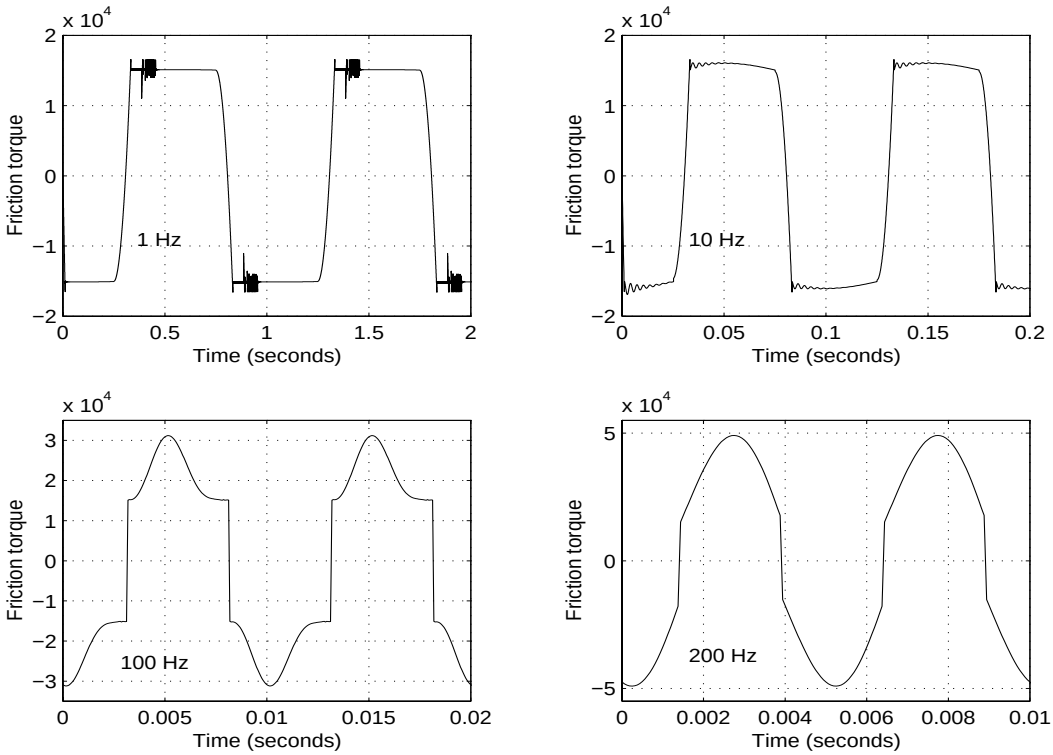

Figure 4.11: Friction torques generated by various input signals.

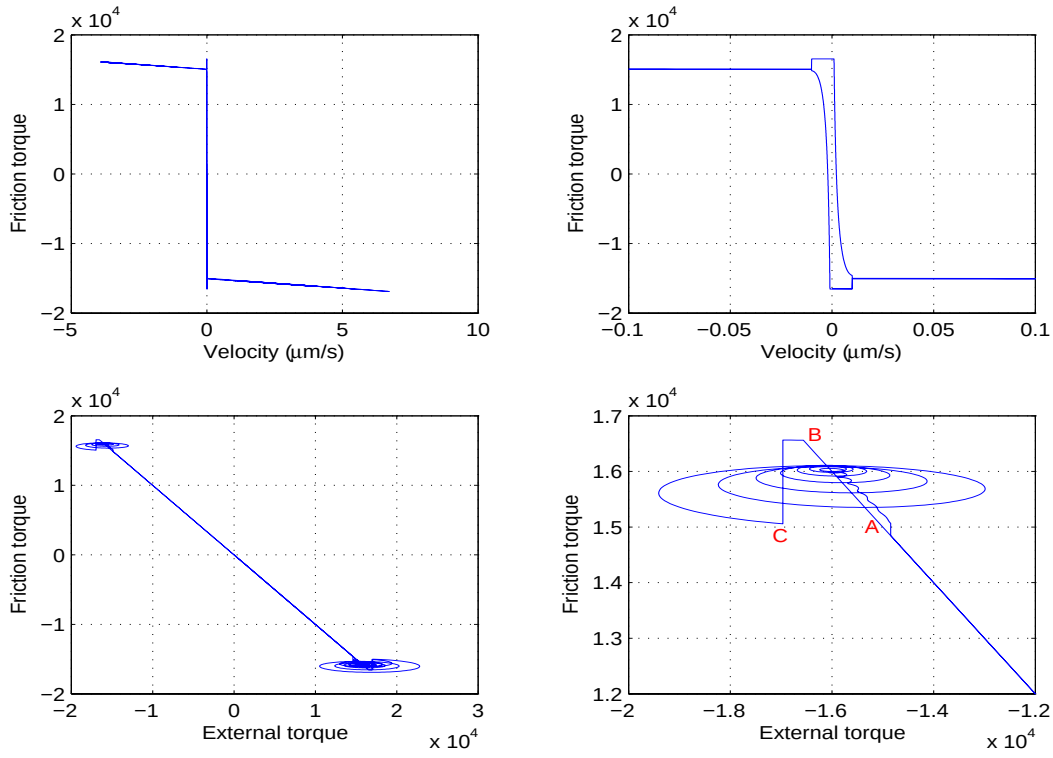

Figure 4.12: Relationships of friction torque with velocity and external torque (10 Hz input).

4.5 Concluding Remarks

In this chapter we have identified a comprehensive model with nonlinearities for a typical VCM actuator used in HDD servo systems. It has been done through a detailed analysis of physical effects of components in the actuator, *e.g.*, the coil, R/W head, pivot bearing and data flex cable. After the model structure has been established, a Monte Carlo process was carried out to identify its parameters. The verification of the identified model shows it indeed captures the comprehensive features of the VCM actuator. The resulting model can be expected to play an important role in eliminating residual errors and improving the performance of HDD head positioning servo systems, as will be seen in the next chapter.

Chapter 5

Design of Micro Hard Disk Drive Servo Systems

In the previous chapter, we have established a comprehensive model of a microdrive voice-coil-motor (VCM) actuator, which explicitly captures the characteristics of pivot bearing friction and flex cable nonlinearity. With this model in hand, we are ready to proceed to servo system design. This chapter focuses on the design of HDD servo systems which are capable of fast and precise tracking, for hard disk drives using the conventional VCM as the head positioning servo mechanism (single-stage servo systems).

5.1 Introduction

In hard disk drives, data is stored on concentric circles or so-called tracks on the surface of disk platters which are stacked along a rotational spindle. A read/write (R/W) head is used to read and write data on every disk surface. The R/W head is driven by a built-in servo system, using a Voice Coil Motor (VCM) as the servo mechanism, to move across disk surface to reach each track while disk platters are spinning at constant speed. To achieve fast and reliable data reading and writing, HDD servo system is expected to move the R/W head from one track to another track as soon as possible (track seeking) and then maintain

the R/W head as close as possible to the target track center (track following) while data is being read or written.

One of the objectives in HDD servo design is to maintain the Track Mis-Registration (TMR) budget, *i.e.*, to keep the position error signal (PES) within the tolerance limit during data reads/writes. So far, many control techniques have been proposed and they significantly improved the performance of HDD servo systems. However, more challenges still lie ahead, as the HDD industry moves towards smaller disk drives with larger capacity which impose a tighter TMR budget for track following. It is known that torque disturbances play a negative role in HDD track following tasks. The so-called torque disturbances, which include bias torque due to flex cable, pivot bearing friction and hysteresis, as well as other unmodelled dynamics, have conventionally been treated as a lumped disturbance or even ignored when a servo controller is being designed. This may be acceptable in those old HDDs with lower track density. However, when we are working with high TPI HDDs, where the TMR budget is at the scale of nanometer, the adverse effects induced by torque disturbances become conspicuous, to be specific, steady-state error (or bias), limit cycles, and performance degradation might occur.

To solve this problem, torque disturbances, especially those dominant contributing factors, such as flex cable nonlinearity and pivot bearing friction, should be sufficiently modeled and identified at the modeling stage, and then integrated into the controller design. In the previous chapter, we have established a comprehensive model, which explicitly incorporates the nonlinear effects of the flex cable and the pivot bearing friction, for an IBM microdrive (model DMDM-10340). The model (omitting high frequency resonant modes) is given as follows:

$$\ddot{y} = 2.35 \times 10^8 u - 6.78445 \times 10^6 \arctan(0.5886y) + \tilde{T}_{\mathrm{f}}, \tag{5.1}$$

where

$$\tilde{T}_{\rm f} = \begin{cases} -\left(\left|1.175\times 10^6 uy + 0.01\dot{y}^2\right| + 1.5\times 10^4\right)\operatorname{sgn}(\dot{y}) - 282.6\dot{y}, & \dot{y}\neq 0, \\ -\tilde{T}_{\rm e}, & \dot{y}=0 \text{ and } |\tilde{T}_{\rm e}|\leq \tilde{T}_{\rm s}, \\ -\tilde{T}_{\rm s}\operatorname{sgn}(\tilde{T}_{\rm e}), & \dot{y}=0 \text{ and } |\tilde{T}_{\rm e}|> \tilde{T}_{\rm s}, \end{cases} \tag{5.2}$$

and where

$$\tilde{T}_{\rm e} = 2.35\times 10^8\Big[u - 0.02887\arctan\left(0.5886y\right)\Big], \tag{5.3}$$

$$\tilde{T}_{\rm s} = 1.293\times 10^6|u_0 y_0| + 1.65\times 10^4, \tag{5.4}$$

with u_0 and y_0 being respectively the corresponding input voltage and the displacement for the case when $\dot{y}=0$.

Based on the above model, we are going to design HDD servo controllers which aim to achieve fast and smooth tracking without static error. Our philosophy here is quite simple and intuitive. Once the model of the friction and nonlinearities of the VCM actuator is obtained, we will try to cancel as much as possible all these unwanted elements in the servo system. As it is impossible to have perfect models for friction and nonlinearities, a perfect cancellation of these elements is unlikely to happen in the real world. We will then formulate our design by treating the uncompensated portion as external disturbances, and a robust control design methodology will be used to minimize their adverse effects on closed-loop performance.

In what follows, we will first design a track following controller for the microdrive using Robust and Perfect Tracking (RPT) control technique combined with nonlinear compensation and integral enhancement. Next, we will apply the enhanced composite nonlinear feedback (CNF) control technique to design a servo system that can perform track seeking and track following all-in-one without any explicit switching element. Simulation and Experiment will be carried out to evaluate the performance of the servo systems.

5.2 Design of a Microdrive Track Following Controller Using RPT Control

In this section, we are going to design a microdrive track following controller, using the Robust and Perfect Tracking (RPT) control technique as outlined in Chapter 2. The RPT technique was proposed by Liu *et al.* [45] and has been successfully used in servo system design for a larger hard disk drive [28]. The same idea applies to the servo problem here, but enhancements will be introduced to improve transient performance and remove steady state error.

5.2.1 Design of the Controller

To proceed, we first need to recast the HDD servo problem into the RPT framework. It is noted that the identified HDD model of (5.1) actually represents a second order system with nonlinear input disturbances. Experimental observation shows that flex cable nonlinearity is more influential than pivot bearing friction. As a natural practice and the first step of controller design, we compensate the term of flex cable nonlinearity which is already identified in clear form. Next, since the model of friction is somewhat messy, we choose to tick out the viscous friction component (the linear part) and incorporate it into the second order model while treating residual components (including other un-modeled torque disturbances) as an unknown lumped disturbance d_i. To be specific, we introduce

$$\bar{u} = u - a \arctan(cy) \tag{5.5}$$

where a and c are the identified parameters corresponding to the flex cable nonlinearity, then the HDD model is recast as

$$\ddot{y} = a_1 \dot{y} + a_0 y + b(\bar{u} + d_i) \tag{5.6}$$

where a_0, a_1 are parameters introduced to cover general second order systems. We define the following state variables

$$x_1 = y,\ x_2 = \dot{y},\ x_3 = \int (y - r)dt \tag{5.7}$$

where r is the reference input, or the desired position/track of the R/W head. Next, we define the controlled output as

$$h = x_1 + \lambda x_3 \tag{5.8}$$

where $\lambda > 0$ is a weighting factor. Now the system can be formulated into the following RPT form:

$$\Sigma : \begin{cases} \dot{x} = Ax + B\bar{u} + Ew, \\ \hat{y} = C_1 x + D_1 w, \\ h = C_2 x + D_2 \bar{u} \end{cases} \tag{5.9}$$

with

$$A = \begin{bmatrix} 0 & 1 & 0 \\ a_0 & a_1 & 0 \\ 1 & 0 & 0 \end{bmatrix},\ B = \begin{bmatrix} 0 \\ b \\ 0 \end{bmatrix},\ E = \begin{bmatrix} 0 & 0 \\ b & 0 \\ 0 & -1 \end{bmatrix} \tag{5.10}$$

$$C_1 = \begin{bmatrix} 1 & 0 & 0 \\ 0 & 0 & 1 \end{bmatrix},\ D_1 = \begin{bmatrix} 0 & 0 \\ 0 & 0 \end{bmatrix},\ C_2 = [\,1 \quad 0 \quad \lambda\,],\ D_2 = [\,0\,] \tag{5.11}$$

$$x = \begin{pmatrix} x_1 \\ x_2 \\ x_3 \end{pmatrix},\ w = \begin{pmatrix} d_i \\ r \end{pmatrix},\ \hat{y} = \begin{pmatrix} x_1 \\ x_3 \end{pmatrix} \tag{5.12}$$

It can be verified that the solvability conditions of the above RPT problem are satisfied, hence the RPT methodology can be applied here. Following the RPT design procedure outlined in chapter 2, we now give a step by step design for the microdrive servo controller.

Step 1 : System augmentation

Note that in HDD servo systems, the dominant task is set point tracking, *i.e.*, to move the R/W head to the desired track, which corresponds to a step reference input characterized by

$$\dot{r}(t) = r \cdot \delta(t) \tag{5.13}$$

If we augment the original state vector x with reference $r(t)$ and define the controlled output as $e = h - r$, we will have

$$\Sigma_{aug} : \begin{cases} \dot{\bar{x}} = \bar{A}\bar{x} + \bar{B}\bar{u} + \bar{E}\bar{w}, \\ \bar{y} = \bar{C}_1\bar{x} + \bar{D}_1\bar{w}, \\ e = \bar{C}_2\bar{x} + \bar{D}_2\bar{u} \end{cases} \tag{5.14}$$

with

$$\bar{x} = \begin{pmatrix} r \\ x \end{pmatrix}, \quad \bar{w} = \begin{pmatrix} d_i \\ r \cdot \delta(t) \end{pmatrix}, \quad \bar{y} = \begin{pmatrix} r \\ \hat{y} \end{pmatrix} \tag{5.15}$$

$$\bar{A} = \begin{bmatrix} 0 & 0 & 0 & 0 \\ 0 & 0 & 1 & 0 \\ 0 & a_0 & a_1 & 0 \\ -1 & 1 & 0 & 0 \end{bmatrix}, \quad \bar{B} = \begin{bmatrix} 0 \\ B \end{bmatrix}, \quad E = \begin{bmatrix} 0 & 1 \\ 0 & 0 \\ b & 0 \\ 0 & 0 \end{bmatrix} \tag{5.16}$$

$$\bar{C}_1 = \begin{bmatrix} 1 & 0 \\ 0 & C_1 \end{bmatrix}, \quad \bar{D}_1 = \begin{bmatrix} 0 \\ D_1 \end{bmatrix}, \quad \bar{C}_2 = [\,-1 \quad C_2\,], \quad \bar{D}_2 = D_2 \tag{5.17}$$

Step 2 : Special Coordinate Basis (SCB) decomposition

We utilize the results of the special coordinate basis [15] to find nonsingular state, input, and output transformation Γ_s, Γ_i and Γ_o to the subsystem $\Sigma_P = (\bar{A}, \bar{B}, \bar{C}_2, \bar{D}_2)$ of Σ_{aug} such that the subsystem under new coordinate basis will explicitly exhibit the invariant and infinite zeros structure as well as the invertibility structure. We have

$$\Gamma_s = \begin{bmatrix} 0 & 1 & 0 & 0 \\ -\lambda & 1 & 1 & 0 \\ \lambda^2 & 0 & -\lambda & 1 \\ 1 & 0 & 0 & 0 \end{bmatrix}, \quad \Gamma_i = \frac{1}{b}, \quad \Gamma_o = 1 \tag{5.18}$$

After the following SCB transformation

$$\bar{x} = \Gamma_s\tilde{x}, \quad e = \Gamma_o\tilde{e}, \quad \bar{u} = \Gamma_i\tilde{u} \tag{5.19}$$

we have

$$\tilde{A} = \Gamma_s^{-1}\bar{A}\Gamma_s = \begin{bmatrix} -\lambda & 0 & 1 & 0 \\ 0 & 0 & 0 & 0 \\ 0 & 0 & 0 & 1 \\ (\lambda+a_1)\lambda^2 - a_0\lambda & a_0 & a_0 - (\lambda+a_1)\lambda & \lambda + a_1 \end{bmatrix} \tag{5.20}$$

and

$$\tilde{B} = \Gamma_s^{-1}\bar{B}\Gamma_i = \begin{bmatrix} 0 \\ 0 \\ 0 \\ 1 \end{bmatrix}, \quad \tilde{C}_2 = \Gamma_o\bar{C}_2\Gamma_s = [\,0 \quad 0 \quad 1 \quad 0\,], \quad \tilde{D}_2 = \Gamma_o\bar{D}_2\Gamma_i = 0 \tag{5.21}$$

It is now quite clear that the above subsystem has an invariant zero at the origin and another at $-\lambda$, and it has an infinity zero of order 2. Moreover, this subsystem is invertible.

Step 3: Design of the parameterized state feedback control law

For the moment, we assume that the state vector $\bar{x}$ is available for feedback control. Since the subsystem Σ_P has only one infinity zero of order 2, we just need to consider one conjugate pair $-\zeta\omega \pm j\omega\sqrt{1-\zeta^2}$, where ζ and ω are respectively the damping ratio and natural frequency of the supposedly closed-loop poles. This conjugate pair corresponds to the following characteristic polynomial:

$$p(s) = s^2 + 2\zeta\omega s + \omega^2 \tag{5.22}$$

Now the parameterized state feedback gain matrix can be given by

$$\begin{aligned} \tilde{F}(\epsilon) &= -\Gamma_i\,[\,(\lambda+a_1)\lambda^2 - a_0\lambda \quad a_0 \quad a_0 - (\lambda+a_1)\lambda + \tfrac{\omega^2}{\epsilon^2} \quad \lambda + a_1 + \tfrac{2\zeta\omega}{\epsilon}\,]\,\Gamma_s^{-1} \\ &= -\tfrac{1}{b}\,[\,-\tfrac{\omega^2}{\epsilon^2} - \tfrac{2\zeta\omega\lambda}{\epsilon} \quad a_0 + \tfrac{\omega^2}{\epsilon^2} + \tfrac{2\zeta\omega\lambda}{\epsilon} \quad a_1 + \lambda + \tfrac{2\zeta\omega}{\epsilon} \quad \tfrac{\omega^2\lambda}{\epsilon^2}\,] \end{aligned} \tag{5.23}$$

where ϵ is the time scale factor which can serve as a tuning parameter.

We partition $\tilde{F}(\epsilon)$ according to the sizes of reference r and state vector x:

$$\tilde{F}(\epsilon) = [\,H(\epsilon) \quad F(\epsilon)\,] \tag{5.24}$$

Now the state feedback control law can be rewritten as:

$$\bar{u} = F(\epsilon)x + H(\epsilon)r \tag{5.25}$$

Step 4: Design of the reduced order measurement feedback controller

In the previous step, we assume the state vector $\bar{x}$ is available. However, this is not the case in real implementation. From (5.9) we know that the variable x_1 and x_3 are directly available, while the variable x_2 is not measurable here and will have to be estimated by an observer. In what follows, we will design a reduced order measurement feedback controller based on the above state feedback control law. First, we define

$$\bar{x}_1 = \begin{pmatrix} x_1 \\ \\ x_3 \end{pmatrix}, \quad \bar{x}_2 = x_2 \tag{5.26}$$

From (5.9), we have

$$\left.\begin{aligned} \begin{pmatrix} \dot{\bar{x}}_1 \\ \\ \dot{\bar{x}}_2 \end{pmatrix} &= \begin{bmatrix} A_{11} & A_{12} \\ \\ A_{21} & A_{22} \end{bmatrix} \begin{pmatrix} \bar{x}_1 \\ \\ \bar{x}_2 \end{pmatrix} + \begin{bmatrix} E_1 \\ \\ E_2 \end{bmatrix} w + \begin{bmatrix} B_1 \\ \\ B_2 \end{bmatrix} \bar{u}, \\ \hat{y} &= \begin{bmatrix} 1 & 0 & 0 \\ \\ 0 & 1 & 0 \end{bmatrix} \begin{pmatrix} \bar{x}_1 \\ \\ \bar{x}_2 \end{pmatrix} + \begin{bmatrix} 0 & 0 \\ \\ 0 & 0 \end{bmatrix} w \end{aligned}\right\} \tag{5.27}$$

where

$$A_{11} = \begin{bmatrix} 0 & 0 \\ \\ 1 & 0 \end{bmatrix}, \quad A_{12} = \begin{bmatrix} 1 \\ \\ 0 \end{bmatrix}, \quad B_1 = \begin{bmatrix} 0 \\ \\ 0 \end{bmatrix}, \quad E_1 = \begin{bmatrix} 0 & 0 \\ \\ 0 & -1 \end{bmatrix}$$

$$A_{21} = [\, a_0 \quad 0 \,], \quad A_{22} = [\, a_1 \,], \quad B_2 = [\, b \,], \quad E_2 = [\, b \quad 0 \,]$$

To estimate $\bar{x}_2$ or equivalently x_2, we define an auxiliary system $\Sigma_{QR} = (A_R, E_R, C_R, D_R)$ with

$$A_R = A_{22},\ E_R = E_2,\ C_R = A_{12},\ D_R = E_1 \tag{5.28}$$

It is easy to verify that (A_R, C_R) is detectable since (A, C_1) is detectable. So we can determine an appropriate dimensional constant matrix K_R such that the eigenvalues of $A_R + K_R C_R$ are all on LHP. For this simple case of first order observer, we choose

$$K_R = [\, -a_1 - L, \quad 0 \,],\ L > 0 \tag{5.29}$$

which places the pole at $-L$. Next we rearrange $F(\epsilon)$ in accordance with $\bar{x}_1$ and $\bar{x}_2$, *i.e.*,

$$F(\epsilon) = [\, F_1(\epsilon) \quad F_2(\epsilon)\,] = -\frac{1}{b}\,[\, a_0 + \tfrac{\omega^2}{\epsilon^2} + \tfrac{2\zeta\omega\lambda}{\epsilon} \quad \tfrac{\omega^2\lambda}{\epsilon^2} \quad | \quad a_1 + \lambda + \tfrac{2\zeta\omega}{\epsilon}\,] \tag{5.30}$$

By now, the reduced order measurement feedback controller can be obtained as

$$\Sigma_{\rm v}(\epsilon): \begin{cases} \dot{x}_{\rm v} = A_{\rm v}(\epsilon)\ x_{\rm v} + B_{\rm y}(\epsilon)\ \hat{y} + B_{\rm r}(\epsilon) r \\ \\ \bar{u}\ = C_{\rm v}(\epsilon)\ x_{\rm v} + D_{\rm y}(\epsilon)\ \hat{y} + D_{\rm r}(\epsilon) r \end{cases} \tag{5.31}$$

with

$$\left.\begin{aligned} A_{\rm v}(\epsilon) &= -\left(a_1 + \lambda + L + \frac{2\zeta\omega}{\epsilon}\right), \\ B_{\rm y}(\epsilon) &= -\left[(a_1 + \lambda + L)(a_1 + L + \frac{2\zeta\omega}{\epsilon}) + \frac{\omega^2}{\epsilon^2}, \qquad \frac{\omega^2\lambda}{\epsilon^2}\right], \\ B_{\rm r}(\epsilon) &= \frac{\omega^2}{\epsilon^2} + \frac{2\zeta\omega\lambda}{\epsilon}, \\ C_{\rm v}(\epsilon) &= -\frac{1}{b}\left(a_1 + \lambda + \frac{2\zeta\omega}{\epsilon}\right), \\ D_{\rm y}(\epsilon) &= -\frac{1}{b}\left[a_0 + (a_1 + \lambda)(a_1 + L) + \frac{\omega^2}{\epsilon^2} + (a_1 + \lambda + L)\frac{2\zeta\omega}{\epsilon}, \qquad \frac{\omega^2\lambda}{\epsilon^2}\right], \\ D_{\rm r}(\epsilon) &= \frac{1}{b}\left(\frac{\omega^2}{\epsilon^2} + \frac{2\zeta\omega\lambda}{\epsilon}\right), \end{aligned}\right\} \tag{5.32}$$

Step 5: Derivation of the final controller

In this step we will combine the first order linear controller of (5.31) with the augmented integration term x_3 and nonlinear compensation term to result in a second order composite controller. Define $x_c = \begin{pmatrix} x_{\rm v} \\ \\ x_3 \end{pmatrix}$, and combining (5.5) and (5.31), we arrive at the following final controller to be implemented onto the real system:

$$\Sigma_{\rm c}(\epsilon): \begin{cases} \dot{x}_{\rm c} = A_{\rm c}(\epsilon)\ x_{\rm c} + B_{\rm c}(\epsilon) \begin{pmatrix} y \\ \\ r \end{pmatrix} \\ \\ u\ = C_{\rm c}(\epsilon)\ x_{\rm c} + D_{\rm c}(\epsilon) \begin{pmatrix} y \\ \\ r \end{pmatrix} + a \arctan(cy) \end{cases} \tag{5.33}$$

$$\left.\begin{aligned}
&\text{with}\\
&A_c(\epsilon) = \begin{bmatrix} -\left(a_1+\lambda+L+\dfrac{2\zeta\omega}{\epsilon}\right) & -\dfrac{\omega^2\lambda}{\epsilon^2} \\ 0 & 0 \end{bmatrix},\\
&B_c(\epsilon) = \begin{bmatrix} -(a_1+\lambda+L)\left(a_1+L+\frac{2\zeta\omega}{\epsilon}\right)-\frac{\omega^2}{\epsilon^2} & \dfrac{2\zeta\omega\lambda}{\epsilon}+\dfrac{\omega^2}{\epsilon^2} \\ 1 & -1 \end{bmatrix},\\
&C_c(\epsilon) = -\frac{1}{b}\left[a_1+\lambda+\frac{2\zeta\omega}{\epsilon}, \quad \frac{\omega^2\lambda}{\epsilon^2}\right],\\
&D_c(\epsilon) = -\frac{1}{b}\left[a_0+(a_1+\lambda)(a_1+L)+\frac{\omega^2}{\epsilon^2}+(a_1+\lambda+L)\frac{2\zeta\omega}{\epsilon}, \quad -\frac{\omega^2}{\epsilon^2}-\frac{2\zeta\omega\lambda}{\epsilon}\right],
\end{aligned}\right\} \tag{5.34}$$

The following remarks are in order.

Remark 5.1. Controller $\Sigma_c(\epsilon)$ of (5.33) is a RPT controller combined with integral and nonlinear compensation, as shown in Figure 5.1. Note that $\Sigma_c(\epsilon)$ is a closed form controller parameterized by $(\epsilon, \zeta, \omega, \lambda, L)$. These parameters can be tuned online to improve control performance. As $\epsilon \to 0$, perfect tracking can be achieved. However, in the actual implementation, we have to take into consideration the physical limitation of the HDD servo system, such as actuator saturation and resonant modes. The parameterized design enables us to easily tune the controller parameters to achieve a good performance.

Remark 5.2. Note that we have redefined the controlled output to be $h = x_1 + \lambda x_3 = x_1 + \lambda \int e$. This is important for the solvability of the RPT problem with integral augmentation. It can be verified that the transfer function from reference r (the desired track) to output displacement y is given by

$$H_{yr}(s) = \frac{\omega(\omega+2\zeta\omega\lambda)}{\epsilon^2} \times \frac{(s+L)(s+\frac{\omega\lambda}{\omega+2\zeta\epsilon\lambda})}{(s+L)(s^2+\frac{2\zeta\omega s}{\epsilon}+\frac{\omega^2}{\epsilon^2})(s+\lambda)} \tag{5.35}$$

As expected, there is a zero/pole cancellation at $-L$. There are three poles at $-\lambda, -\frac{\zeta\omega}{\epsilon} \pm j\frac{\omega}{\epsilon}\sqrt{1-\zeta^2}$ respectively and one zero at $-\frac{\omega\lambda}{\omega+2\zeta\epsilon\lambda}$. As $\frac{\omega}{\epsilon} \to \infty$, $\frac{\omega\lambda}{\omega+2\zeta\epsilon\lambda} \to \lambda$, there will be a zero/pole cancellation at $-\lambda$, and the closed loop system will behave like a second order system. Finally, it is easy to verify, the static gain, $H_{yr}(0) = 1$, which guarantees a zero steady-state error for set point tracking.

Remark 5.3. The term of nonlinear compensation in our controller directly cancels out a major part of the torque disturbances in the microdrive. Usually, in the absence of a clear model of disturbances, one will resort to a high bandwidth design to reject disturbances.

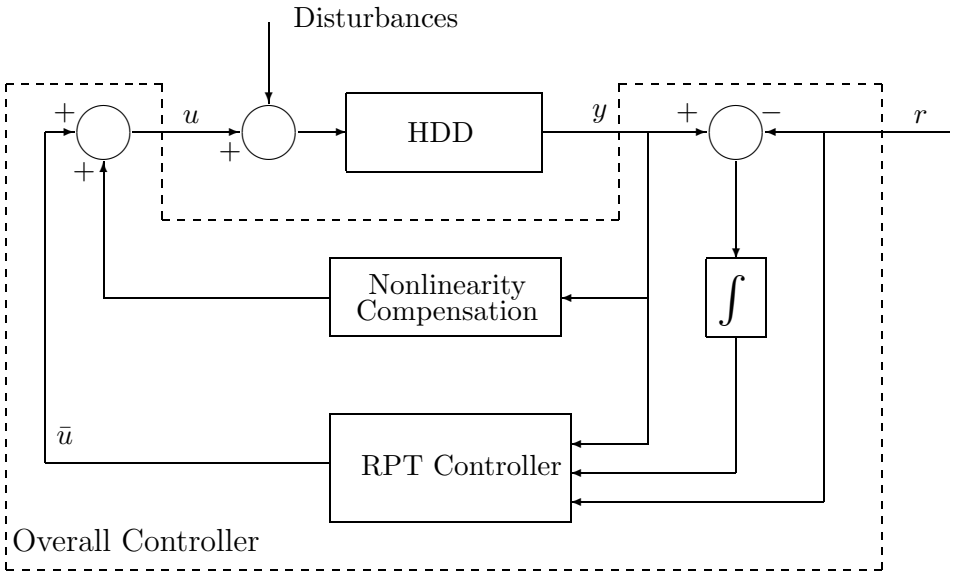

Figure 5.1: Control scheme for the microdrive servo system (with RPT control).

However, as the bandwidth is pushed higher, more noises are allowed into the control loop, which may result in performance degradation in the output response and even trigger the resonant modes in the plant. By using a nonlinear compensation, we are able to properly design a moderately high bandwidth controller, which maintains a good balance between time domain and frequency domain specifications. Due to the lack of a perfect model for friction and nonlinearities, a perfect cancellation of these elements is unlikely to happen in the physical system. Anyway, the un-cancelled components can be handled by the robustness of this controller.

Remark 5.4. In our design of the HDD track following controller, we only use the nominal model of the micro hard disk drive. However, it is crucial to include the high frequency resonant modes in simulation before one carries out the implementation of the controller to the actual hardware. The simulation result obtained in the next section is done with all the resonant modes of (4.33)–(4.37) being included.

5.2.2 Simulation and Experimental Results

Simulations and experiments have been carried out to evaluate the performance of the above designed controller in HDD track following task. The microdrive (IBM model DMDM-10340, with its cover and platters removed) used in our experiments, is the same one as in the modeling stage in Chapter 4. In the experiments, the only measurable output is the relative displacement of the R/W head which is measured by a Laser Doppler Vibrometer (LDV). Control algorithm is implemented on a dSpace DSP board installed in a personal computer. The sampling rate is $20kHz$. For this specific microdrive with an assumed track density of $50KTPI$, its track pitch is around $0.5\mu m$. Hence the so-called TMR budget, which is defined here as 5% of track pitch, is about $0.025\mu m$. A desirable controller is expected to bring the R/W head into the $0.025\mu m$ neighborhood of the target track as soon as possible.

Since $\Sigma_c(\epsilon)$ is a parameterized controller, we can easily tune its parameters$(\epsilon, \zeta, \omega, \lambda, L)$ online to achieve satisfactory results. For this microdrive, we have

$$b = 2.35 \times 10^8,\ a_0 = 0,\ a_1 = -282.6,\ a = 0.02887,\ c = 0.5886.$$

By online tuning, we find that the following controller parameters give the best performance:

$$\epsilon = 1, \zeta = 1.2, \omega = 2400\pi, \lambda = 80, L = 6000.$$

The final controller is then given by

$$\begin{cases} \dot{x}_c = \begin{bmatrix} -2.3893 \times 10^4 & -4.5479 \times 10^9 \\ 0 & 0 \end{bmatrix} x_c + \begin{bmatrix} -1.949 \times 10^8 & 5.8297 \times 10^7 \\ 1 & -1 \end{bmatrix} \begin{pmatrix} y \\ r \end{pmatrix}, \\ \bar{u} = [\,-7.614 \times 10^{-5} \quad -19.353\,]\, x_c + [\,-0.6834 \quad 0.2481\,] \begin{pmatrix} y \\ r \end{pmatrix} \end{cases} \tag{5.36}$$

and

$$u = \bar{u} + 0.02887 \arctan(0.5886y). \tag{5.37}$$

The above controller can achieve a settling time of $0.75ms$ and $0.83ms$ respectively for $0.5\mu m$ and $1\mu m$ tracking following in simulation (see Figure 5.2 and 5.3); While in experiments, the corresponding settling time are $0.9ms$ and $1.1ms$ respectively (see Figure 5.4 and 5.5). Here settling time is defined as the time it takes for the R/W head to enter and remain in the $0.025\mu m$ neighborhood of the target track center.

For comparison, we also design a conventional PID controller with the same nonlinearity pre-compensation, and a conventional RPT controller which does not include integral enhancement and nonlinear compensation.

The PID controller is given by:

$$\begin{pmatrix} \dot{z} \\ \dot{x}_{\rm d} \end{pmatrix} = \begin{bmatrix} 0 & 0 \\ 0 & -10^5 \end{bmatrix} \begin{pmatrix} z \\ x_{\rm d} \end{pmatrix} + \begin{bmatrix} 1 \\ 1 \end{bmatrix} (r - y) \tag{5.38}$$

and

$$\bar{u} = 2.181(r - y) + 30z - 2.139 \times 10^5 x_{\rm d}. \tag{5.39}$$

The conventional RPT controller is designed based on the double integrator model (*i.e.*, $\ddot{y} = bu$) of VCM actuator, and is given by

$$\begin{cases} \dot{x}_v = -(L + \frac{2\zeta\omega}{\epsilon})x_v - (L^2 + \frac{2\zeta\omega L}{\epsilon} + \frac{\omega^2}{\epsilon^2})y + \frac{\omega^2}{\epsilon^2} r, \\ u = -\frac{1}{b}[\frac{2\zeta\omega}{\epsilon} x_v + (\frac{2\zeta\omega L}{\epsilon} + \frac{\omega^2}{\epsilon^2})y - \frac{\omega^2}{\epsilon^2} r] \end{cases} \tag{5.40}$$

with the following best tuned parameters:

$$\epsilon = 1,\ \zeta = 0.8,\ \omega = 2600\pi,\ L = 6000.$$

The performances of the three controllers for $0.5\mu m$ and $1\mu m$ tracking following are shown in Figure 5.2 and 5.3 for simulation, Figure 5.4 and 5.5 for implementation respectively. Table 5.1 summarizes the performances in terms of settling time achieved by the three controllers. It is easy to see that in both simulation and experiments, the conventional RPT controller is not able to bring the R/W head into the $0.025\mu m$ neighborhood of the target track center, *i.e.*, there is a significant bias at the steady-state output. Although we

may try to reduce such bias by using a larger ω or smaller ϵ, which means higher closed-loop bandwidth, it is likely to activate the high frequency resonant modes. The conventional PID controller results in a large overshoot in the output response and hence a sluggish settling. The RPT controller with integral and nonlinearity compensation achieves a fast and smooth settling. This can be attributed to two factors: First, as mentioned before, there is a nonlinear compensation term in the controller, which directly cancels the flex cable nonlinearity and hence speeds up the motion of the R/W head; Second, the integral enhancement serves as inner mode control for constant disturbance, which helps remove steady-state error at the output displacement y.

However, we do notice that there is a minor offset on the output response in the simulation result of the RPT controller with integral compensation. This offset is due to the accumulated error of the integral term which is supposed to overcome the unmodeled disturbances, and it may take quite some time to wipe out this offset eventually. This problem becomes more serious for track seeking (say, reference $r = 10\mu m$), where there will be large overshoot and hence sluggish settling. To alleviate this negative effect, some researchers suggest using integral reset when the system output enters the neighborhood of target reference. This trick normally works in simulation, but in implementation we have found that it can easily lead to oscillation, probably due to some unidentified yet persistent bias torque in the physical system. As an alternative, we here propose to adapt the integration parameter λ to different tracking tasks. By intuition, we should use a weaker integration (accordingly a smaller weighting parameter λ) for larger range tracking. With this idea in mind, we suggest the following scheduling law for parameter λ based on target reference r:

$$\lambda = \frac{160}{1 + |r|}. \tag{5.41}$$

With the above law, the value of λ will be adjusted automatically for different tracking tasks (*i.e.*, different r), but the controller structure remains the same. As a result, closed-loop

Table 5.1: Comparison of settling time (ms) and stability margins.

Controller	PID	RPT with integral	RPT
Simulation($0.5\mu m$)	1.54	0.75	∞
Implementation($0.5\mu m$)	2.1	0.9	∞
Simulation($1\mu m$)	1.85	0.83	∞
Implementation($1\mu m$)	2.3	1.1	∞
Gain margin (dB)	4.24	8.46	9.71
Phase margin (deg)	68.3	57.8	49.7

stability is maintained while performance can be improved. It can be verified that the above law works well for a wider range of target reference r in both track following and seeking tasks.

Figure 5.6 shows the open loop properties associated with the three controllers. Figure 5.7 is the plot of the sensitivity and complementary sensitivity functions of the RPT controller with integral and pre-compensation. From the bode plots we observe that the RPT controller with integral and pre-compensation achieves a phase margin of 57.8 degree and a gain margin of 8.46 dB (see also Table 5.1), which are quite desirable in engineering context. Judging from the stability margins, it seems that there is still scope for performance improvement by using more aggressive control or higher gain feedback. However, the feasibility will be limited by the resonant modes, since in physical systems, the resonant frequencies may somewhat drift or deviate, which eventually ends up violating the stability margins.

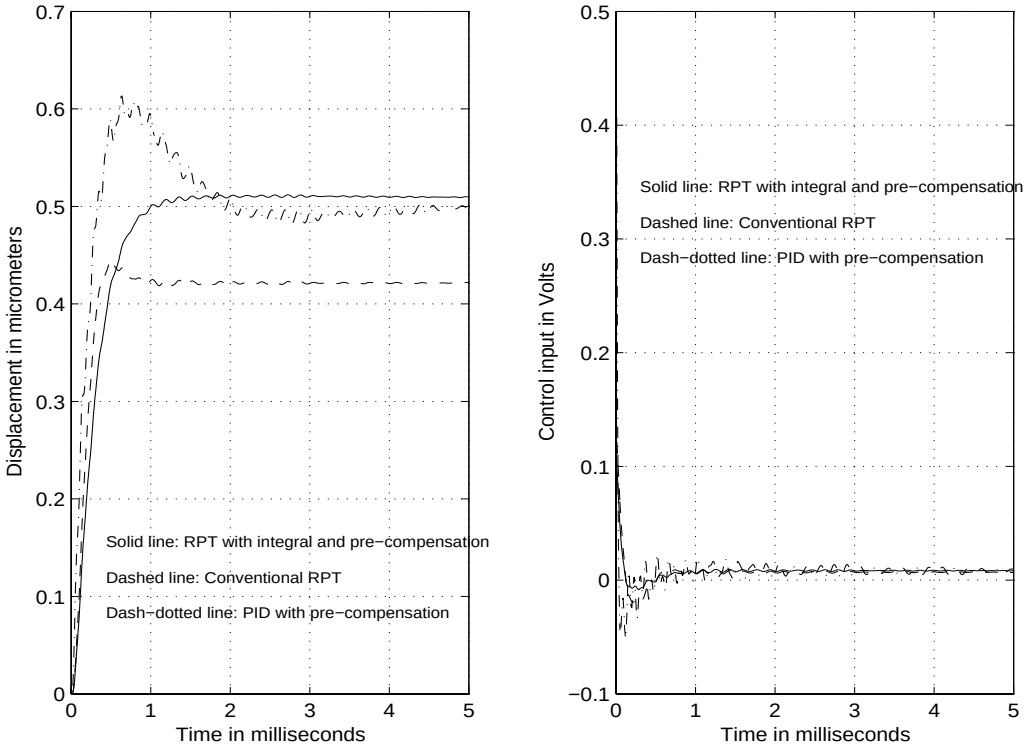

Figure 5.2: Simulation result: $0.5\mu m$ track following.

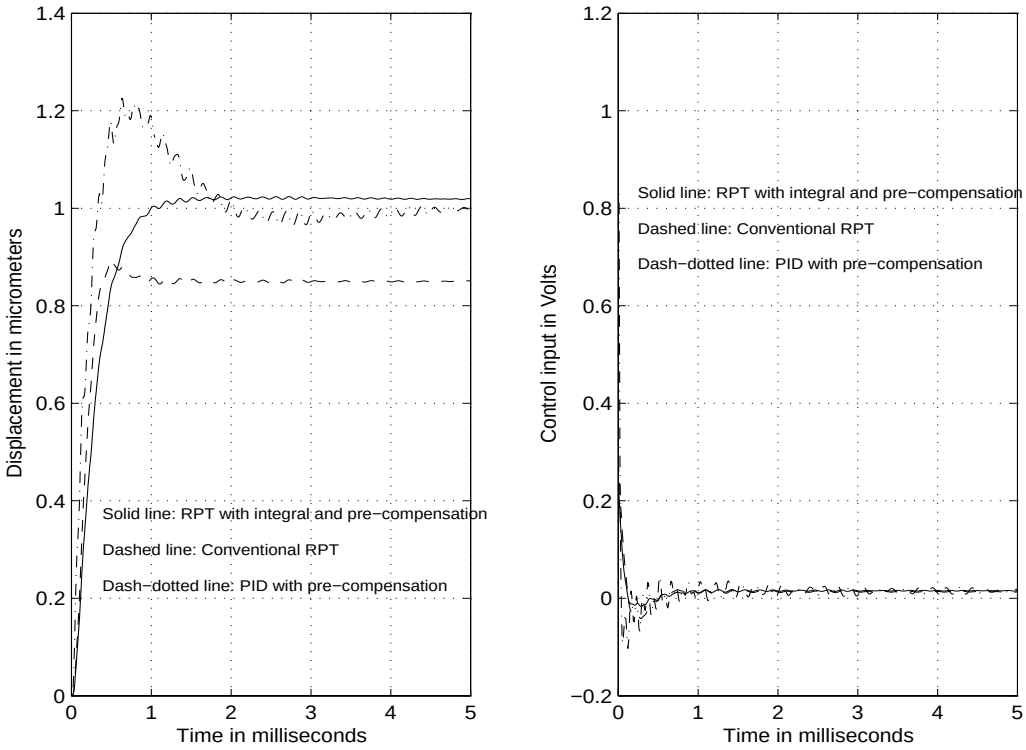

Figure 5.3: Simulation result: $1\mu m$ track following.

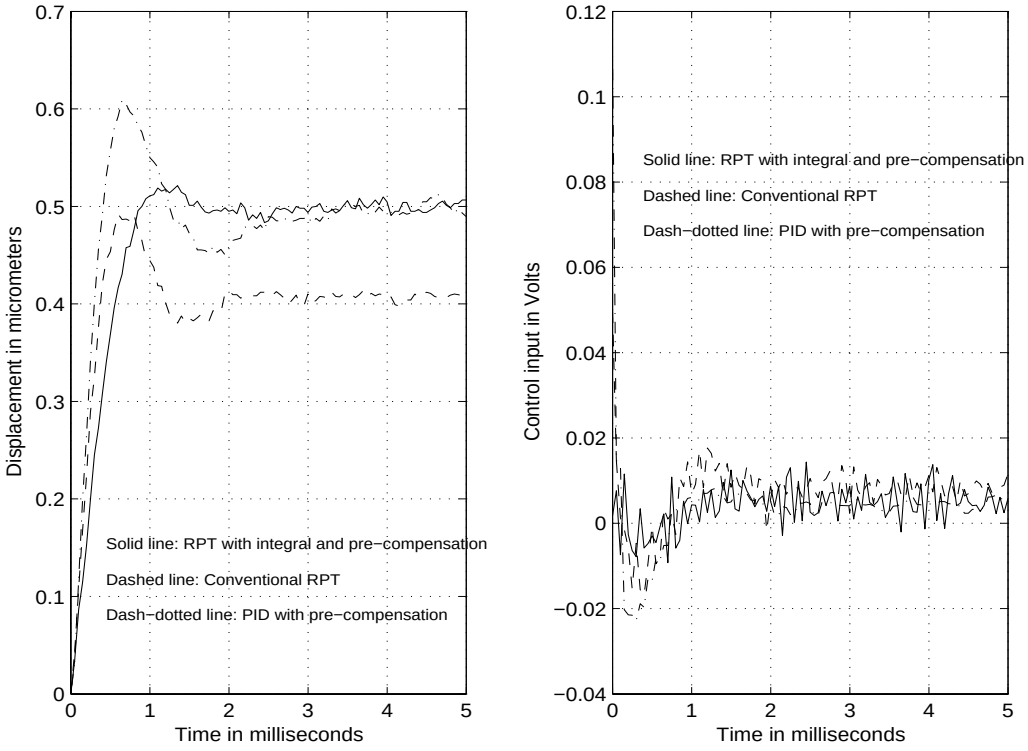

Figure 5.4: Experimental result: $0.5\mu m$ track following.

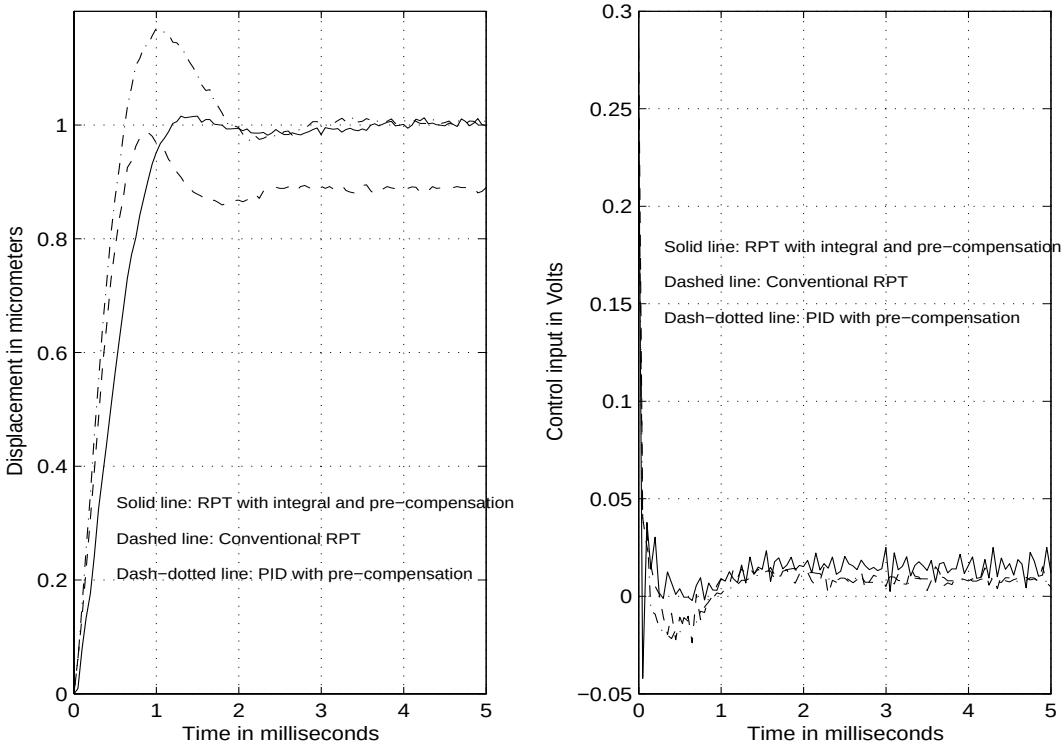

Figure 5.5: Experimental result: $1\mu m$ track following.

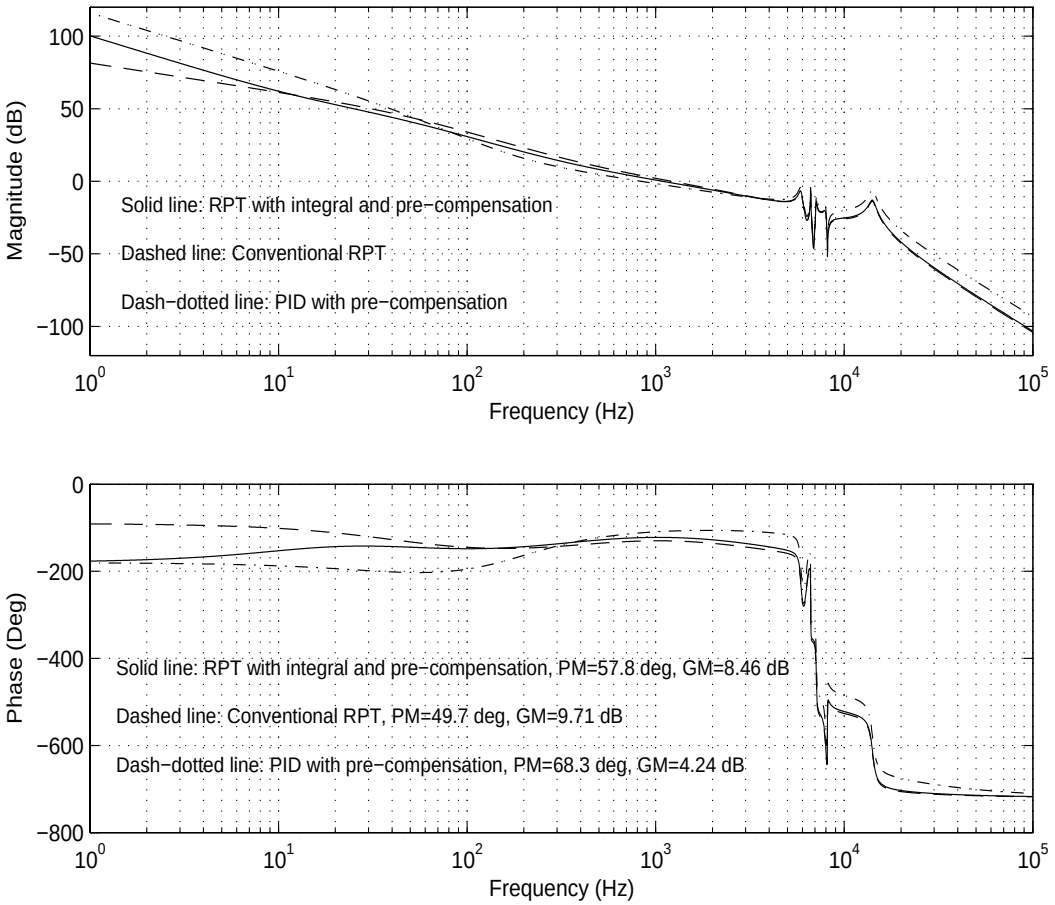

Figure 5.6: Bode plot of the open loop transfer functions.

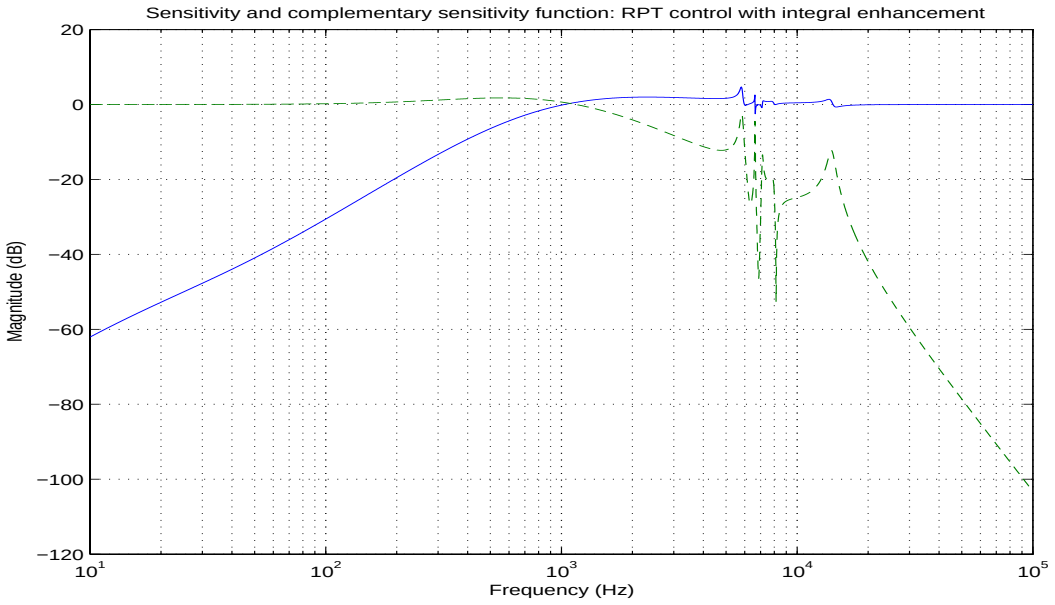

Figure 5.7: Plot of the sensitivity and complementary sensitivity functions.

5.3 A Microdrive Servo System Design Using Enhanced CNF Control

In the previous section, we have designed a servo controller for the microdrive with excellent performance in track following tasks. However, track following is just one aspect of HDD servo problem. For a complete solution, we still have to consider track seeking tasks in HDDs. Ideally, we expect a servo system that can perform track seeking and track following all-in-one without any explicit switching element. In this section we will try to fulfill such an expectation. The control strategy we are going to use is the so-called enhanced Composite Nonlinear Feedback (CNF) control technique combined with a simple friction and nonlinearity pre-compensation scheme. The enhanced CNF technique has a feature of removing the uncompensated portion of friction and nonlinearities while maintaining those nice properties of the original CNF technique, such as fast response and little or no overshoot in set point tracking tasks. Simulations and experiments will be carried out to verify the effectiveness of our approach.

5.3.1 Servo System Design

We proceed to design a servo system for both track seeking and track following in the microdrive. The design philosophy here is roughly the same as in the previous section. We will make full use of the obtained model of the friction and nonlinearities of the VCM actuator to design a pre-compensator, which would cancel as much as possible all the unwanted elements in the servo system. As it is impossible to have a perfect cancellation of the friction and nonlinearities, we will then formulate our design by treating the uncompensated portion as external disturbances. The enhanced CNF control technique of Chapter 2 will then be employed to design an effective servo controller. The overall control scheme for the servo system is depicted in Figure 5.8.

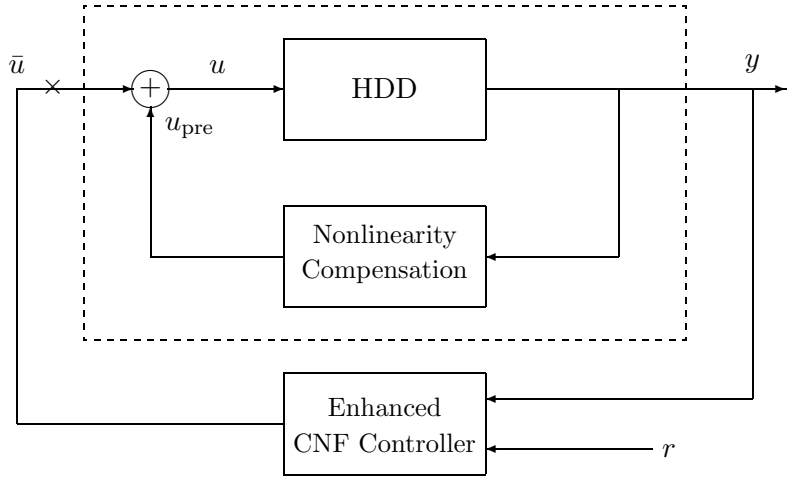

Figure 5.8: Control scheme for the microdrive servo system (with CNF control).

Same as before, we first introduce a nonlinearity pre-compensation,

$$u_{\text{pre}} = u - \bar{u} = 0.02887 \arctan(0.5886\, y), \tag{5.42}$$

which would eliminate the majority of nonlinearities in the data flex cable. The HDD model can then be simplified as the following:

$$\begin{cases} \dot{x} = \begin{bmatrix} 0 & 1 \\ 0 & 0 \end{bmatrix} x + \begin{bmatrix} 0 \\ 2.35 \times 10^8 \end{bmatrix} \text{sat}(\bar{u}) + \begin{bmatrix} 0 \\ 2.35 \times 10^8 \end{bmatrix} w, \\ y = h = [\,1 \quad 0\,]\, x, \end{cases} \tag{5.43}$$

where the disturbance, w, represents uncompensated nonlinearities, and $y = h$ is the relative displacement of the R/W head (in micrometer). The control input, $\bar{u}$, is to be limited within $\pm\bar{u}_{\max}$ with $\bar{u}_{\max} = 3$V. The corresponding augmented plant to be used in the enhanced CNF design is then given by

$$\begin{cases} \dot{\bar{x}} = \begin{bmatrix} 0 & 1 & 0 \\ 0 & 0 & 1 \\ 0 & 0 & 0 \end{bmatrix} \bar{x} + \begin{bmatrix} 0 \\ 0 \\ 2.35 \times 10^8 \end{bmatrix} \text{sat}(\bar{u}) + \begin{bmatrix} -1 \\ 0 \\ 0 \end{bmatrix} r + \begin{bmatrix} 0 \\ 0 \\ 2.35 \times 10^8 \end{bmatrix} w, \\ \bar{y} = \begin{bmatrix} 1 & 0 & 0 \\ 0 & 1 & 0 \end{bmatrix} \bar{x}, \\ h = [\,0 \quad 1 \quad 0\,]\, \bar{x}. \end{cases} \tag{5.44}$$

We will focus on our design for short span track seeking and track following stages of the microdrive servo system. The initial state, $x(0)$, is assumed to be 0. Note that the nonlinearities in the flex cable and pivot friction are relatively less influential in the track seeking stage.

Following the procedures given in Section 2.3 and with the help of the CNF control toolkit, we obtain a state feedback gain matrix,

$$F = -\left[\, 8.2317 \times 10^{-4} \quad 0.0823 \quad 2.2459 \times 10^{-5} \,\right], \tag{5.45}$$

such that the closed-loop system (matrix $\bar{A} + \bar{B}F$) has an integration pole at -0.01 and another two conjugate poles with damping ratio 0.6 and natural frequency 1400π. This arrangement work very well for the microdrive servo system. Next, we choose W to be a diagonal matrix with diagonal elements being 7.4536×10^{-4}, 0.0135 and 7.0057×10^{-11}, respectively. Solving the Lyapunov equation of (6.14), we obtain

$$P = \begin{bmatrix} 0.0373 & 1.0182 \times 10^{-5} & 1.9266 \times 10^{-9} \\ 1.0182 \times 10^{-5} & 3.2591 \times 10^{-6} & 3.5028 \times 10^{-10} \\ 1.9266 \times 10^{-9} & 3.5028 \times 10^{-10} & 7.3005 \times 10^{-14} \end{bmatrix} > 0. \tag{5.46}$$

The reduced order observer gain matrix is selected as

$$K_{\mathrm{R}} = -6000, \tag{5.47}$$

which places the observer pole at -6000, and the nonlinear gain function is selected as follows:

$$\rho(r, h) = -4.7459 \left| \mathrm{e}^{-|h-r|} - \mathrm{e}^{-|h(0)-r|} \right|. \tag{5.48}$$

Finally, the reduced order enhanced CNF control law for the microdrive servo system is given by

$$\begin{pmatrix} \dot{z} \\ \dot{x}_{\mathrm{v}} \end{pmatrix} = \begin{bmatrix} 0 & 0 \\ 0 & -6000 \end{bmatrix} \begin{pmatrix} z \\ x_{\mathrm{v}} \end{pmatrix} + \begin{bmatrix} 1 \\ -3.6 \times 10^{7} \end{bmatrix} y + \begin{bmatrix} 0 \\ 2.35 \times 10^{8} \end{bmatrix} \mathrm{sat}(\bar{u}) - \begin{bmatrix} 1 \\ 0 \end{bmatrix} r, \tag{5.49}$$

and

$$\bar{u}=\Big(\rho(r,h)\,[0.4527 \;\; 0.0823 \;\; 1.7156\times10^{-5}]-[8.2317\times10^{-4} \;\; 0.0823 \;\; 2.2459\times10^{-5}]\Big)\begin{pmatrix} z \\ y-r \\ x_{\rm v}+6000y \end{pmatrix}. \tag{5.50}$$

To see the effectiveness of the nonlinearity pre-compensation, we design a normal reduced order CNF control law for the original plant without the pre-compensation using the technique reported in [13], which is given by

$$\dot{x}_{\rm v} = -6000x_{\rm v} - 3.6\times10^{7}y + 2.35\times10^{8}\,\mathrm{sat}(u), \tag{5.51}$$

and

$$u = (-\,[\,0.0823 \quad 2.2459\times10^{-5}\,] + \rho(r,h)\,[\,0.0823 \quad 1.7156\times10^{-5}\,])\begin{pmatrix} y-r \\ \\ x_{\rm v}+6000y \end{pmatrix}, \tag{5.52}$$

where $\rho(r,h)$ is the same as in (5.48).

To compare the result of the enhanced CNF technique with conventional control techniques, we also design a PID controller,

$$\begin{pmatrix} \dot{z} \\ \\ \dot{x}_{\rm d} \end{pmatrix} = \begin{bmatrix} 0 & 0 \\ \\ 0 & -N/T \end{bmatrix}\begin{pmatrix} z \\ \\ x_{\rm d} \end{pmatrix} + \begin{bmatrix} 1 \\ \\ 1 \end{bmatrix}(r-y), \tag{5.53}$$

and

$$\bar{u} = \left(k_{\rm p}+\frac{N}{T}k_{\rm d}\right)(r-y) + k_{\rm i}z - \frac{N^2}{T^2}k_{\rm d}x_{\rm d}, \tag{5.54}$$

for the pre-compensated system. The parameters in (5.54) are tuned to yield the best possible implementation result under this control structure, which are given as:

$$N=10, \quad T=10^{-4}, \quad k_{\rm p}=0.0605, \quad k_{\rm d}=2.8876\times10^{-5}, \quad k_{\rm i}=50. \tag{5.55}$$

5.3.2 Simulation and Experimental Results

For simulation, we use the nonlinear model of the microdrive in (5.1) together with all its identified resonant modes given in (4.33)–(4.37). The simulations are done in a continuous

Table 5.2: Settling time (ms): enhanced CNF control versus PID control.

Controller	PID	eCNF	Improvement
Simulation($r = 1\mu m$)	1.7	0.8	53%
Implementation($r = 1\mu m$)	4.5	1.1	76%
Simulation($r = 10\mu m$)	5.75	1.48	74%
Implementation($r = 10\mu m$)	6.8	2.7	60%

setting, and $|\dot{y}| \leq 0.01\mu$m/s is considered to be 0. The simulation results are shown in Figure 5.9 for $1\mu m$ track following and in Figure 5.11 for $10\mu m$ short span track seeking. Experiments are done on the actual HDD with its cover removed. The HDD is placed on a vibration-free platform and an LDV is used to measure the displacement of the R/W head of the HDD. The controllers are implemented using a dSpace DSP installed in a desktop computer. The sampling frequency is set to be 10 kHz, a typical sampling frequency used in HDD servo systems. The experimental results are shown in Figure 5.10 for $1\mu m$ track following and in Figure 5.12 for $10\mu m$ short span track seeking. From the figures, we can see that in both track following and short span track seeking, the enhanced CNF controller achieves fast and smooth settling, whereas the normal CNF controller (without integral and pre-compensation) can not settle into the desired neighborhood of the target reference, i.e., there is a noticeable static bias on the output response. The PID controller leads to a large overshoot and consequently slow settling, especially in $10\mu m$ track seeking. Moreover, oscillation can be observed in the output responses associated with the PID controller, which suggests that the high frequency resonance may have been activated. We summarize the tracking performances (in terms of settling time characterized by 5% track width for 50K TPI) in Table 5.2. Clearly, the performance of the enhanced CNF control is much better than that of the PID control.

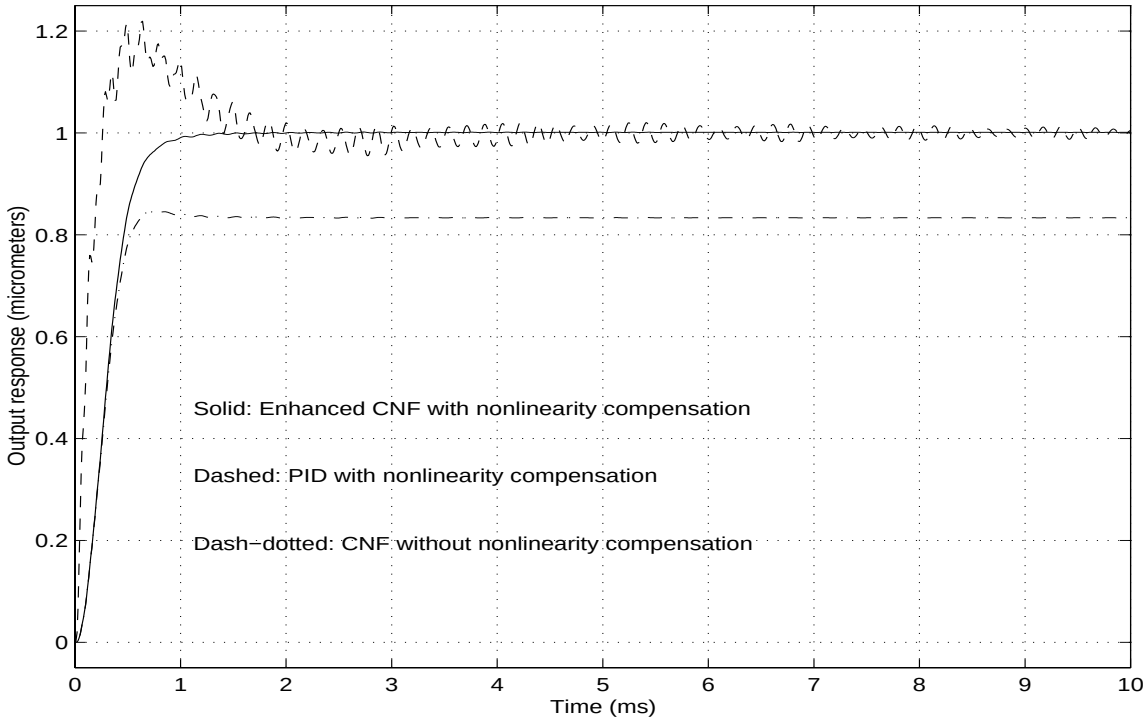

a. Output response.

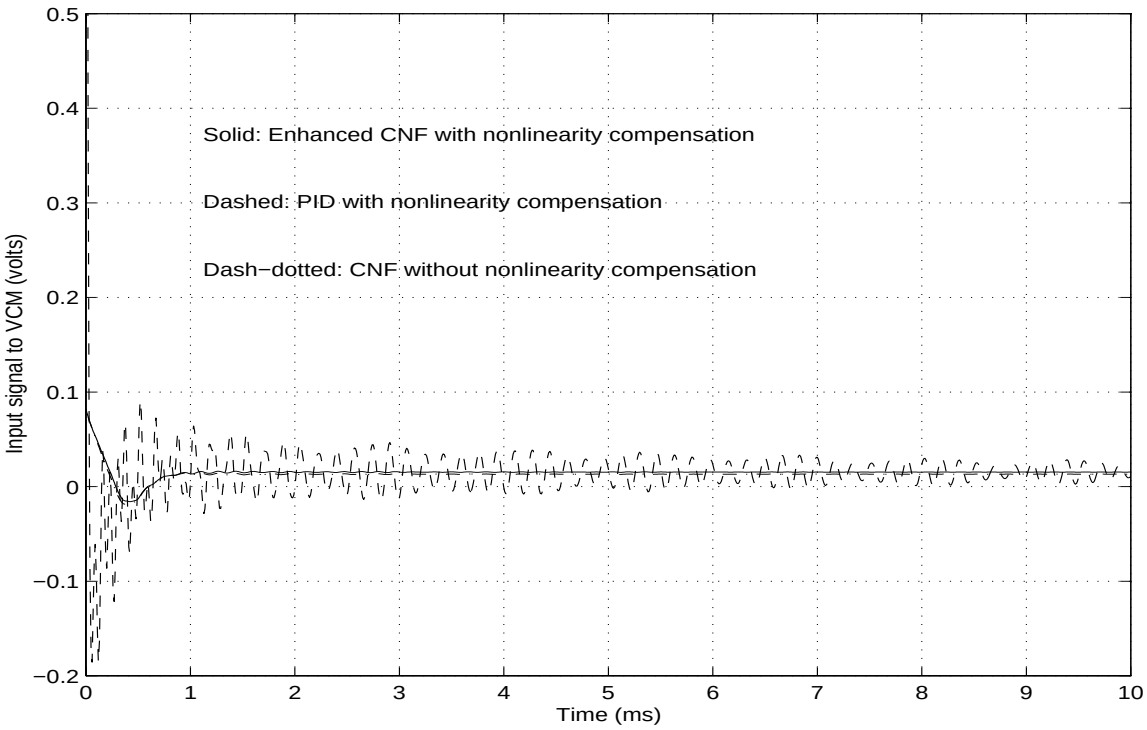

b. Input signal to VCM.

Figure 5.9: Simulation results ($r = 1\mu m$).

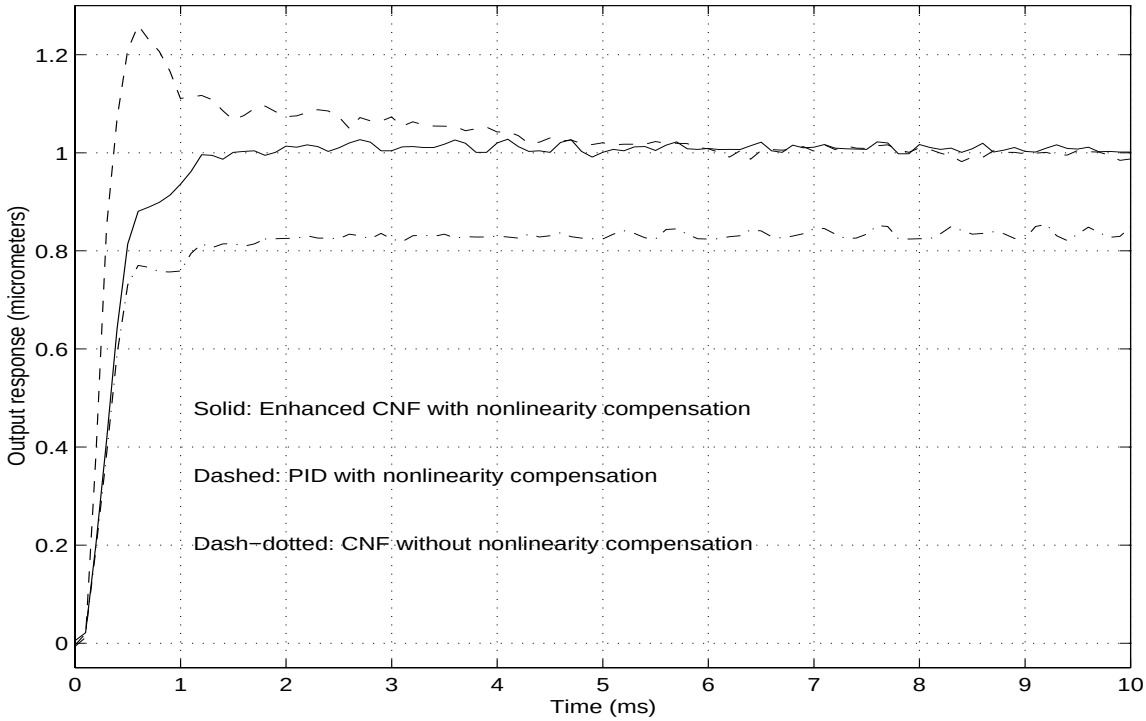

a. Output response.

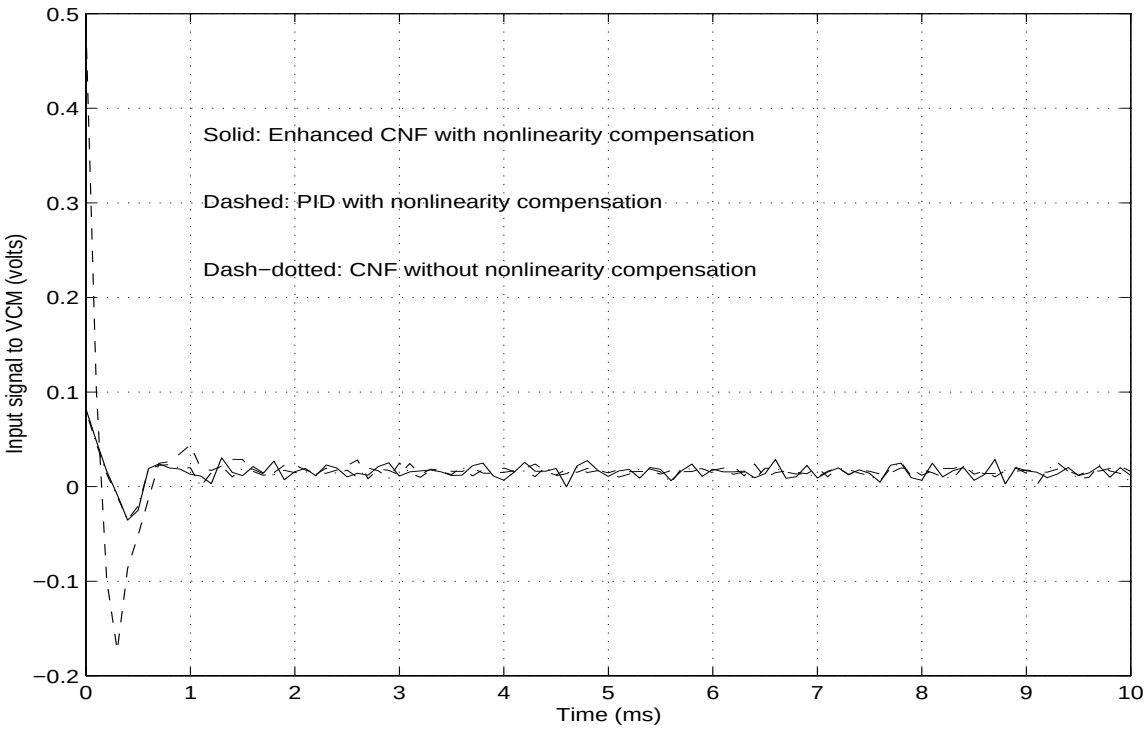

b. Input signal to VCM.

Figure 5.10: Experimental results ($r = 1\mu m$).

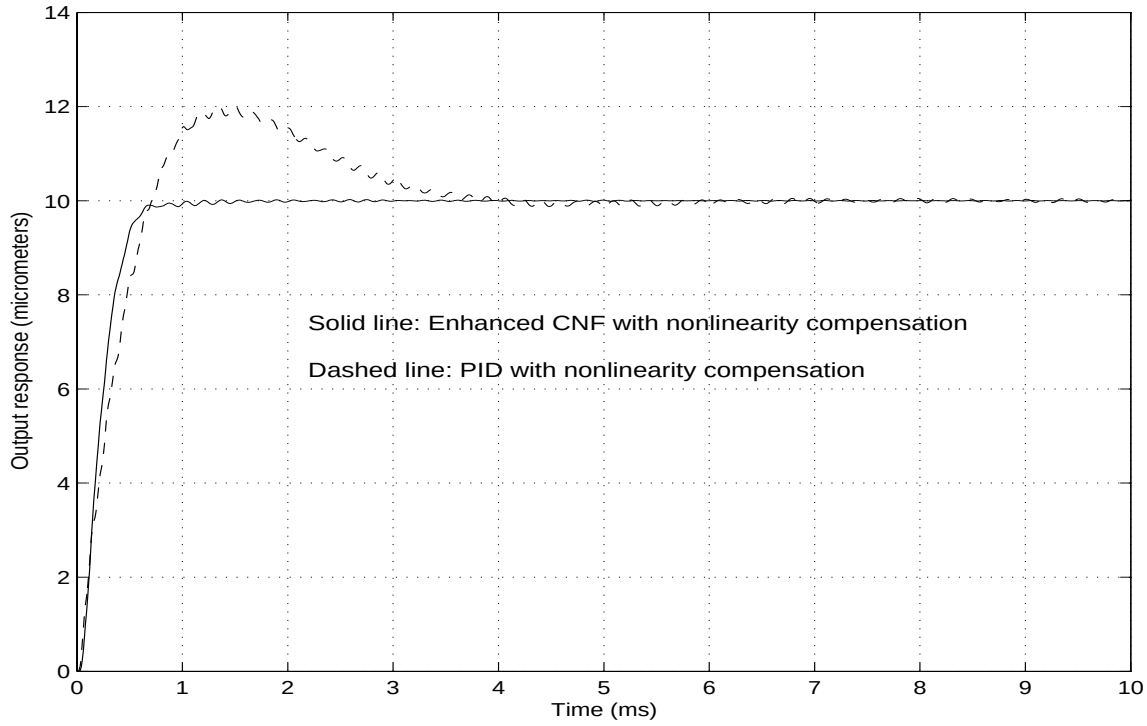

a. Output response.

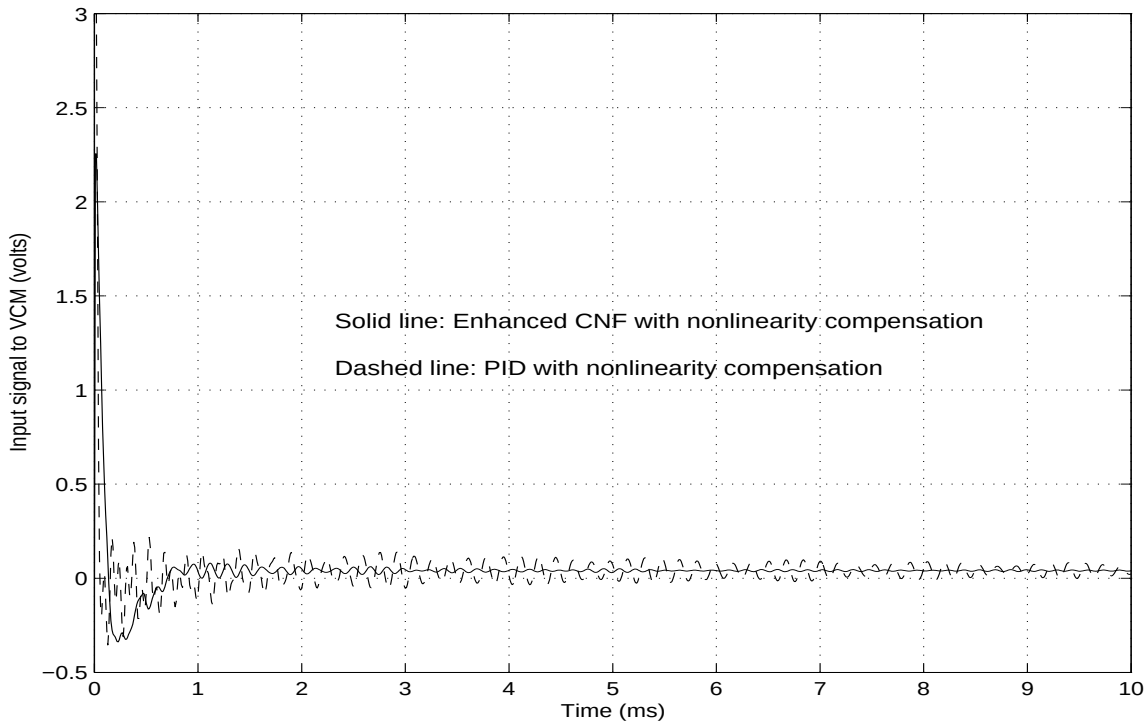

b. Input signal to VCM.

Figure 5.11: Simulation results ($r = 10\mu m$).

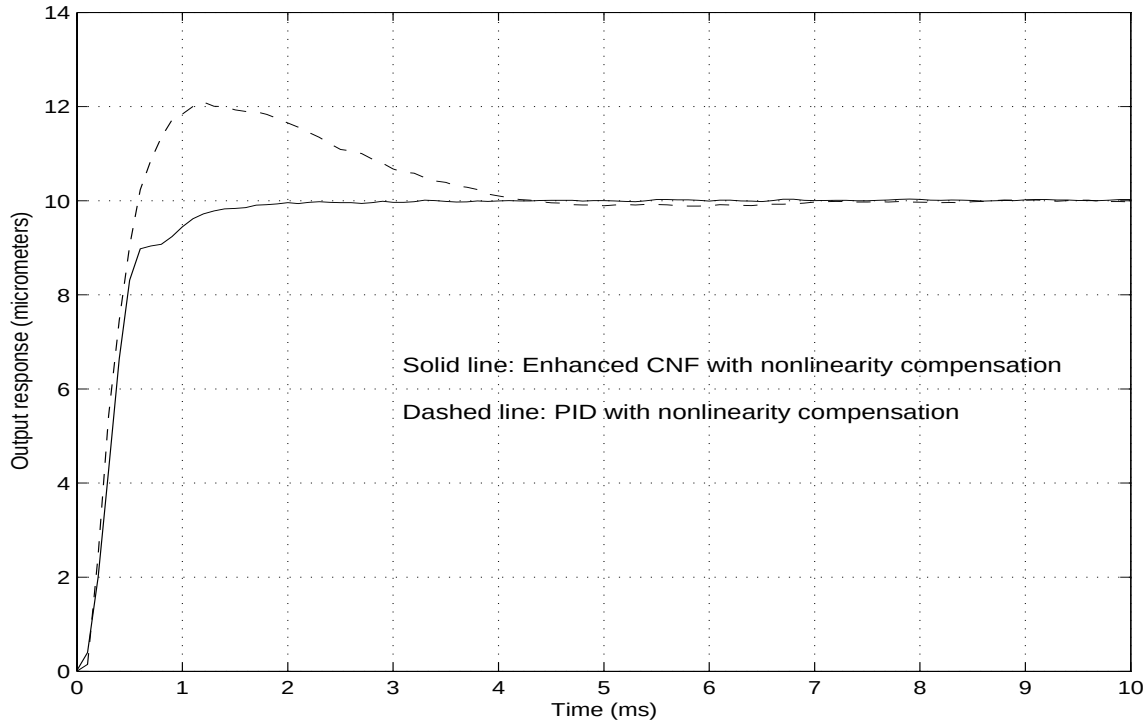

a. Output response.

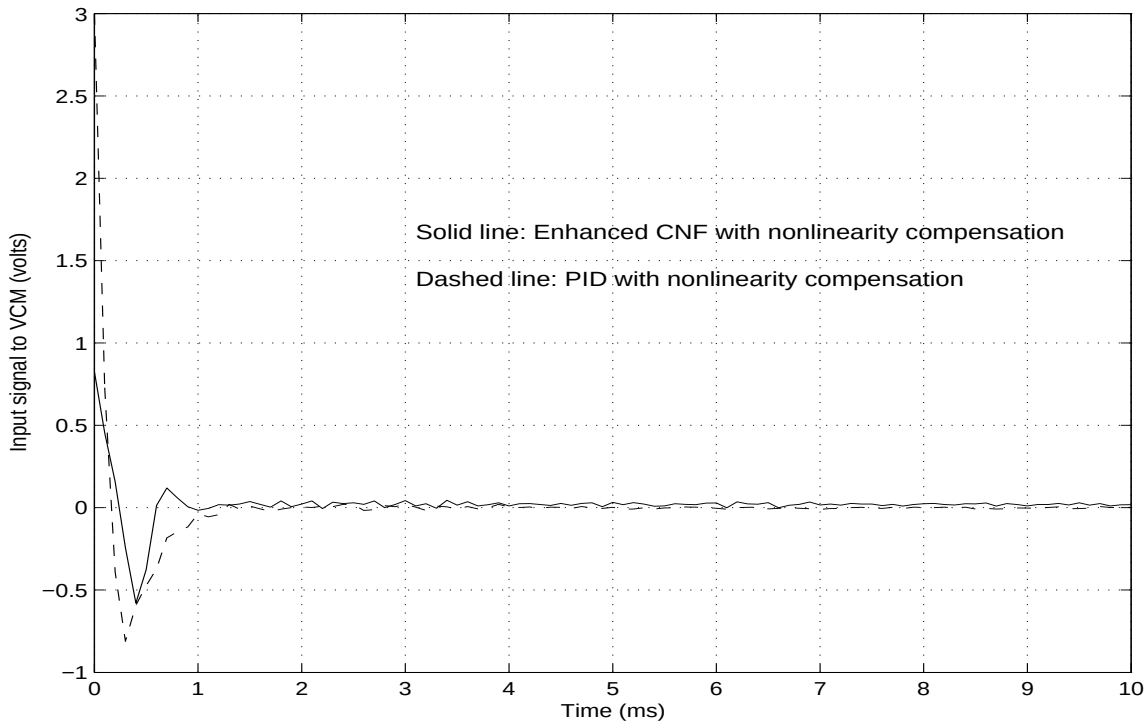

b. Input signal to VCM.

Figure 5.12: Experimental results ($r = 10\mu m$).

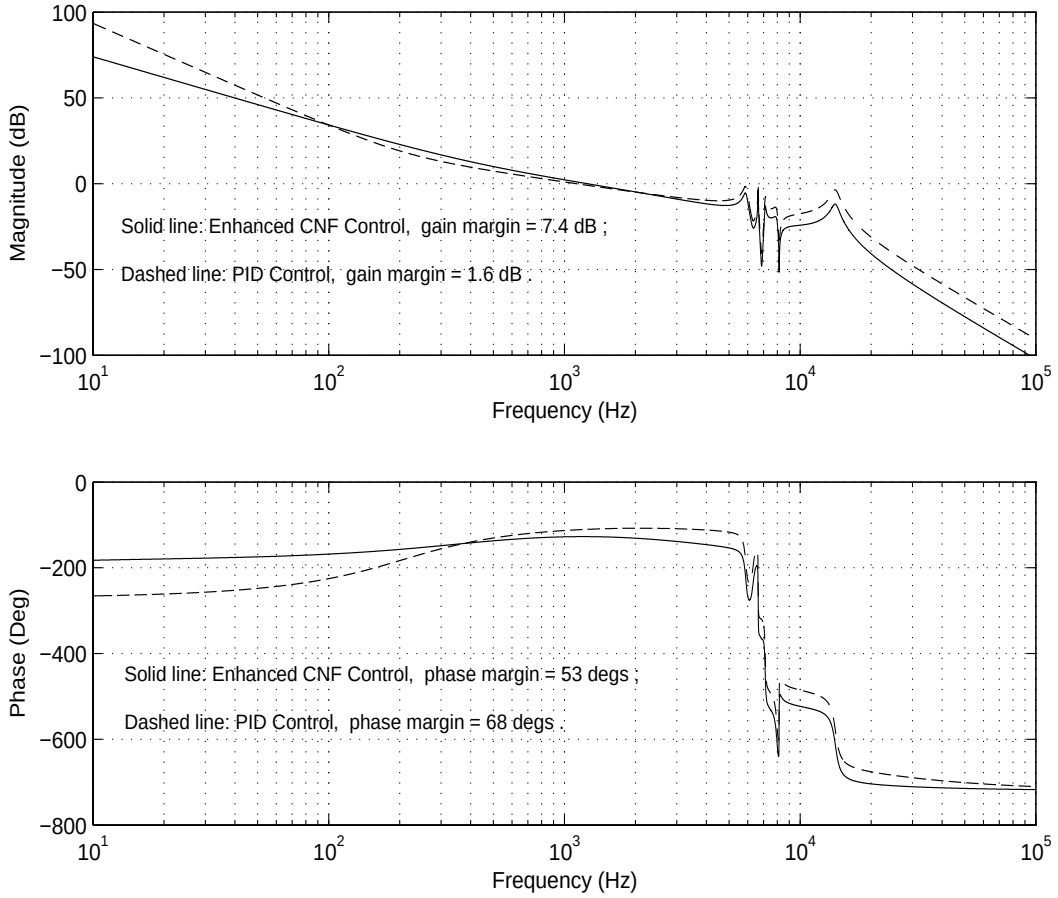

Figure 5.13: Frequency responses of the open-loop system.

We next examine the frequency domain properties of the servo system by breaking the loop at the input point to the pre-compensated plant (marked '$\times$' in Figure 5.8) and computing its open-loop frequency response with the reference input, r, being set to 0. For the CNF control, which is nonlinear, we replace $\rho(r, h)$ by $\rho^* = -3$, representing the steady state situation of such a control scheme. The resulting frequency responses of the servo system shown in Figure 5.13 clearly indicate that the servo system with the enhanced CNF controller has a gain margin of 7.4 dB and a phase margin of 53°, while the one with the PID controller has a gain margin of 1.6 dB and a phase margin of 68°. The gain margin in the PID control is not acceptable in practical situations. This could be due to the fact that we have tuned the response of the PID control a bit too fast, although it is very slow compared to that of the enhanced CNF control.

5.4 Concluding Remarks

In this chapter, two servo system designs have been presented for a microdrive, based on its comprehensive model which explicitly identifies the characteristics of pivot bearing friction and flex cable nonlinearity. We first designed a track following controller for the microdrive, using the Robust and Perfect Tracking (RPT) methodology enhanced with integral and nonlinear compensation. Simulation and experiments show that this enhanced RPT controller can achieve faster settling and eliminate static bias, which is a significant improvement over a conventional RPT controller and a PID controller. Next, we applied the enhanced CNF technique developed in Chapter 2 to design a microdrive servo system, which is capable of fast and smooth track seeking and following without steady state bias. Simulation and implementation results show that the enhanced CNF control has outperformed the conventional PID control in settling time by a high percentage. The techniques and relevant ideas can be adopted to solve other servomechanism problems as well.

Chapter 6

Design of a Piezoelectric Dual-stage HDD Servo System

The previous chapter is focused on the design of single-stage servo system, where the VCM actuator is the sole positioning mechanism for R/W heads in HDDs. In this chapter, we consider the design and implementation of a dual-stage actuated HDD servo system, in which an additional piezoelectric microactuator is mounted on top of the conventional VCM actuator to provide a faster and finer positioning, while the existing VCM actuator is used to move the R/W head assembly for large but coarse positioning onto a target track.

6.1 Introduction

The HDD industry has been undergoing rapid progress for the past two decades and it is now moving towards smaller disk drives with higher capacity. As the areal density continues to increase and track spacing (or track pitch) becomes tighter, a more stringent TMR (track mis-registration) budget is imposed for servo design. To meet the tougher requirement, the servo bandwidth must be expanded. However, the conventional VCM actuator has significant mechanical modes (or resonant modes) that limit the achievable bandwidth. To circumvent this headache, many approaches have been tested. The first is loop-shaping

based design for suppressing the resonant modes (*e.g.*, using notch filter). The second is the so-called multi-sensing servo control design, which damps the resonant modes by attaching an acceleration sensor or a strain sensor to the actuator and feeding back the vibration signal of the inner analog loop. The third approach, now seemingly the most promising one, is the so-called dual-stage servo design, in which the existing VCM actuator is used as a primary stage to perform large but coarse movement, while a secondary micro-actuator is employed to provide finer and faster positioning. The secondary micro-actuator could be, in some designs, a push pull piezoelectric (such as PZT) actuator that typically would be mounted between the R/W head suspension and the actuator arm, or in other designs, an electrostatic or electromagnetic MEMS-based actuator sandwiched between the suspension gimbal and slider. The dual-stage actuated system has been extensively studied by the HDD servo community during the past ten years, and has demonstrated superb performance in some experiments. It is predicted that dual-stage actuator will be integrated into commercial hard disk drives in the near future.

In most PZT-based dual-stage systems, the displacement of the R/W head relative to the VCM arm, or the so-called Relative Position Signal (RPS), is generally not available, while for MEMS-based micro-actuators, capacitive or piezoresistive sensing can be used to measure the RPS [70]. Dual-stage servo design should aim to use the two different actuators to their advantages, so as to enhance the combined performance. For this, special attention must be paid to ensure the cooperation between the two actuator control loops. Several configurations have been proposed to deal with this problem [30]. The baseline is the so-called parallel configuration, where two separate controllers are designed for VCM and micro-actuator to work in low and high frequency regions respectively, using the PES (Position Error Signal) as the feedback information, and usually no special actions are taken to coordinate the two actuators in the mid-frequency handoff region. In this configuration,

the two actuators might end up interfering destructively. The next one is the master-slave configuration, which is basically a variant of the parallel configuration except that the RPS signal, instead of the PES, is used as the input for the VCM control loop (the slave loop). This configuration eases the design for actuator coordination, but the two actuator loops is still coupled. Moreover, feeding back the RPS signal is dependent on its availability. However, when the RPS signal is available, it is more desirable to feedback the summation of the RPS and the PES, which is actually the relative position error signal of the VCM, into the VCM control loop, and the result is the so-called decoupled configuration, where the two actuator loops are now totally decoupled. In this circumstance controllers can be designed independently for the two actuator loops to optimize their sensitivity functions. In the case when the RPS is not measurable or too costly to measure, an observer based on the micro-actuator model can be used to estimate the RPS, and the decoupled configuration may still be used, but the robustness must be checked carefully [42]. In all the above configurations, whenever the RPS signal is available, a minor feedback loop using the RPS can be applied to damp the resonance of the micro-actuator (the so-called active damping, [70]), resulting in a well-behaved dual-stage system which makes it easier for servo design.

Many design schemes for dual-stage HDD servo systems have been reported in recent years. They are mostly based on the aforementioned configurations, probably with some modifications (see *e.g.*, [31, 35, 38, 41, 54, 57, 60, 61]). Especially, Peng *et al.* [57] combined the Composite Nonlinear Feedback (CNF) control with filtering technique within a model-based decoupled configuration to design a dual-stage servo system with a piezoelectric actuator, which achieved significant improvement over single-stage counterpart in HDD track following.

In this chapter, we consider the design and implementation of a piezoelectric dual-stage actuated HDD servo system. In our design, the low frequency characteristics of the

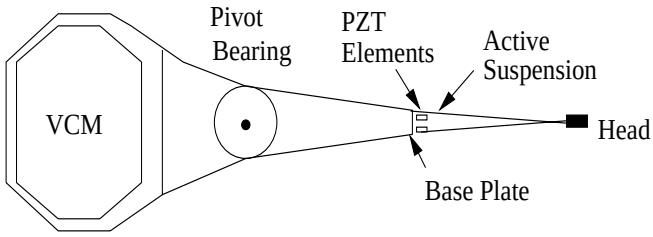

Figure 6.1: A dual-stage HDD actuator.

piezoelectric microactuator are utilized to estimate its displacement and accordingly the displacement of the VCM actuator. Based on the concept of open loop inverse control, the microactuator will be controlled by a simple static gain together with an appropriately designed filter, and the VCM actuator will be controlled using some well-established single-stage servo design methodology, specifically, the RPT (robust and perfect tracking), CNF(composite nonlinear feedback) and PID respectively. Simulation and implementation will then be carried out to evaluate the performance of the dual-stage servo system.

The remaining part of this chapter is organized as follows. Section 6.2 deals with the identification of the mathematical models of the VCM actuator and the piezoelectric microactuator, which are used to form the dual-stage actuated HDD servo system. We will proceed to design controllers for the dual-stage servo system in Section 6.3. Especially, one controller for the microactuator and three alternative controllers for the VCM will be designed. Simulation and implementation results of the dual-stage servo system will be presented and analyzed in Section 6.4. Finally, we draw some concluding remarks in Section 6.5.

6.2 Modeling of the Dual-stage Actuated HDD system

Figure 6.1 is a simple illustration of the dual-stage actuator considered in this chapter. The microactuator here is a piezoelectric actuator. When driven by voltage, the microactuator produces relative motion of the R/W head along the active suspension or the radial direction

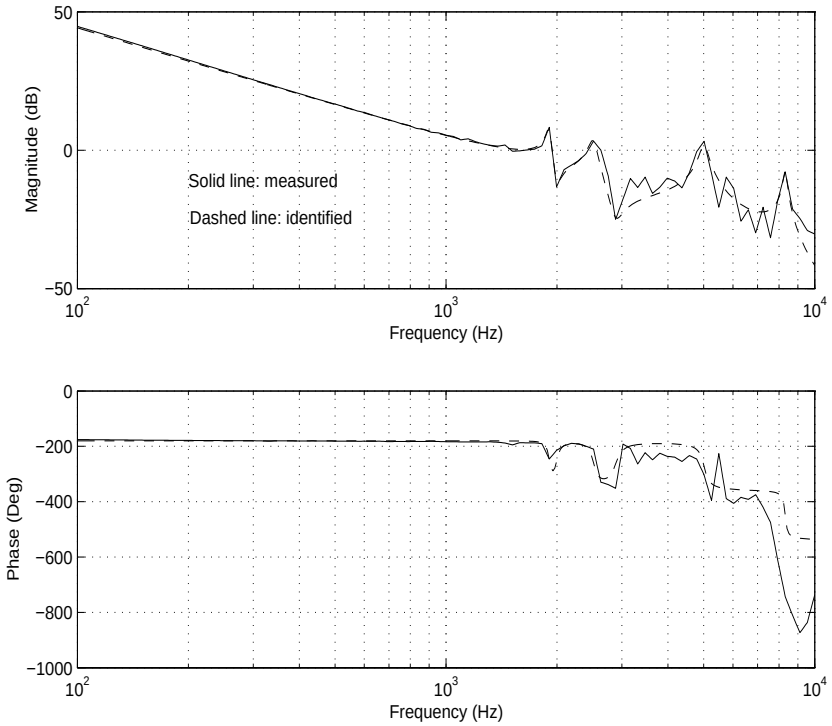

Figure 6.2: Frequency response characteristics of the VCM actuator.

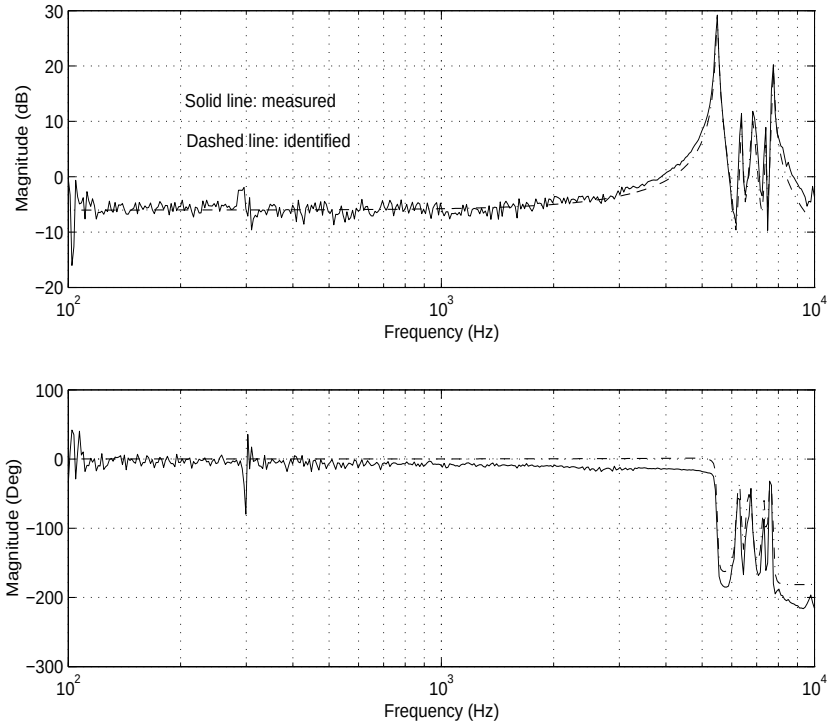

Figure 6.3: Frequency response characteristics of the microactuator.

in the center of the pivot (see *e.g.*, [23] and [30]), while the VCM actuator rotates the base plate and active suspension to move the microactuator and the R/W head across disk surface.

In what follows, the mathematical models of the VCM actuator and the microactuator are derived to compose the model of the dual-stage actuated HDD servo system. These models are identified through frequency response characteristics obtained from experiments using a laser Doppler vibrometer (LDV) and a dynamic signal analyzer. We would like to note that in our experimental setup, the cover of the hard disk drive and the disk plates are removed. The displacement of the HDD R/W head is measured by the LDV. The frequency responses are measured for the two actuators one by one with the input signal to the other actuator being set to zero. The frequency response characteristics of the VCM actuator and the microactuator used in our experiment are respectively shown in Figures 6.2 and 6.3. Using these measured data from the actual system, and the algorithms of [24] and [67], omitting the flexible modes in higher frequency, we obtain a tenth order model for the VCM actuator together with its driver (a converter from voltage to electric current),

$$G_{\rm v}(s) = \frac{6.4013\times10^7}{s^2} \cdot \frac{0.912s^2+457.4s+1.433\times10^8}{s^2+359.2s+1.433\times10^8} \cdot \frac{0.7586s^2+962.2s+2.491\times10^8}{s^2+789.1s+2.491\times10^8} \cdot \frac{9.917\times10^8}{s^2+1575s+9.917\times10^8} \cdot \frac{2.731\times10^9}{s^2+2613s+2.731\times10^9} \tag{6.1}$$

whose input $u_{\rm v}$ is in volts with $|u_{\rm v}| \leq 3$ volts. The output $y_{\rm v}$ is in μm. We obtain also a tenth order model for the microactuator together with its driver (a linear amplifier from voltage to voltage),

$$G_{\rm m}(s) = 0.5 \times \frac{0.7938s^2+767.9s+1.189\times10^9}{s^2+344.8s+1.189\times10^9} \cdot \frac{0.955s^2+978.6s+1.605\times10^9}{s^2+400.6s+1.605\times10^9} \cdot \frac{0.8912s^2+1013s+1.843\times10^9}{s^2+1073s+1.843\times10^9} \cdot \frac{0.9772s^2+460.1s+2.167\times10^9}{s^2+465.5s+2.167\times10^9} \cdot \frac{2.376\times10^9}{s^2+487.4s+2.376\times10^9} \tag{6.2}$$

in which the input $u_{\rm m}$ is again in volts with $|u_{\rm m}| \leq 2$ volts. The output $y_{\rm m}$ is in μm. The

only measurement output for the whole system, y, is the combination of $y_{\rm v}$ and $y_{\rm m}$, *i.e.*,

$$y = y_{\rm v} + y_{\rm m}. \tag{6.3}$$

We note that in practical situations, it is required to design a single servo controller that works for a whole batch of drives with resonant modes varying from drive to drive. As such, we have to design a controller that is robust enough to cope with different resonant modes. Also, in order to simplify our design procedure, we first set aside the resonant modes and approximate the model of the VCM actuator as follows:

$$\Sigma_{\rm v}: \begin{cases} \dot{x}_{\rm v} &= \begin{bmatrix} 0 & 1 \\ 0 & 0 \end{bmatrix} x_{\rm v} + \begin{bmatrix} 0 \\ b \end{bmatrix} \mathrm{sat}(u_{\rm v}) \\ y_{\rm v} &= \begin{bmatrix} 1 & 0 \end{bmatrix} x_{\rm v} \end{cases} \tag{6.4}$$

with $b = 6.4013 \times 10^7$.

Next, by adding an appropriately designed filter, the microactuator model can be approximated as:

$$\Sigma_{\rm m}: \quad y_{\rm m} = 0.5\, \mathrm{sat}(u_{\rm m}). \tag{6.5}$$

It can be seen soon that such approximations on the actuator models are working properly in our design. We would like to note that the simulation results obtained in Section 6.4 are actually done using the models with resonant modes, *i.e.*, the models in (6.1) and (6.2).

6.3 Design of the Dual-stage Actuated HDD Servo System

We now carry out the design of servo system for HDDs with a dual-stage actuator. We would like to design our servo system according to the following requirements.

1. The control input to the VCM actuator should not exceed ± 3 V, whereas the control input to the microactuator should be within ± 2 V.

2. The displacement of the microactuator should not exceed 1 μm. Moreover, it should

settle down to zero in the steady state so that the microactuator can be further used for the next move.

3. The combined displacement of the dual-stage system should settle into the 0.05μm (*i.e.*, 5% of one track pitch) neighborhood of the target track, as fast as possible, and without large overshoot or undershoot. The R/W head of HDDs can start reading or writing data on the disk when it is within 5% of one track pitch from the target track.

4. The gain margin is not less than $6dB$ and the phase margin is not less than $40deg$.

Note that in this dual-stage actuated HDD servo system, the only available measurement is the displacement of the R/W head, which is a combination of the displacement of the VCM actuator and that of the microactuator. Practically, we have to control both actuators using one measurement only, which poses a difficulty for the servo system design. Figure 6.4 is the control configuration we are going to use for the dual-stage servo design. Here MA stands for microactuator, and M_0 is its nominal model, which will be used to estimate the relative position signal (RPS) of the microactuator when this RPS is not measurable. Once this relative displacement is estimated (or measured, if possible) as $\hat{y}_m$, the displacement of the VCM can be derived as $\hat{y}_{\rm v} = y - \hat{y}_m$. The controller C_v is designed so that the output displacement of the VCM actuator will follow the target reference r, and controller C_m is then designed to make the microactuator follow the position error of the VCM, *i.e.*, $r - \hat{y}_{\rm v}$. As a result, the combined output of the dual-stage system will follow the target reference r, hopefully faster than the VCM alone. Since the microactuator can only work within limited stroke, the position error signal of the VCM has to go through a saturation block before it is applied to the controller C_m. Here, the saturation block (with a saturation limit of $1\mu m$) acts as a command generator for the microactuator control loop.

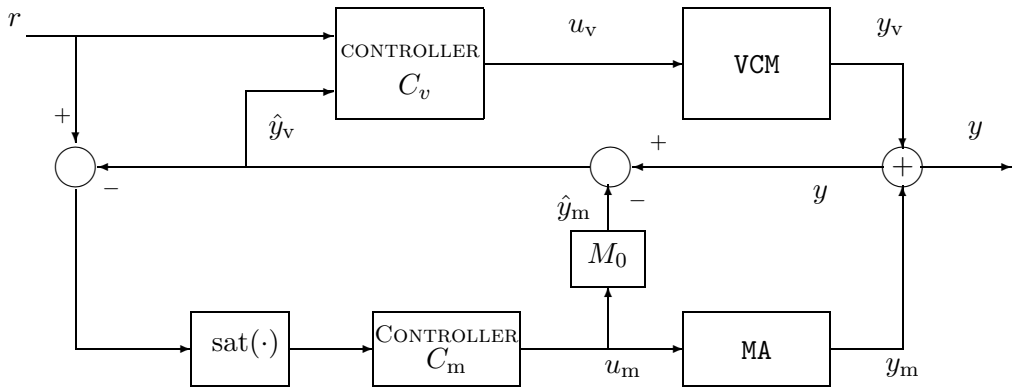

Figure 6.4: The schematic representation of a dual-stage actuator control.

6.3.1 Design of the Microactuator Controller

From the frequency response of the microactuator as shown in Figure 6.3, we find that at low frequency region it is nothing more than a constant gain with a value of $k_0 = 0.5$. This property will be valid so long as we do not push the speed of the microactuator too fast. Based on this observation, the microactuator can be approximated by a nominal model $M_0 : k_0 = 0.5$ and the displacement y_m of the microactuator can be estimated directly from its input $u_{\rm m}$ as $\hat{y}_{\rm m} = k_0 u_{\rm m}$. The design of controller C_m can also be simplified using the characteristics of the microactuator. The concept of open loop inverse control is adopted here. We design the controller C_m as follows,

$$C_m(s) = k_m H_m(s) \tag{6.6}$$

where k_m is a DC gain with a maximal value of $\frac{1}{k_0} = 2$. The maximal value corresponds to the ideal case such that the controlled output of the microactuator fully matches the position error of the VCM. Over here, we will treat this k_m as a tuning parameter so as to improve overall performance. Note that when $k_m = 0$, the microactuator control loop is inactive, and the resulting dual-stage system is equivalent to single stage case. $H_m(s)$ is a series of filters for suppressing resonance and noises along the microactuator control loop.

Its transfer function is given by

$$H_{\mathrm{m}}(s) = \frac{(4000\pi)^2}{s^2 + \sqrt{2} \cdot 4000\pi s + (4000\pi)^2} \cdot \frac{s^2 + 1100\pi s + (11000\pi)^2}{s^2 + 22000\pi s + (11000\pi)^2}, \tag{6.7}$$

where the first item is a second-order Butterworth filter with a cut-off frequency at 2000 Hz and the latter is a notch filter with a central frequency at 5500 Hz. This combined filter is used to attenuate the microactuator resonant modes and high frequency noises. Figures 6.5 clearly shows that the microactuator together with this filter can be nicely approximated by a static gain at low frequency region up to $1kHz$.

6.3.2 Design of the VCM Controller

This subsection deals with the design of controller C_{v} for the VCM actuator loop. The design here is basically the same as in single stage servo design, except that we now have to use the estimated displacement $\hat{y}_{\mathrm{v}}$ instead of a measured one.

First, we introduce a notch filter to reduce the effects of the resonant modes in the VCM actuator,

$$H_{\mathrm{v}}(s) = \frac{s^2 + 238.8s + 1.425 \times 10^8}{s^2 + 2388s + 1.425 \times 10^8} \cdot \frac{s^2 + 314.2s + 2.467 \times 10^8}{s^2 + 6283s + 2.467 \times 10^8}. \tag{6.8}$$

With the notch filter in place and within the working bandwidth of interest, the VCM model can be safely approximated by a double integrator as in (6.4).

Next, we proceed to design controller for the compensated VCM loop, using three different control techniques, ı.e.,, the RPT, CNF, and PID control.

VCM Controller Design 1: Using RPT Control

The first controller for the compensated VCM loop is based on the Robust and Perfect Tracking (RPT) control technique. The RPT technique enables control engineers to design a low-order parameterized controller which still results in a closed-loop system with fast tracking speed and low overshoot as well as strong robustness. This technique has been

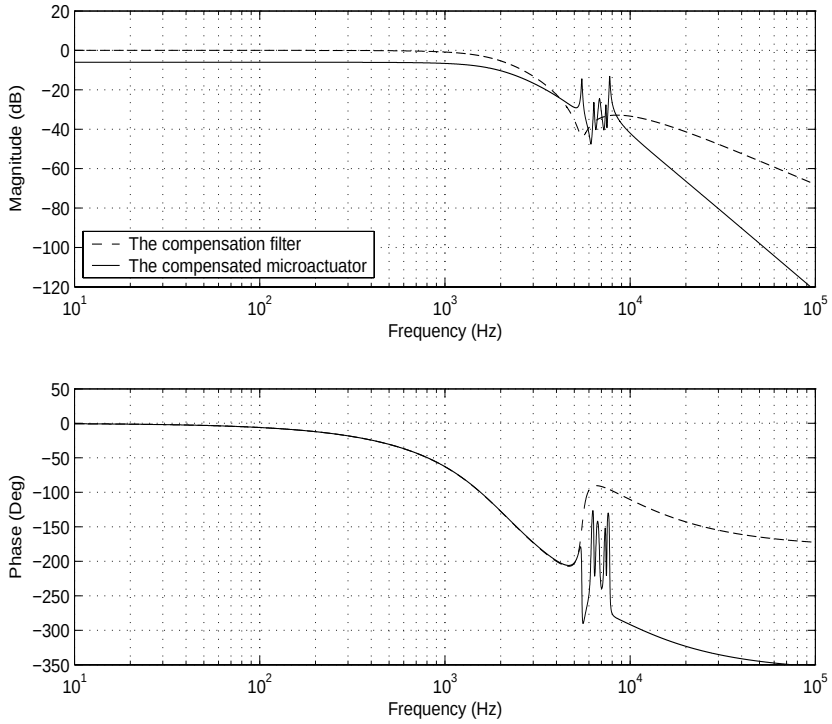

Figure 6.5: Frequency responses of the microactuator with the compensation filter.

successfully utilized to design a microdrive track following controller in the previous chapter. The same idea applies to the control problem here, and a reduced order measurement feedback RPT controller with integral enhancement can be obtained as

$$\begin{cases} \dot{x}_c = A_r(\epsilon)x_c + B_r(\epsilon)\begin{pmatrix} \hat{y}_{\rm v} \\ \\ r \end{pmatrix}, \\ \\ \bar{u}_{\rm v} = C_r(\epsilon)x_c + D_r(\epsilon)\begin{pmatrix} \hat{y}_{\rm v} \\ \\ r \end{pmatrix} \end{cases} \tag{6.9}$$

with

$$\begin{cases} A_r(\epsilon) = \begin{bmatrix} -(\lambda + L + \frac{2\zeta\omega}{\epsilon}) & -\frac{\omega^2\lambda}{\epsilon^2} \\ \\ 0 & 0 \end{bmatrix} \\ \\ B_r(\epsilon) = \begin{bmatrix} -[(\lambda+L)(L+\frac{2\zeta\omega}{\epsilon}) + \frac{\omega^2}{\epsilon^2}] & \frac{2\zeta\omega\lambda}{\epsilon} + \frac{\omega^2}{\epsilon^2} \\ \\ 1 & -1 \end{bmatrix} \\ \\ C_r(\epsilon) = -\frac{1}{b}\left[\lambda + \frac{2\zeta\omega}{\epsilon}, \quad \frac{\omega^2\lambda}{\epsilon^2}\right] \\ \\ D_r(\epsilon) = -\frac{1}{b}\left[\lambda L + (\lambda+L)\frac{2\zeta\omega}{\epsilon} + \frac{\omega^2}{\epsilon^2}, \quad -\frac{\omega^2}{\epsilon^2} - \frac{2\zeta\omega\lambda}{\epsilon}\right] \end{cases} \tag{6.10}$$

where ϵ is the time scale factor which can serve as a tuning parameter; ζ and ω are respectively the damping ratio and natural frequency of the supposedly dominant closed-loop conjugate poles; λ is the integral weighting factor; $L > 0$ is a parameter for the reduced order observer, corresponding to the pole at $-L$.

The control input to the VCM actuator is given by

$$u_{\rm v} = H_{\rm v}(s) \cdot \bar{u}_{\rm v}, \tag{6.11}$$

where $H_{\rm v}(s)$ is the notch filter as defined in (6.8).

It is noted that an integration action (moderately weak) is needed for the VCM actuator to overcome the bias torque induced by the pivot bearing friction and flex cable nonlinearity, so that the output displacement of the VCM will settle into the target track center without static error, and accordingly the relative displacement of the microactuator will return to zero and be ready for next movement.

For the above RPT controller, we choose the following parameters:

$$\epsilon = 1,\ \zeta = 0.8,\ \omega = 800\pi,\ \lambda = 15,\ L = 5000$$

Meanwhile, the DC gain for the microactuator controller C_m is chosen as $k_m = 1.3$. The combined controller $(C_m + C_{\rm v})$ achieves a gain margin of $11.3dB$ and a phase margin of $42.6deg$. Note that these parameters can be tuned for better performance, especially for larger range seeking, the value of λ may have to be scaled down to reduce the overshoot caused by integration.

VCM Controller Design 2: Using Enhanced CNF Control

The second controller we design for the VCM is based on the enhanced composite nonlinear feedback (CNF) control technique developed in Chapter 2. This enhanced CNF technique preserves the nice properties of the original CNF control technique developed by Chen et al. [13], *i.e.*, fast and smooth settling without any explicit switching element in set

point tracking tasks. Moreover, this new technique has an additional feature of removing constant bias and rejecting disturbances. In the case of HDD servo system, we know there are friction and nonlinearities in the VCM actuator, which may cause static bias in tracking tasks. Hence the enhanced CNF technique comes into the picture. In the previous chapter, the enhanced CNF technique has been successfully applied to design a micro HDD servo system that is able to perform track seeking and track following all-in-one with superior performance. The same technique will be used to design the VCM controller over here.

Following the design procedure given in Chapter 2, we first augment the nominal model of VCM with an integration term of the tracking error $y_{\rm v} - r$, the corresponding augmented plant to be used in the enhanced CNF design is then given by

$$\begin{cases} \dot{\bar{x}} = \bar{A}\bar{x} + \bar{B}\text{sat}(u_{\rm v}) + \bar{B}_r r, \\ \bar{y} = \begin{bmatrix} 1 & 0 & 0 \\ 0 & 1 & 0 \end{bmatrix} \bar{x}, \\ h = \begin{bmatrix} 0 & 1 & 0 \end{bmatrix} \bar{x}. \end{cases} \tag{6.12}$$

where

$$\bar{A} = \begin{bmatrix} 0 & 1 & 0 \\ 0 & 0 & 1 \\ 0 & 0 & 0 \end{bmatrix}, \ \bar{B} = \begin{bmatrix} 0 \\ 0 \\ b \end{bmatrix}, \ \bar{B}_r = \begin{bmatrix} -1 \\ 0 \\ 0 \end{bmatrix},$$

with $b = 6.4013 \times 10^7$. For the above system we choose an appropriate state feedback gain $F = [\, f_0 \quad f_1 \quad f_2 \,]$, such that the resulting closed-loop system has an integration pole at $-\lambda$ and a pair of conjugate poles with a low damping ratio ζ and a natural frequency ω. Next, to design the nonlinear feedback law of CNF, we choose a diagonal matrix W as follows:

$$W = \begin{bmatrix} 2\gamma f_0^2 & & \\ & 2f_1^2 & \\ & & -\frac{2\eta f_1}{b} \end{bmatrix} \tag{6.13}$$

with γ and η being positive tuning parameters. It can be checked that $W > 0$. We solve the following Lyapunov equation:

$$(\bar{A} + \bar{B}F)'P + P(\bar{A} + \bar{B}F) = -W, \tag{6.14}$$

for a positive definite matrix P,

$$P = \begin{bmatrix} (1+\gamma)f_0 f_1 & 0 & -\frac{\gamma f_0}{b} \\ 0 & \frac{\gamma f_0}{b} + f_1 f_2 - \frac{(1+\eta)f_1^2}{b f_2} & -\frac{f_1}{b} \\ -\frac{\gamma f_0}{b} & -\frac{f_1}{b} & \frac{(1+\eta)f_1}{b^2 f_2} \end{bmatrix}. \tag{6.15}$$

The feedback gain matrix of the nonlinear part of CNF control law is then given by

$$F_n = \bar{B}' P = [\, -\gamma f_0 \quad -f_1 \quad \tfrac{(1+\eta)f_1}{b f_2} \,]. \tag{6.16}$$

Finally, choosing a reduced order observer with a pole at $-L$, we obtain a reduced order enhanced CNF control law as follows:

$$\begin{cases} \dot{x}_{\rm e} = \hat{y}_{\rm v} - r, \\ \dot{x}_{\rm c} = -L x_{\rm c} - L^2 \hat{y}_{\rm v} + b \cdot \mathrm{sat}\,(u_{\rm v}), \end{cases} \tag{6.17}$$

and

$$\bar{u}_{\rm v} = \{[\, f_0 \quad f_1 \quad f_2 \,] + \rho(r, \hat{y}_{\rm v})\, [\, -\gamma f_0 \quad -f_1 \quad \tfrac{(1+\eta)f_1}{b f_2} \,]\} \times \begin{pmatrix} x_{\rm e} \\ \hat{y}_{\rm v} - r \\ x_{\rm c} + L\hat{y}_{\rm v} \end{pmatrix}, \tag{6.18}$$

$$u_{\rm v} = H_{\rm v}(s) \cdot \bar{u}_{\rm v}, \tag{6.19}$$

where

$$\begin{cases} f_0 = -\frac{\lambda \omega^2}{b}, \\ f_1 = -\frac{2\zeta\omega\lambda + \omega^2}{b}, \\ f_2 = -\frac{\lambda + 2\zeta\omega}{b}. \end{cases} \tag{6.20}$$

and

$$\rho(r, \hat{y}_{\rm v}) = -\beta |e^{-\alpha |r - \hat{y}_{\rm v}|} - e^{-1}|, \tag{6.21}$$

with $\alpha = 1$, $\beta = 2.0$, $\gamma = 200$, $\eta = 0.1$, $\zeta = 0.3$, $\omega = 600\pi$, $\lambda = 0.1$ and $L = 5000$ being the nominal values for $r = 1\mu m$. Note that these parameters can be fine tuned for better performance. For the above controller, the DC gain for the microactuator controller C_m is chosen accordingly as $k_m = 1.3$.

Although the above CNF control law is basically a nonlinear one, stability margins can be verified for the steady state case when the tracking error $r - \hat{y}_{\rm v}$ approaches zero and the

nonlinear function ρ converges to a constant value of $-\beta(1-e^{-1})$. At the steady state, the CNF controller reduces to a linear feedback controller, hence the loop transfer function can be derived and stability margins obtained. The combined controller $(C_m + C_{\rm v})$ achieves a gain margin of $8.8dB$ and a phase margin of $45.3deg$.

VCM Controller Design 3: Using PID Control

The third controller we design for the VCM is based on the conventional PID control. The design process is trivial. A PID controller with low-pass filtering and the notch filter of (6.8) is given as follows,

$$u_{\rm v} = H_{\rm v}(s) \cdot \left(k_p + \frac{k_d s}{1 + \frac{sT}{N}} + \frac{k_i}{s} \right) \cdot (r - \hat{y}_{\rm v}) \tag{6.22}$$

with

$$k_p = 6.6705 \times 10^{-3},\ k_d = 1.2250 \times 10^{-5},\ k_i = 0.4,\ T = 5 \times 10^{-5},\ N = 10$$

For this PID controller, we choose the DC gain for the microactuator controller C_m to be $k_m = 1.8$. The combined controller $(C_m + C_{\rm v})$ achieves a gain margin of $6.1dB$ and a phase margin of $55.3deg$.

We have so far designed three alternative controllers for the VCM control loop. The Open loop frequency characteristics of the HDD servo systems with the three designs are shown in Figures 6.6, 6.7 and 6.8 respectively. The gain margins and phase margins of these designs are summarized in Table 6.1, which verifies that the designed control laws meet the stability margin requirements. Over here, the single-stage refers to the case when $k_m = 0$, *i.e.*, the microactuator control loop is inactive.

6.4 Simulation and Experimental Results

Simulations and experiments are carried out to evaluate the performance of the above designed dual-stage servo controllers in HDD track following and seeking tasks. The simu-

Table 6.1: Gain margin (GM) and phase margin (PM).

Design method	Single-stage		Dual-stage	
	GM (dB)	PM (deg)	GM (dB)	PM (deg)
RPT	10.8	42.3	11.3	42.6
CNF	9.1	45.0	8.8	45.3
PID	6.9	55.3	6.1	55.3

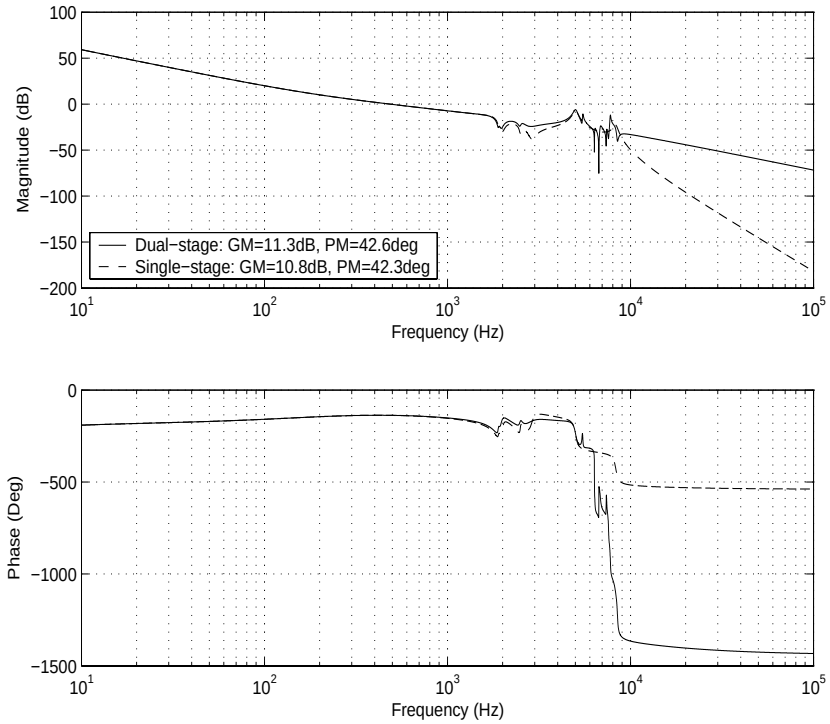

Figure 6.6: Open loop frequency characteristics of the servo systems with RPT control.

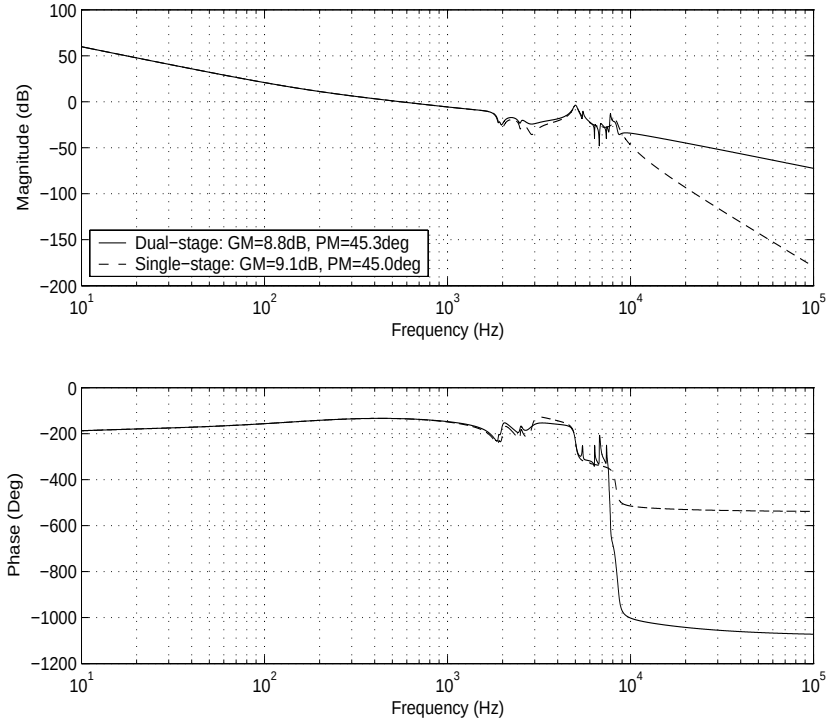

Figure 6.7: Open loop frequency characteristics of the servo systems with CNF control.

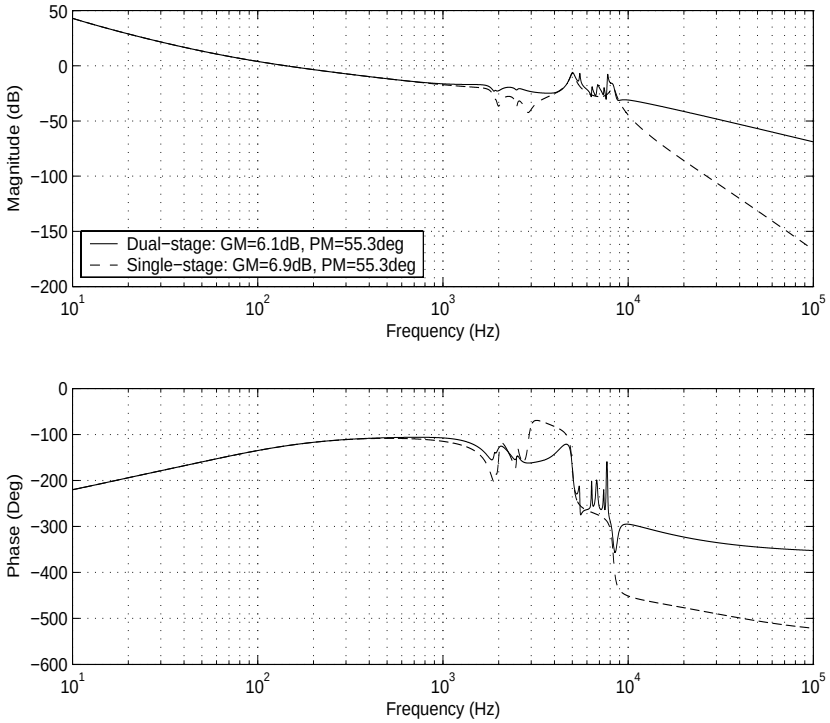

Figure 6.8: Open loop frequency characteristics of the servo systems with PID control.

lations are done in a continuous-time setting. The experiments are carried out at a sampling frequency of 20 kHz. Note that the hard disk drive used in our experiment has all its cover and disk plates removed, and is placed on a vibration-free table. The displacement of the R/W head is measured by a laser Doppler vibrometer, and the real-time control is implemented using a dSpace package. The results of the dual-stage actuated HDD servo system will then be compared with those of the servo system with a single-stage actuator VCM. The latter is done on the same drive by keeping the microactuator control loop inactive throughout the implementation process.

6.4.1 Track Seeking and Following Test

We first test the performance of the dual-stage actuated servo system in track seeking and track following ($r \leq 1\mu m$) tasks. The simulation results of $r = 1\mu m$ (track following) are shown in Figures 6.9, 6.10 and 6.11 for the three different designs based on RPT, CNF and PID respectively. Figures 6.12 to 6.14 compare the experimental results for $r = 1\mu m$ track following between the three dual-stage designs and their single-stage counterparts. One can easily see that the microactuator plays an active role here. Figures 6.15 to 6.17 compare the experimental results for $r = 10\mu m$ (track seeking). From the results, we notice that in track following, all the designs achieve satisfactory results, thanks to the contribution of the microactuator. However, in track seeking, the VCM plays a major role instead. Hence, the different designs for VCM control loop exhibit significant performance variation. But still, the microactuator can improve the precision of R/W head positioning at the steady state, and facilitate the settling process of track seeking tasks. It is observed that for $10\mu m$ seeking, the PID design results in a sluggish settling process. We know that the performance of the PID design is limited by its structure (one degree of freedom) and the stability margin requirement. Both RPT and CNF designs have a fast and smooth settling while fulfilling the stability margin requirement. Table 6.2 summarizes the tracking performances in terms

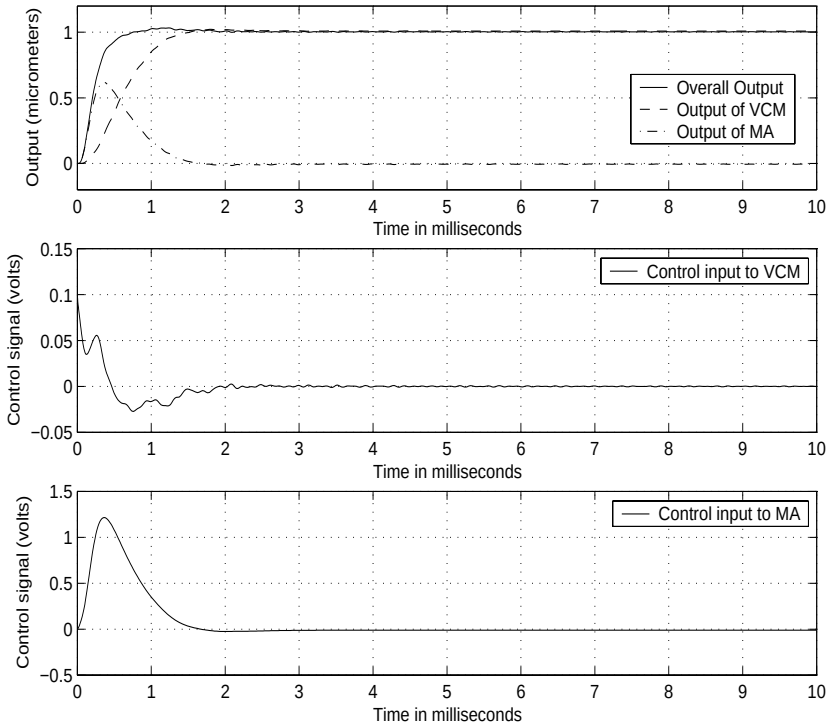

Figure 6.9: Simulation results for $r = 1\mu$m: RPT control.

of settling time.

6.4.2 Position Error Signal Test

The disturbances in a real HDD are usually considered as a lumped disturbance at the plant output, also known as runouts. Repeatable runouts (RROs) and nonrepeatable runouts (NRROs) are the major sources of track following errors. RROs are caused by the rotation of the spindle motor and consists of frequency components that are multiples of the spindle frequency. NRROs can be perceived as coming from three main sources: vibration shocks, mechanical disturbances and electrical noises. NRROs are usually random and unpredictable by nature, unlike repeatable runouts. They are also of a lower magnitude. A perfect servo system for HDDs should reject both the RROs and NRROs.

As mentioned earlier, the cover and disk plates of the hard disk drive are removed in our experiment. As such, some disturbances of the actual system, *e.g.*, the runout disturbances, are no longer existent. In order to test the robustness of our design against

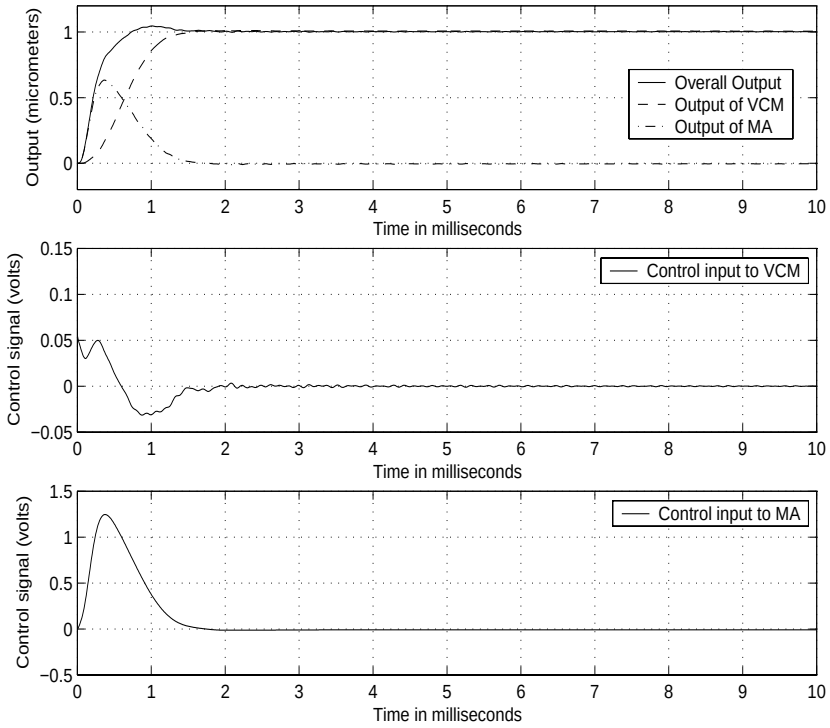

Figure 6.10: Simulation results for $r = 1\mu$m: CNF control.

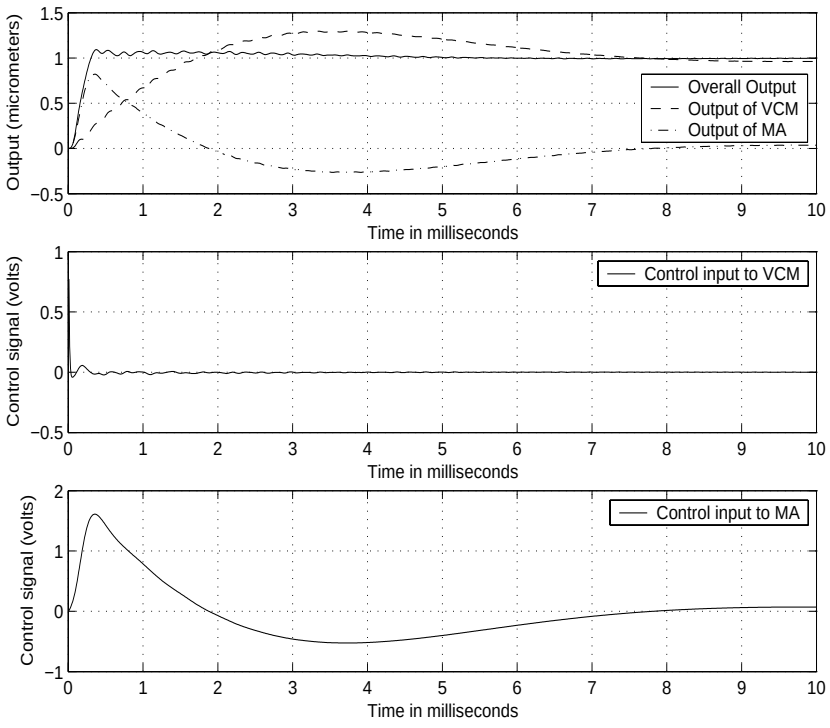

Figure 6.11: Simulation results for $r = 1\mu$m: PID control.

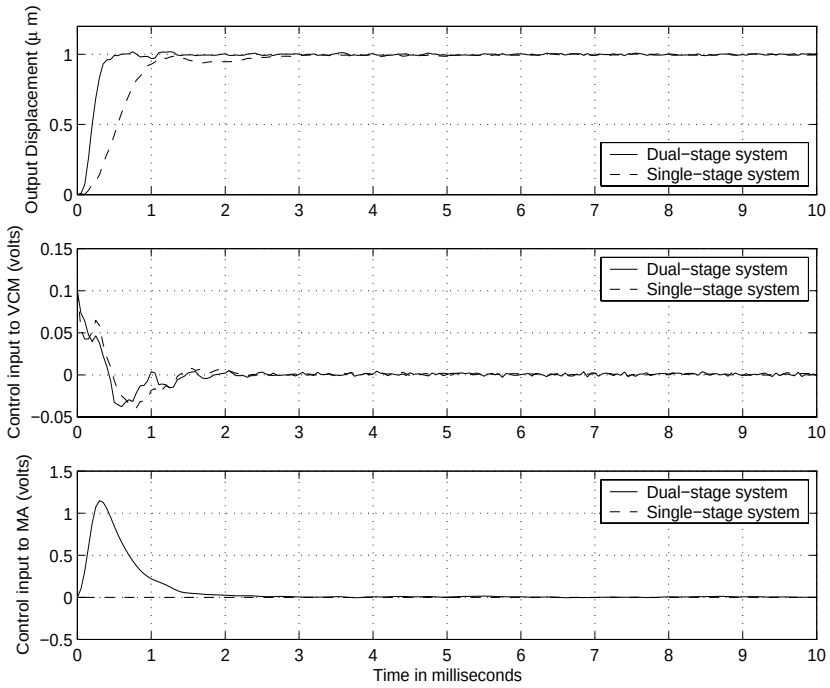

Figure 6.12: Experimental results for $r = 1\mu$m: RPT design(dual- versus single-stage).

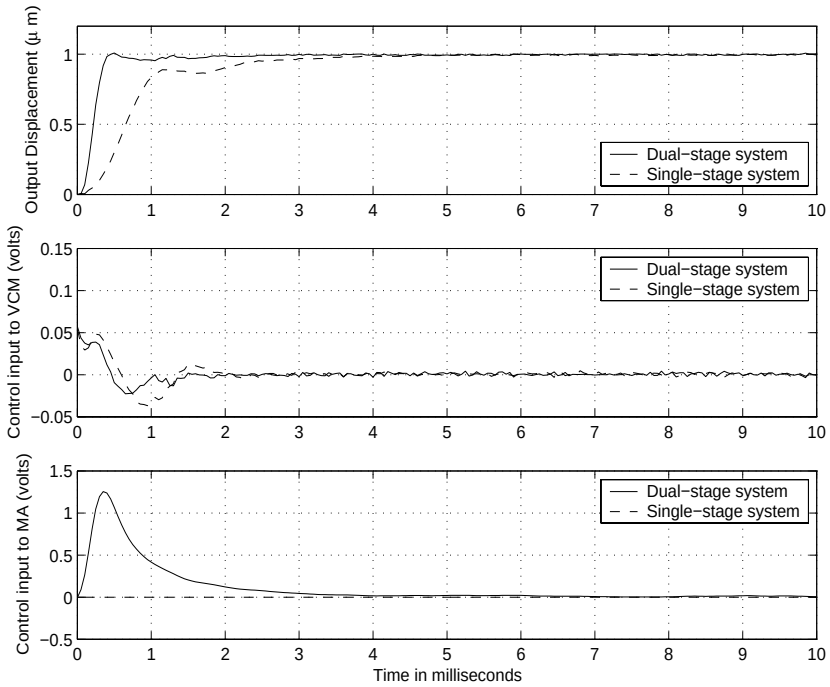

Figure 6.13: Experimental results for $r = 1\mu$m: CNF design (dual- versus single-stage).

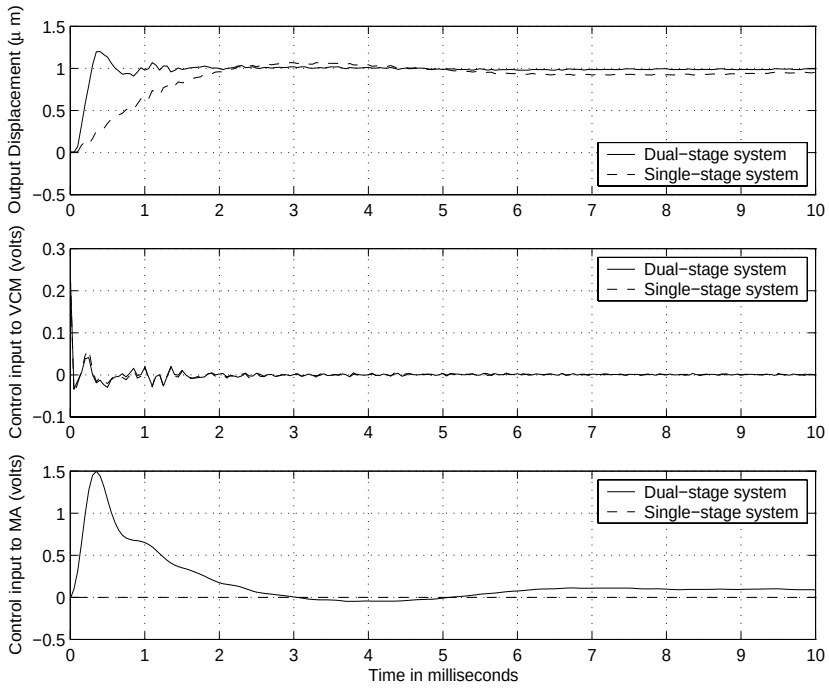

Figure 6.14: Experimental results for $r = 1\mu$m: PID design (dual- versus single-stage).

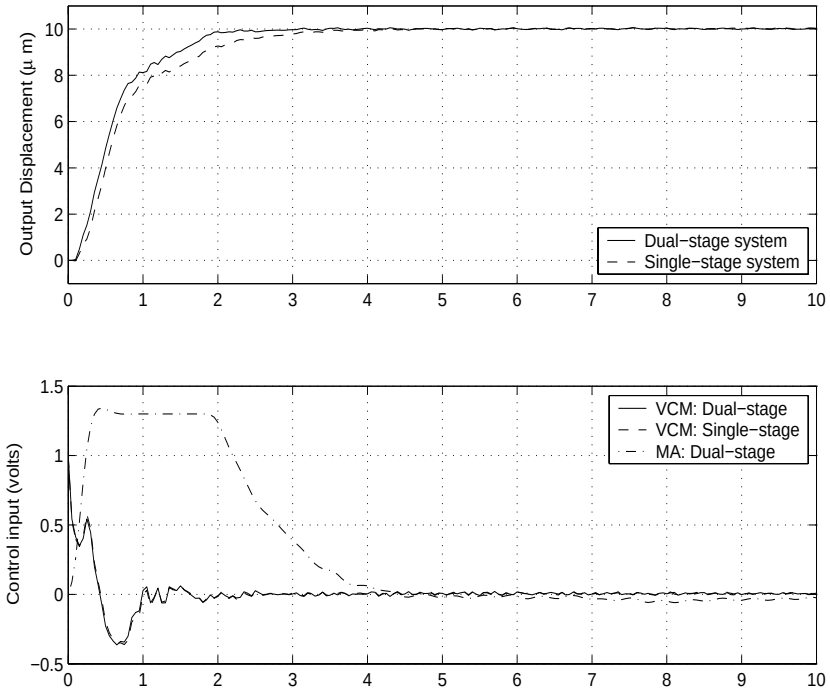

Figure 6.15: Experimental results for $r = 10\mu$m: RPT design (dual- versus single-stage).

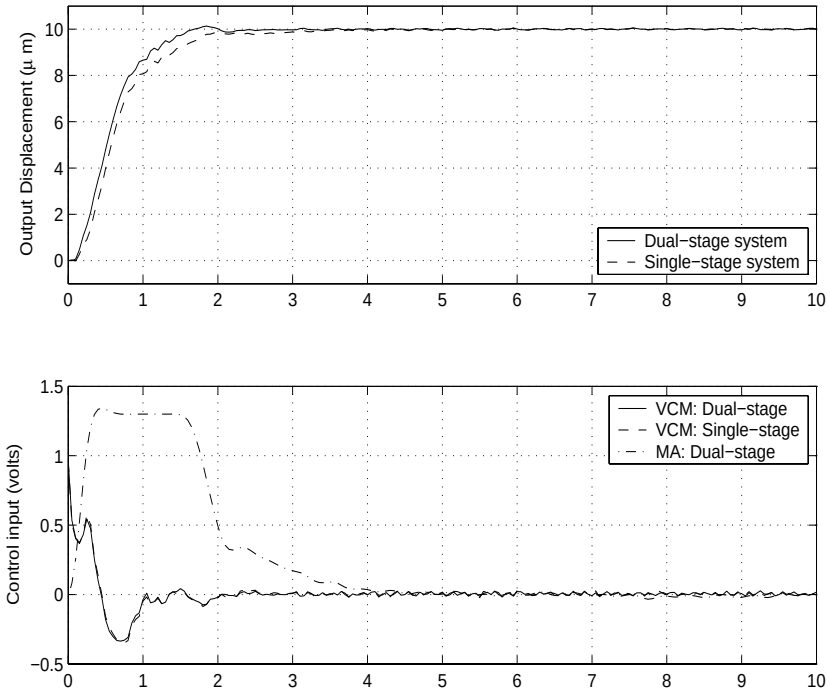

Figure 6.16: Experimental results for $r = 10\mu$m: CNF design (dual- versus single-stage).

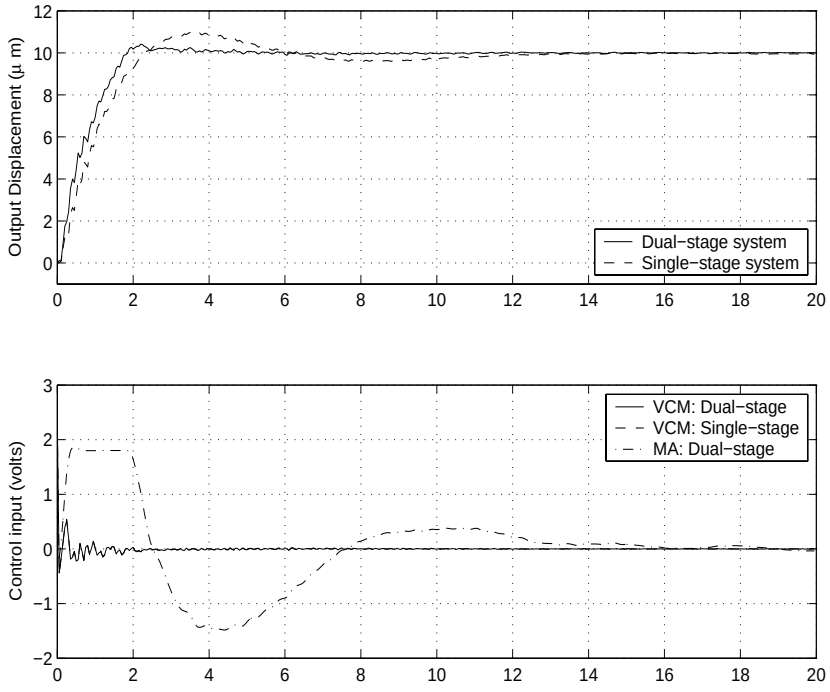

Figure 6.17: Experimental results for $r = 10\mu$m: PID design (dual- versus single-stage).

Table 6.2: Performances of dual-stage HDD servo systems.

(a) Settling time (ms) for $1\mu m$ track following

Design	Simulation	Experiment
RPT	0.54	0.60
CNF	0.61	0.5
PID	2.95	1.15

(b) Settling time (ms) for $10\mu m$ track seeking

Design	Simulation	Experiment
RPT	2.3	2.8
CNF	2.2	2.5
PID	8.1	8.4

these disturbances, we need to artificially add the runouts and other disturbances into the system. Based on previous experiments, we know that the runouts in real disk drives are composed mainly of RROs, which are basically sinusoidal with a fundamental frequency corresponding to the spin rate of the spindle motor. By manually adding this "noise" to the output while keeping the reference signal at zero, we can then read off the subsequent position signal as the expected position error signal (PES) in the presence of runouts. In disk drive applications, the deviation of the R/W head from the center of the track during track following, which can be directly read off as the PES, is very important. Track following servo systems have to ensure that the PES is kept to a minimum. Having deviations that are above the tolerance of the disk drive would result in too many read or write errors, making the disk drive unusable. The measure of track mis-registration (TMR) in HDDs, which is closely related to the maximum achievable track density, is defined as three times of the standard deviation of the PES readings, *i.e.*, $3\sigma_{\text{pes}}$.

Table 6.3: Position error signal (PES) tests: $3\sigma_{\text{pes}}$ values (μm).

	Single	Dual	improvement (%)
RPT	0.033	0.017	47
CNF	0.032	0.016	48
PID	0.075	0.020	73

We conduct the PES tests for the complete single- and dual-stage actuated servo systems (using nominal parameter values) by injecting a fictitious runout signal with a fundamental frequency of $55Hz$(corresponding to a spindle speed of $3300RPM$),

$$w(t) = 0.5 + 0.1\cos(110\pi t) + 0.05\sin(220\pi t) + 0.02\sin(440\pi t) + 0.01\sin(880\pi t) \quad (6.23)$$

into the actual system. The unit for $w(t)$ is in micrometer. The results, *i.e.*, the actual output responses and the histograms of the PES tests, are given in Figures 6.18 and 6.19 respectively. The $3\sigma_{\text{pes}}$ values of the PES tests for the single- and dual-stage actuated servo systems are summarized in Table 6.3. It is obvious that the dual-stage system can effectively reject the RROs disturbance, even with a conventional PID design.

6.5 Concluding Remarks

We have presented in this chapter the design of a piezoelectric dual-stage actuated HDD servo system using three different control approaches, namely, RPT, CNF and PID. The designs are facilitated by the low frequency property of the piezoelectric microactuator. Simulation and experimental results confirm that our designs achieve desirable performance while at the same time maintaining the stability margin requirements. Especially, the dual-stage systems show excellent performance in track following tasks and rejecting repeatable runout disturbance. This was actually the original motivation for introducing a microactuator into HDD servo systems.

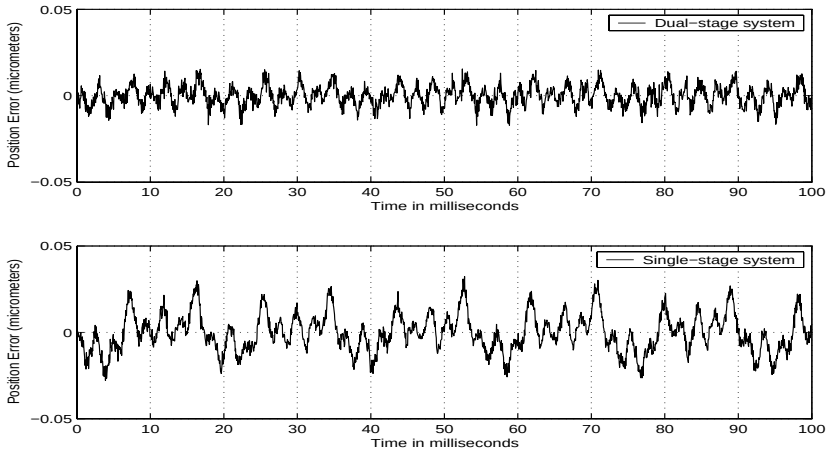

(a) RPT design

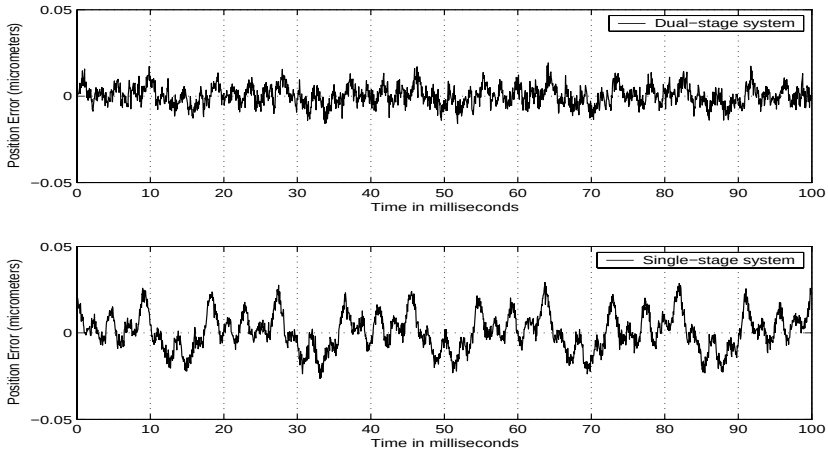

(b) CNF design

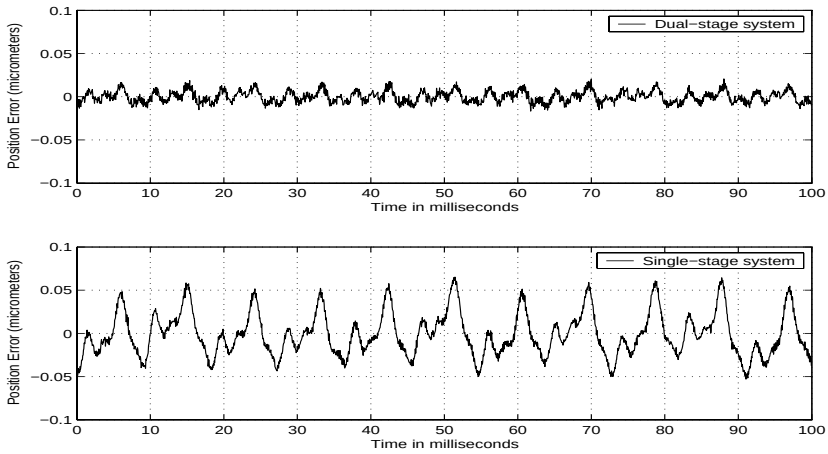

(c) PID design

Figure 6.18: Experimental results: Responses to a runout disturbance.

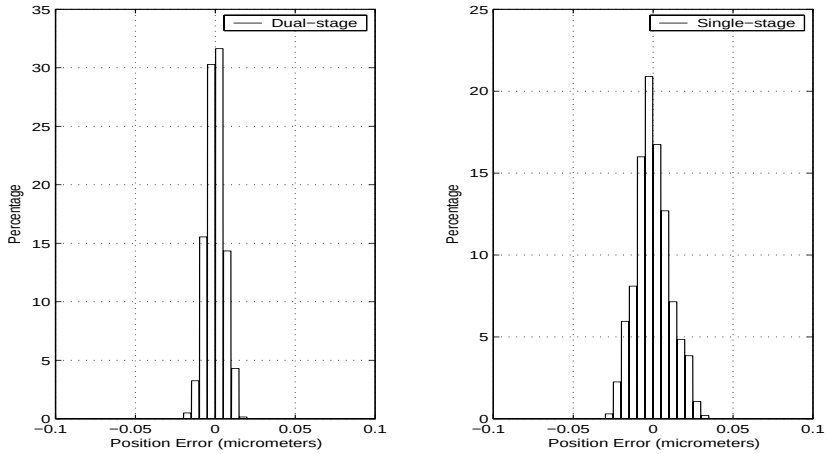

(a) RPT design

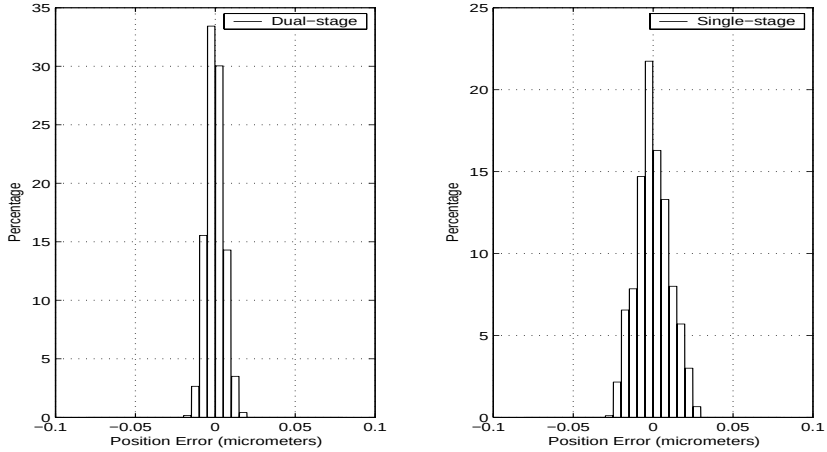

(b) CNF design

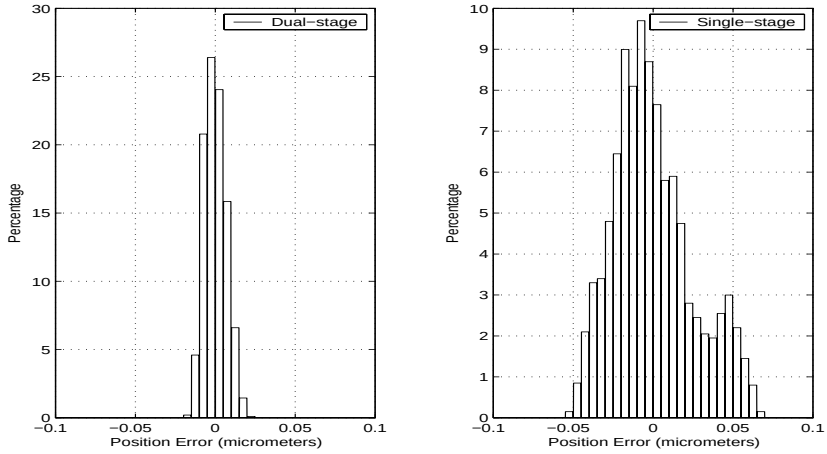

(c) PID design

Figure 6.19: Experimental results: PES test histograms.

Chapter 7

Conclusion and Further Research

7.1 Conclusion

This research attempted to develop a servo design methodology for the new generation hard disk drives which are characterized by smaller form factor and larger capacity. To be specific, the task of this research boiled down to three aspects. First, it aimed to establish a comprehensive HDD model which accurately identifies the dynamics of the HDD servo mechanism, with special attention to the coupled nonlinearity which has long been ignored but has now become prominent in the new generation HDDs. Next, it sought to explore new control techniques that can be used to design a servo controller with superior performance for HDD tracking tasks. Third, it sought to develop software toolkit to support controller design for HDD servo systems and relevant servo systems as well.

Our research has resulted in a full-fledged HDD model which captures not only the dominant linear dynamics of HDD servo mechanism, but also its coupled nonlinearities, *i.e.*, pivot bearing friction and flex cable nonlinearity. This model was derived by first studying the physical effects in and between the electromechanical parts of HDD VCM actuator and then applying Monte Carlo and system identification methods to determine the model parameters. Based on the established model, we have developed an effective control strategy for HDD servo system. Our idea is that, a nonlinearity that has been identified in clear form can be simply pre-compensated and the residual nonlinearity can be treated as

disturbances, and subsequent controller design should aim to minimize the adverse effects of the disturbances on the closed-loop performance of servo systems. With this idea in mind, we proceeded to design a microdrive track following controller using Robust and Perfect Tracking (RPT) control with integral enhancement. Furthermore, we have developed the enhanced Composite Nonlinear Feedback (CNF) control technique, which is basically an extension of its existing counterpart. And we have successfully applied this control technique to design a microdrive servo system which can perform track following and short span track seeking as well. The RPT and CNF techniques have also found applications in the design of a dual-stage actuated HDD servo system with a piezoelectric microactuator as the secondary actuator.

MATLAB simulations and real-time experiments have been carried out to verify our HDD model and test the performance of our servo controllers. Both time domain responses and frequency responses of our HDD model display a close match with those from experimental measurement, which verifies that our model correctly captures the linear and nonlinear dynamics of the physical disk drives. Simulation and experimental results of HDD set-point tracking consistently demonstrate that our servo controllers designed using nonlinear pre-compensation (if possible) plus integral enhancement together with either RPT or CNF can achieve fast settling and remove steady state bias in HDD tracking tasks, which is a major improvement over existing servo controllers.

Our research work also led to the so-called CNF control toolkit, which can be utilized to design a fast and smooth tracking controller for general linear systems with actuator and other nonlinearities, external disturbances, and high frequency resonance. The toolkit has been built on the popular MATLAB and SIMULINK environment with a user-friendly interface. All design parameters can be easily tuned online on the panels of the toolkit. The two illustrated examples on the servo design for a hard disk drive and a magnetic tape

drive fully show the great potential of the CNF control toolkit in design of servo systems that require fast target tracking and good robustness.

To sum up, the comprehensive VCM model, the servo design methodology using RPT/CNF control techniques combined with nonlinearity pre-compensation and integral enhancement, the servo design scheme for piezoelectric dual-stage system, together with the CNF toolkit provide a complete solution for servo design for the new generation disk drives. These results should be helpful for practicing servo engineers in the HDD industry. Although our research here is focused on HDD servo systems, the modeling methodology and control techniques we developed are actually not restricted to HDD systems. This can be seen from the corresponding theoretical formulations, which apply to a wide class of servo systems. Hence, it is reasonable to expect that our methodology and techniques may come in handy for solving general servo problems.

7.2 Further Research

The major part of this research are the modeling and subsequent servo system designs for a microdrive produced by IBM (now with the brand of Hitachi). However, there are other manufacturers in this industry, *e.g.*, Maxtor, Seagate, to name a few. It is possible that hard disk drives from these manufacturers might display subtle variation in the coupled nonlinearity in the servo mechanism. For future research, it is meaningful to explore the variation of the coupled nonlinearity in hard disk drives across various brands, and check whether our HDD model can serve as a unified model that characterizes the major brands.

Through out the research, the disk drives used in our experiments had their covers opened and disk platters removed. Hence, some disturbance sources, such as disk flutter, windage, repeatable run-outs, shock and vibrations caused by the spindle motor, are no longer existent, and we were not able to study their effects on the performance of the servo

systems we designed. For our servo systems to come to practical application in working environment, future research should include those factors in the designs and experiments.

For the dual-stage servo design, we are heavily dependent on the property of the piezoelectric microactuator, which simplifies the estimation of its relative displacement and subsequent design of servo system. However, this may not be the case for other types of microactuator, *e.g.*, an MEMS-based microactuator is generally identified as a second order system. More efforts need to be devoted to the servo design with such kind of microactuators. Moreover, it should be worthwhile to explore the coupling effects, which we have actually ignored, between the VCM and microactuator, and identify a multivariable model for the dual-stage system and then apply multi-variable control technology to design a servo controller in one shot.

For dual-stage servo experiments, we actually used a conventional 3.5 inch disk drive, due to the difficulty in mounting a microactuator on the tiny VCM arm of a microdrive. For future work, a dual-stage system comprising microdrive and microactuator should be available to study their synergy effects, in an effort to provide better servo solutions for future generation HDDs.

For the enhanced CNF control technique, it is now able to achieve fast and accurate set-point tracking for linear systems subject to actuator saturation and constant disturbances. Recently, extension has been made to track a non-step reference signal. However, further extensions are needed to cover systems with uncertainty, such as unknown parameters or parameter perturbation, and/or non-constant (*e.g.*, sinusoidal) disturbances.

As for the CNF control toolkit, it has significantly reduced the efforts involved in CNF design. However, parameter tuning is still a headache, especially with the choice of the matrix W. It is desirable to provide some guidelines for choosing W, *e.g.*, the zeros-assignment approach as suggested in [13]. Moreover, for MIMO systems, the design gets

tougher. Generally, it is quite difficult to obtain satisfactory performance for all output channels. In this regard, a decoupling control may be helpful. Hence, it is worthwhile to add a decoupling option to the CNF toolkit, which can be utilized if needed, to decouple an MIMO system into several SISO systems for which CNF design are actually carried out.

Last but not least, it should be interesting to apply the modeling methodology and control techniques here to other servo systems, such as robot manipulator, X-Y table, *etc.* These systems have been extensively studied and are still being used as benchmark platforms for evaluation of control techniques by the control community.

Bibliography

[1] D. Abramovitch, F. Wang and G. Franklin, "Disk drive pivot nonlinearity modeling Part I: Frequency domain," *Proceedings of the 1994 American Control Conference*, Baltimore, USA, pp. 2600-2603, 1994.

[2] D. Abramovitch and G. Franklin, "A brief history of disk drive control," *IEEE Control Systems Magazine*, vol. 22, no. 3, pp. 28-42, 2002.

[3] B. Armstronghelouvry, P. Dupont, C. Canudas de Wit, "A survey of models, analysis tools and compensation methods for the control of machines with friction," *Automatica*, vol. 30, pp. 1083-1138, 1994.

[4] C. Canudas de Wit and P. Lischinsky, "Adaptive friction compensation with partially known dynamic friction model," *International Journal of Adaptive Control and Signal Processing*, vol. 11, pp. 65-80, 1997.

[5] C. Canudas de Wit, H. Olsson, K. J. Astrom and P. Lischinsky, "A new model for control of systems with friction," *IEEE Transactions on Automatic Control*, vol. 40, pp. 419-425, 1995.

[6] C. Canudas de Wit, H. Olsson, K. J. Astrom and P. Lischinsky, "Dynamic friction models and control design," *Proceedings of the 1993 American Control Conference*, San Francisco, USA, pp. 1920-1926, 1993.

[7] W.-J. Cao, J.-X. Xu, "Fourier series-based repetitive learning variable structure control of hard disk drive servos," *IEEE Transactions on Magnetics*, vol. 36, pp. 2251-2254, 2000.

[8] H. S. Chang, S. E. Baek, J. H. Park and Y. K. Byun, "Modeling of pivot friction using relay function and estimation of its functional parameters," *Proceedings of the American Control Conference*, San Francisco, USA, pp. 3784-3789, 1999.

[9] J. K. Chang, and H. T. Ho, "LQG/LTR frequency loop shaping to improve TMR budget," *IEEE Transactions on Magnetics*, vol. 35, pp. 2280-2282, 1999.

[10] B. M. Chen, *Theory of Loop Transfer Recovery for Multivarible Linear Systems*, Ph.D. Dissertation, Washington State University, 1991.

[11] B. M. Chen, *Robust and $H\infty$ Control*, Springer, London, 2000.

[12] B. M. Chen, T. H. Lee and V. Venkataramanan, *Hard Disk Drive Servo Systems*, Springer-Verlag, New York, 2002.

[13] B. M. Chen, T. H. Lee, K. Peng and V. Venkataramanan, "Composite nonlinear feedback control: Theory and an application," *IEEE Transactions on Automatic Control*, vol. 48, no. 3, pp. 427-439, 2003.

[14] B. M. Chen and D. Z. Zheng, "Simultaneous finite and infinite zero assignments of linear systems," *Automatica*, vol. 31, pp. 643-648, 1995.

[15] B. M. Chen, Z. Lin and Y. Shamash, *Linear Systems Theory: A Structural Decomposition Approach*, Birkhauser, Boston, 2004.

[16] Y. Chen, P. Huang and J. Yen, "Frequency-domain identification algorithms for servo systems with friction," *IEEE Transactions on Control Systems Technology*, vol. 10, no. 5, pp. 654-665, 2002.

[17] S. Cho and I. Ha, "A learning approach to tracking in mechanical systems with friction," *IEEE Transactions on Automatic Control*, vol. 45, no. 1, pp. 111-116, 2000.

[18] D. Dammers, P. Binet, G. Pelz and L. M. Vobkarper, "Motor modeling based on physical effect models," *Proceedings of the 2001 IEEE International Workshop on Behavioral Modeling and Simulation*, Santa Rosa, USA, pp. 78-83, 2001.

[19] H. Du and S. S. Nair, "Modeling and compensation of low-velocity friction with bounds," *IEEE Transactions on Control Systems Technology*, vol. 7, no. 1, pp. 110-121, 1999.

[20] A. Dubi, *Monte Carlo Applications in Systems Engineering*, John Wiley, New York, 2000.

[21] R. Ehrlich, J. Adler and H. Hindi, "Rejecting oscillatory, non-synchronous mechanical disturbances in hard disk drives," *IEEE Transactions on Magnetics*, vol. 37, pp. 646-650, 2001.

[22] M. Evans and T. Swartz, *Approximating Integrals via Monte Carlo and Deterministic Methods*, Oxford University Press, London, 2000.

[23] R. B. Evans, J. S. Griesbach and W. C. Messner, "Piezoelectric microactuator for dual stage control," *IEEE Transactions on Magnetics*, vol. 35, pp. 977-982, 1999.

[24] P. Eykhoff, *System Identification - Parameter and State Estimation*, John Wiley, New York, 1981.

[25] M. Feemster, P. Vedagarbha, D.M. Dawson and D. Haste, "Adaptive control techniques for friction compensation," *Mechatronics*, vol.9, pp. 125-145, 1999.

[26] G. F. Franklin, J. D. Powell and M. L. Workman, *Digital Control of Dynamic Systems, Third Edition*, Addison-Wesley, Reading, Massachusetts, 1998.

[27] S. S. Ge, T. H. Lee and S. X. Ren, "Adaptive friction compensation of servomechanisms," *International Journal of Systems Science*, vol. 32, pp. 523-532, 2001.

[28] T. B. Goh, Z. Li, B. M. Chen, T. H. Lee and T. Huang, "Design and implementation of a hard disk drive servo system using robust and perfect tracking approach,"*IEEE Transactions on Control Systems Technology*, vol. 9, no. 2, pp. 221-233, 2001.

[29] J. Q. Gong, L. Guo, H. S. Lee and B. Yao, "Modeling and cancellation of pivot nonlinearity in hard disk drives," *IEEE Transactions on Magnetics*, vol. 38, pp. 3560-3565, 2002.

[30] L. Guo, D. Martin and D. Brunnett, "Dual-stage actuator servo control for high density disk drives," *Proceedings of the 1999 IEEE/ASME International Conference on Advanced Intelligent Mechatronics*, Atlanta, USA, pp. 132-137, 1999.

[31] W. Guo, L. Yuan, L. Wang, G. Guo, T. Huang, B. M. Chen and T. H. Lee, "Linear quadratic optimal dual-stage servo control systems for hard disk drives," *Proceedings of the 24th Annual Conference of the IEEE Industrial Electronics Society*, Aachen, Germany, vol. 3, pp. 1405-1410, 1998.

[32] Y. He, B. M. Chen and C. Wu, "Composite nonlinear control with state and measurement feedback for general multivariable systems with input saturation," *Proceedings of the 42nd IEEE Conference on Control and Decision*, Maui, Hawaii, USA, pp. 4469-4474, 2003.

[33] R. M. Hirschorn and G. Miller, "Control of nonlinear systems with friction," *IEEE Transactions on Control Systems Technology*, vol. 7, no. 5, pp. 588-595, 1999.

[34] T. Hu and Z. Lin, *Control Systems with Actuator Saturation: Analysis and Design*, Birkhäuser, Boston, 2001.

[35] X. Hu, W. Guo, T. Huang and B. M. Chen, "Discrete time LQG/LTR dual-stage controller design and implementation for high track density HDDs," *Proceedings of American Control Conference*, San Diego, California, USA, pp. 4111-4115, 1999.

[36] J. Ishikawa and M. Tomizuka, "A novel add-on compensator for cancellation of pivot nonlinearities in hard disk drives," *IEEE Transactions on Magnetics*, vol. 34, pp. 1895-1897, 1998.

[37] J. Ishikawa and M. Tomizuka, "Pivot friction compensation using an accelerometer and a disturbance observer for hard disk drives," *IEEE/ASME Transactions on Mechatronics*, vol. 3, pp. 194-201, 1998.

[38] Y.-H. Kim, and S.-H. Lee, "An approach to dual-stage servo design in computer disk drives," *IEEE Transactions on Control Systems Technology*, vol. 12, no. 1, pp. 12-20, 2004.

[39] M. Kobayashi, S. Nakagawa, T. Atsumi and T. Yamaguchi, "High-bandwidth servo control designs for magnetic disk drives," *Proceedings of IEEE/ASME International Conference on Advanced Intelligent Mechatronics*, Como, Italy, pp. 1124-1129, 2001.

[40] H. S. Lee, "Controller optimization for minimum position error signals of hard disk drives," *IEEE Transactions on Industrial Electronics*, vol.48, pp. 945-950, 2001.

[41] S.-H. Lee, and Y.-H. Kim, "Minimum destructive interference design of dual-stage control systems for hard disk drives," *IEEE Transactions on Control Systems Technology*, vol. 12, no. 4, pp. 517-531, 2004.

[42] Y. Li, and R. Horowitz, "Mechatronics of electrostatic microactuators for computer disk drive dual-stage servo systems ," *IEEE/ASME Transactions on Mechatronics*, vol.6, no. 2, pp. 111-121, 2001.

[43] Z. Li, G. Guo, B. M. Chen and T. H. Lee, "Optimal control design to achieve highest track-per-inch in hard disk drives," *Journal of Information Storage and Processing Systems*, vol. 3, no. 1-2, pp. 27-41, 2001.

[44] Z. Lin, M. Pachter and S. Banda, "Toward improvement of tracking performance – Nonlinear feedback for linear system," *International Journal of Control*, vol. 70, pp. 1-11, 1998.

[45] K. Liu, B. M. Chen and Z. Lin, "On the problem of robust and perfect tracking for linear systems with external disturbances," *International Journal of Control*, vol. 74, no. 2, pp. 158-174, 2001.

[46] X. Liu and J. C. Liu, "Analysis and measurement of torque hysteresis of pivot bearing in hard disk drive applications," *Tribology International*, vol. 32, pp. 125-130, 1999.

[47] L. Ljung, *System Identification - Theory for the User*, Second Edition, Prentice Hall, New York, 1999.

[48] A. Al Mamun, T.H. Lee, T.S. Low, "Frequency domain Identification of transfer function model of a disk drive actuator," *Mechatronics*, vol. 12, no. 4, pp. 563-574, 2001.

[49] H. A. Maria and I. D. Abrahams, "Active control of friction-driven oscillations," *Journal of Sound and Vibration*, vol. 193, pp. 417-426, 1996.

[50] G. A. Mikhailov, *Parametric Estimates by the Monte Carlo Method*, V.S.P. International Science, Utrecht, The Netherlands, 1999.

[51] H. Olsson and K. J. Astrom, "Observer-based friction compensation," *Proceedings of the 35th IEEE Conference on Decision and Control*, Kobe, Japan, pp. 4345-4350, 1996.

[52] H. Olsson, K. J. Astrom, C. Canudas de Wit, M. Gafret and P. Lischinsky, "Friction models and friction compensation," *European Journal of Control*, vol. 3, pp. 176-195, 1998.

[53] H. Olsson and K. J. Astrom, "Friction generated limit cycles," *IEEE Transactions On Control Systems Technology*, vol. 9, no. 4, pp. 629-636, 2001.

[54] C. K. Pang, G. Guo, B. M. Chen and T. H. Lee, "Nanoposition sensing and control in HDD dual-stage servo systems," *Proceedings of the 2004 IEEE Conference on Control Applications*, Taipei, Taiwan, pp. 551-556, 2004.

[55] E. Panteley, R. Ortega and M. Gafvert, "An adaptive friction compensator for global tracking in robot manipulators," *Systems & Control Letters*, vol. 33, pp. 307-313, 1998.

[56] K. Peng, B. M. Chen, G. Cheng and T. H. Lee, "Friction and nonlinearity compensation in hard disk drive servo systems using robust composite nonlinear feedback control," *Proceedings of the 5th Asian Control Conference*, Melbourne, Australia, pp. 58-63, 2004.

[57] K. Peng, B. M. Chen, T. H. Lee and V. Venkataramanan, "Design and implementation of a dual-stage actuated HDD servo system via composite nonlinear control approach," *Mechatronics*, vol. 14, no. 9, pp. 965-988, 2004.

[58] J. Ryu, J. Song and D. Kwon, "A nonlinear friction compensation method using adaptive control and its practical application to an in-parallel actuated 6-DOF manipulator," *Control Engineering Practice*, vol. 9, no. 2, pp. 159-167, 2001.

[59] P. Sannuti and A. Saberi, "A special coordinate basis of multivariable linear systems — finite and infinite zero structure, squaring down and decoupling," *International Journal of Control*, vol. 45, pp. 1655-1704, 1987.

[60] S. J. Schroeck, W. C. Messner and R. J. McNab,"On compensator design for linear time-invariant dual-input single-output systems," *IEEE/ASME Transactions on Mechatronics*, vol. 6, pp. 50-57, 2001.

[61] S.-M. Suh, C. C. Chung and S.-H. Lee, "Discrete-time LQG/LTR dual-stage controller design in magnetic disk drives,"*IEEE Transactions on Magnetics*, vol. 37, pp. 1891-1895, 2001.

[62] P. Vedagarbha, D. M. Dawson and M. Feemster, "Tracking Control of Mechanical Systems in the Presence of Nonlinear Dynamic Friction Effects," *IEEE Transactions on Control Systems Technology*, vol. 7, no. 4, pp. 446-456, 1999.

[63] V. Venkataramanan, B. M. Chen, T. H. Lee and G. Guo, "A new approach to the design of mode switching control in hard disk drive servo systems," *Control Engineering Practice*, vol. 10, no. 9, pp. 925-939, 2002.

[64] F. Wang, D. Abramovitch and G. Franklin, "A method for verifying measurements and models of linear and nonlinear systems," *Proceedings of the 1993 American Control Conference*, San Francisco, USA, pp. 93-97, 1993.

[65] F. Wang, T. Hurst, D. Abramovitch and G. Franklin, "Disk drive pivot nonlinearity modeling Part II: Time domain," *Proceedings of the 1994 American Control Conference*, Baltimore, USA, pp. 2604-2607, 1994.

[66] F. Wang, *Modeling and Adaptive Control of Time-Varying Friction in a Small Disk Drive*, Ph.D. Dissertation, Stanford University, 1995.

[67] L. Wang, L. Yuan, B. M. Chen and T. H. Lee, "Modeling and control of a dual-stage servo system for hard disk drives," *Proceedings of the 1998 International Conference on Mechatronics Technology*, Hsinchu, Taiwan, pp. 533-538, 1998.

[68] Z. Wang, H. Melkote and F. Khorrami, "Robust adaptive friction compensation in servo-drives using position measurement only," *Proceedings of the 2000 IEEE International Conference on Control Applications*, Alaska, USA, pp. 178-183, 2000.

[69] M. White, M. Tomizuka and C. Smith,"Improved track following in magnetic disk drives using a disturbance observer," *IEEE/ASME Transactions on Mechatronics*, vol. 5, pp. 3-11, 2000.

[70] M. T. White, and T. Hirano, "Use of the relative position signal for microactuators in hard disk drives," *Proceedings of the 2003 American Control Conference*, Denver, USA, pp. 2535-2540, 2003.

[71] M. L. Workman, *Adaptive Proximate Time Optimal Servomechanisms*, Ph.D. Dissertation, Stanford University, 1987.

[72] D. Wu, G. Guo, and T. C. Chong, "Adaptive compensation of microactuator resonance in hard disk drives," *IEEE Transactions on Magnetics*, vol. 36, pp. 2247-2250, 2000.

[73] T. Yan and R. Lin, "Experimental modeling and compensation of pivot nonlinearity in hard disk drives," *IEEE Transactions on Magnetics*, vol. 39, pp. 1064-1069, 2003.

Published/Submitted Papers

Journal Papers

1. G. Cheng, K. Peng, B. M. Chen and T. H. Lee, "A microdrive track following controller design using robust and perfect tracking control with nonlinear compensation," *Mechatronics*, vol. 15, no. 8, pp. 933-948, 2005.

2. K. Peng, B. M. Chen, G. Cheng and T. H. Lee, "Modeling and compensation of nonlinearities and friction in a micro hard disk drive servo system with nonlinear feedback control," *IEEE Transactions on Control Systems Technology*, vol. 13, no. 5, pp. 708-721, 2005.

3. K. Peng, B. M. Chen, G. Cheng and T. H. Lee, "Friction and nonlinearity compensation in hard disk drive servo systems using robust composite nonlinear feedback control," *Australian Journal of Electrical & Electronics Engineering*, vol. 2, no. 1, pp. 81-90, 2005 (invited; in Special Issue for Selected Papers of 2004 Asian Control Conference).

4. K. Peng, G. Cheng, B. M. Chen and T. H. Lee, "On the improvement of transient performance in tracking control for discrete-time systems with input saturation and disturbances," *IEE Proceedings - Control Theory & Applications*, in press.

5. G. Cheng, B. M. Chen, K. Peng and T. H. Lee, "A Matlab toolkit for composite nonlinear feedback control — improving transient response in tracking control," Submitted for journal publication.

Conference Papers

1. K. Peng, G. Cheng, B. M. Chen and T. H. Lee, "Design of discrete time composite nonlinear feedback control with measurement for hard disk drive servo systems," *Proceedings of the 4th Asian Control Conference*, Singapore, pp. 676-681, September 2002.

2. K. Peng, G. Cheng, B. M. Chen and T. H. Lee, "Design of multi-stage composite nonlinear feedback control for hard disk drives," Proceedings of the 17th IEEE International Symposium on Intelligent Control, Vancouver, Canada, pp. 734-739, October 2002.

3. K. Peng, G. Cheng, B. M. Chen and T. H. Lee, "Comprehensive modeling of friction in a hard disk drive actuator," *Proceedings of the 2003 American Control Conference*, Denver, USA, pp. 1380-1385, June 2003.

4. K. Peng, G. Cheng, B. M. Chen and T. H. Lee, "Modeling and analysis of micro hard disk drives, " *Proceedings of the 4th International Conference on Control and Automation*, Montreal, Quebec, Canada, pp. 952-956, June 2003.

5. K. Peng, G. Cheng, B. M. Chen and T. H. Lee, "Improvement on an HDD servo system design through friction and disturbance compensation," *Proceedings of the 2003 IEEE/ASME International Conference on Advanced Intelligent Mechatronics*, Kobe, Japan, pp. 1160-1165, July 2003.

6. K. Peng, B. M. Chen, G. Cheng and T. H. Lee, "Friction and nonlinearity compensation in hard disk drive servo systems using robust composite nonlinear feedback control," *Proceedings of the 5th Asian Control Conference*, Melbourne, Australia, pp. 58-63, July 2004 (won the Best Industrial Control Application Prize).

7. G. Cheng, K. Peng, B. M. Chen and T. H. Lee, "Improvement of HDD tracking performance using nonlinear compensation and RPT control," *Proceedings of the 5th Asian Control Conference*, Melbourne, Australia, pp. 84-89, July 2004.

8. G. Cheng, B. M. Chen, K. Peng and T. H. Lee, "A Matlab toolkit for composite nonlinear feedback control," *Proceedings of the 8th International Conference on Control, Automation, Robotics and Vision*, Kunming, China, pp. 878-883, December 2004.

9. K. Peng, G. Cheng, B. M. Chen and T. H. Lee, "On the improvement of transient performance in tracking control for discrete-time systems with input saturation and disturbances," *Proceedings of the 5th International Conference on Control and Automation*, Budapest, Hungary, pp. 437-442, June 2005.

10. G. Cheng, K. Peng, B. M. Chen and T. H. Lee, "Generalized composite nonlinear feedback control technique to track non-step references," Submitted to the 6th World Congress on Intelligent Control and Automation, Dalian, China, June 2006.